ISSN: 2164-5388 Volume 9, Number 3, July 2019

Scientific Research Publishing

Open Journal of Biophysics

ISSN: 2164-5388

www.scirp.org/journal/ojbiphy

Journal Editorial Board

ISSN Print: 2164-5388 ISSN Online: 2164-5396
http://www.scirp.org/journal/ojbiphy

Associate Editors

Editorial Board

Scientific Research Publishing

Open Journal of Biophysics, 2019, 9, 147-237
http://www.scirp.org/journal/ojbiphy
ISSN Online: 2164-5396
ISSN Print: 2164-5388

Table of Contents

Volume 9 Number 3 July 2019

Open Journal of Biophysics (OJBIPHY)
Journal Information

SUBSCRIPTIONS

The *Open Journal of Biophysics* (Online at Scientific Research Publishing, www.SciRP.org) is published quarterly by Scientific Research Publishing, Inc., USA.

Subscription rates:
Print: $79 per issue.
To subscribe, please contact Journals Subscriptions Department, E-mail: sub@scirp.org

SERVICES

Advertisements
Advertisement Sales Department, E-mail: service@scirp.org

Reprints (minimum quantity 100 copies)
Reprints Co-ordinator, Scientific Research Publishing, Inc., USA.
E-mail: sub@scirp.org

COPYRIGHT

PRODUCTION INFORMATION

For manuscripts that have been accepted for publication, please contact:
E-mail: ojbiphy@scirp.org

Scientific Research Publishing

Open Journal of Biophysics, 2019, 9, 147-154
http://www.scirp.org/journal/ojbiphy
ISSN Online: 2164-5396
ISSN Print: 2164-5388

Easy Determination of Radiation Absorption in Brain Tissue from Mobile Phones Using Finite Element Method

Abubakar Yakubu[1], Zulkifly Abbas[2], Zainab Yunusa[3]

[1]Department of Physics, Kebbi State University of Science and Technology, Aliero, Nigeria
[2]Department of Physics, Universiti Putra Malaysia, Selangor, Malaysia
[3]Department of Mechatronics, Bayero University, Kano, Nigeria
Email: a.yaks@ksusta.edu, ngabulect73@yahoo.com

How to cite this paper: Yakubu, A., Abbas, Z. and Yunusa, Z. (2019) Easy Determination of Radiation Absorption in Brain Tissue from Mobile Phones Using Finite Element Method. *Open Journal of Biophysics*, **9**, 147-154.
https://doi.org/10.4236/ojbiphy.2019.93011

Received: August 25, 2018
Accepted: May 18, 2019
Published: May 21, 2019

Abstract

Brain tissue plays a significant role in both cognitive and psychomotor behavior of humans. However, their interaction with radiation emanating from hand held mobile devices is still not fully understood. This research was aimed at investigating radiation absorption in brain tissue. Bovine brain tissues ranging from lesser than 1 year to greater than 10 years of age were bought from a specialty store (Sigma-Aldrich). The tissues were used within 72 h of extraction for *ex vivo* brain experiments. The brain tissue was stored at 6˚C and then 16˚C for 24 h in the MRI room to reach thermal equilibrium before any experiments were undertaken. The averages for the dielectric constant were measured from 1 - 4 GHz using open ended coaxial probe (OECP) (85,070E; Agilent Technologies). The results obtained for the dielectric properties were then used as raw data in the numerical computation and simulation of the radiation absorption by the brain tissues for both adolescent and adults bovine brain tissue using finite element method (FEM). The measured dielectric constants varied for the different brain tissue from 54.39 to 39.29. Analysis showed that adolescents tissue absorbed more radiation than adults from mobile phoneradiation which is due to the higher dielectric property of adolescent brain tissue. The results obtained can be applied to human brain tissue since bovine shares the same compositional properties with humans.

Keywords

Bovine Brain Tissue, Dielectric Constant, Mobile Phones, Coaxial Probe, Finite Element Method

1. Introduction

Current usage of mobile telephones has plunged the industry into critical thinking of how to curb the menace of electromagnetic interference (EMI) pollution arising from the ever growing number of the telecommunication users via mobile telephones, local area networks, wide area networks and radar systems [1]. Electromagnetic fields are part of our daily life which includes, mobile phones, radio, Wi-Fi, etc. This research work is focused primarily on mobile telephony. The waves associated with mobile phones are numerous and also vary depending on the platform of operation such as Wi-Fi, Bluetooth, GSM antennas, 2G, UMTS or 3G, power grids. All the mentioned radiations are possible potentials to high health hazards. This research determines radiation absorption by brain tissue from brain tissue measurements in accordance with institutional and regulatory requirements.

It is reported in [2] that the Council of Europe recommended limitations on the use of mobile phones and internet access in all schools across the continent to protect young children from potentially harmful radiation. In [3], their study found that low-dose ionizing radiation exposure affects cognitive skills in exposed children later in life. It is reported that high doses of ionizing radiation to the head (20 - 50 Gy) lead to severe learning and memory impairment which is characteristic for Alzheimer's at old age [4] [5]. It is reported in [6] that 2.4 GHz Wi-Fi radiation emitted from wireless internet equipment altered the expression of two of five miRNAs.

Humans are exposed to an increasing amount of non-ionizing electromagnetic radiation emitted from sources such as cell phones, power transmission lines, radars, and medical equipment, causing public health concerns [7]. Safety standards defining upper limits for the specific absorption rates (SARs) were thus established to serve as guidelines for equipment manufacturers in various fields [8]. The Federal Communications Commission (FCC) in the United States has set an SAR limit of 1.6 W/kg averaged over 1 g of tissue for partial-body exposure, whereas the Council of the European Union allows a limit of 2.0 W/kg averaged over 10 g of tissue [9] [10]. Extensive cell phone use is known to present the highest radio frequency (RF) exposure to the general public [11].

Cell phone radiation exposure generally depends on emitted RF power, but to some extent this radiation depends on other parameters such as RF, antenna position relative to the head, duration of exposure and the material properties of the absorbing tissue. The maximum RF power emitted from handsets available today varies as mobile technology has evolved through generations. Brain tissue has a variable iron concentration that causes magnetic susceptibility heterogeneity induced contrast in EM imaging [12]. Moreover, such difference in magnetic and electrical properties of the brain tissue varies with age, causing variations in both EM imaging and absorption. Due to the explosive growth of the telecommunication industry, radiation emission doses are on the increase. Therefore, it is important to understand the relationship between electromagnetic fields radi-

ation absorption with brain tissue.

In the light of the above, this research is focused on investigating the effects of the cell phone radiation on human brain and does not investigate any medical or physiological, effects of cell phone radiation on humans. The question pertinent to ask is, what are the risks of mobile phones on human health? For possible answers to this question, there is need to practically measure and analyze the amount of radiation absorbed by brain tissue during mobile telephony conversation. Depicted in Figure 1 are the possible effects of ionizing radiation to the brain.

2. Methodology

The purchased human brain tissue is placed inside a sample holder after initial preservation for dielectric measurement. The tissue for the less than 1 year was first measured and repeated for about five times. The same experimental procedure is repeated for the other brain tissues. The average of the results were then recorded further use.

2.1. Procedure

After standardize calibration of the open ended coaxial sensor, the probe is place in contact with the tissue avoiding any air gap between the probe and the tissue. The results obtained for the measurements are analysed for the dielectric constant and loss factor. Figure 2(a) & Figure 2(b) are typical bovine brain tissue after extraction and OECP set-up for measurement of dielectric properties of the brain. All measurements were carried out at room temperature.

2.2. Simulation

The human brain is modelled to transit through a microstrip antenna using the

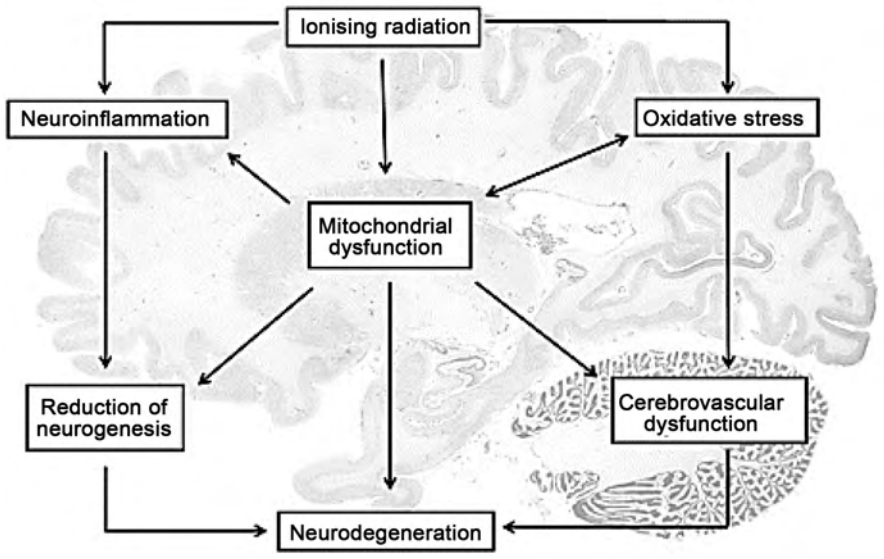

Figure 1. Possible neurodegeneration of the brain after exposure to ionizing radiation [13].

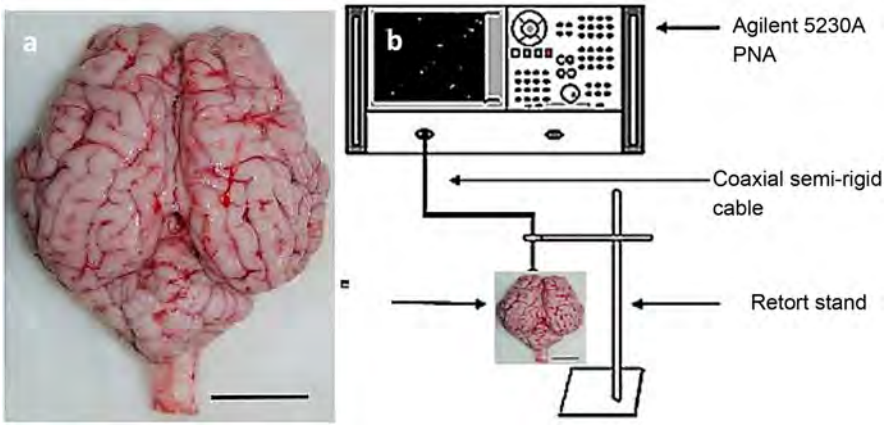

Figure 2. Typical bovine Brain. (a) Typical adolescent bovine brain tissue (b) Measurement set-up.

finite element method (FEM) COMSOL Software V4.5b, America. FEM imaging offers sufficient spatial and temporal resolution to characterize the hot spots from absorbed cell phone radiation in both aqueous media and biological tissues. The microstrip antenna is commercially available which are machined according to specification. In this work, the tissue was excited with RF radiation power of 2500 mW power.

A typical microstrip has a flat conducting walls anchored with SMA at the ends. In the simulating the tissue placed on the microstrip, the walls of the microstrip was approximated as perfect conductors [14]. **Figure 3** is a meshed human brain tissue simulated using the finite element method version 4.5b. The mesh brain tissue is assumed to be a perfect conductor at the boundaries of the microstrip. They are perfect conductor due to the salt like and moist nature of the brain.

3. Results

The variation in dielectric constant for all bovine brain tissues between 1 GHz and 4 GHz using OECP is shown in **Figure 4**. Careful observation and computation showed that the average values for the dielectric constant are 54.39, 48.14, 44.62 and 39.21 for <1 yr, 5 yrs, 10 yrs and >10 yrs old bovine brain tissues, respectively.

Further analysis clearly shows that, the tissues of the young bovine possess higher dielectric constant at frequency of 2.4 GHz which is mostly associated with all Wi-Fi (Mobile phones).

The high dielectric constant of the lesser than 1 year tissue could be attributed to higher iron content of the brain tissue. Results also showed that dielectric constant decreases as frequency increases for all brain tissue. This behavior is in accordance with the theory of [15] who stated that, for semi-liquid dielectric medium, as frequency increases, the dielectric constant decreases. Based on Pozar theory, it is concluded that our measurement and findings conforms to law.

The radiation imaging for the different categories of bovine brain are shown in **Figure 5**. The yellow and blue color represents the intensity of the electric

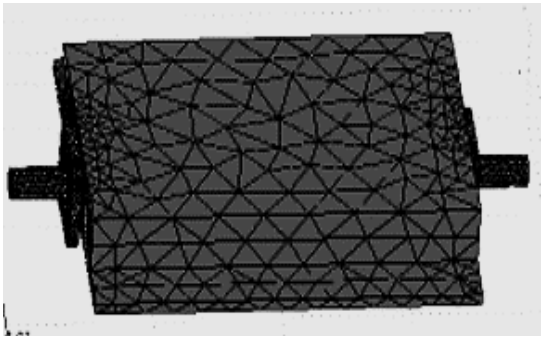

Figure 3. Meshed humanbrain tissue.

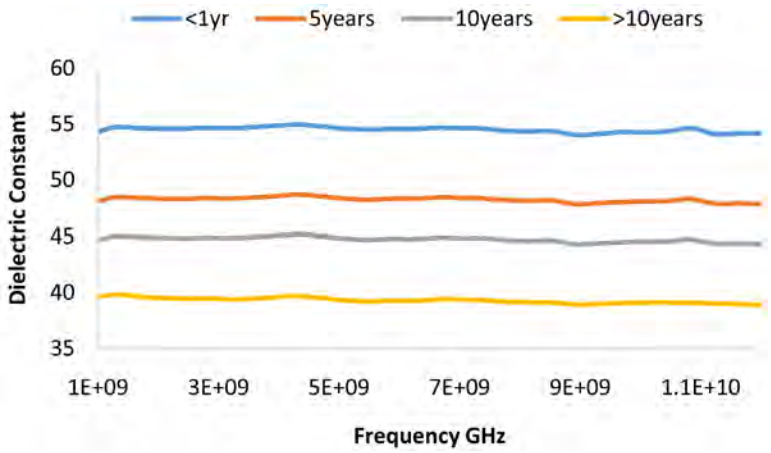

Figure 4. Variations in dielectric constant for all tissues.

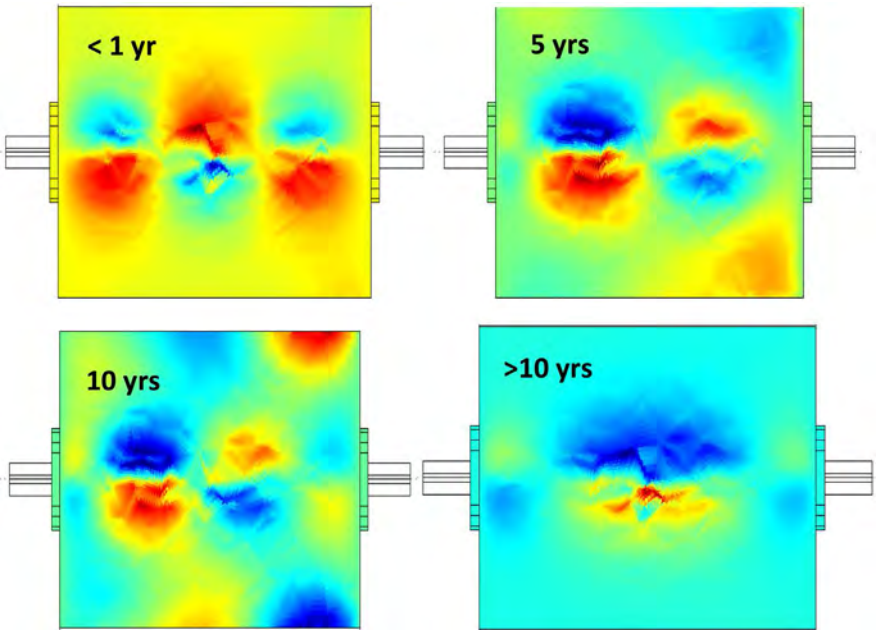

Figure 5. Variation in radiation scattering for different bovine brain tissues.

field within the simulated brain tissue. The blue represent area not affected by radiation while the red color stands for areas affected by radiation (hot spot).

Observation and analysis on the imaging shows that there is high amount of radiation for the less than 1 year tissue.

Further observations shows that the intensity of the radiation decreased as dielectric constant decreases. As expected higher permittivity gives rise to higher absorption of electromagnetic wave through a sample. Hence, the increase in radiation intensity as shown in the simulation is in complete agreement with the permittivity result obtained for the different bovine tissues. The result is also evident in **Figure 6** where the highest absorption at 2.4 GHz is for the less than 1 year old tissue. The results confirmed that radiation absorption distribution in the brain tissue is highly dependent on permittivity values of the tissue. The difference in the bovine brain tissue used in the simulation was to show the amount of radiation that can be absorbed by the tissue depending on age. Based on the result, it is confirmed that young bovine tissue absorb more radiation than older tissue.The human brain is embedded with Ribo Nucleic Acid (RNA) for the normal functioning of the brain [16]. Furthermore, it is believed that RNA-interference can affect both the level of pathological proteins (Aβ, tau protein) and the onset [17] [18], hence any alteration on the RNA can lead to major brain defects.

Generally, human and bovine brains are similar in functionalities. Recent advances have shown that all vertebrate brains share a common evolutionary origin. The bovine and human brains are architecturally the same as both brains consists globally of five parts, the Medulla, Medulla oblongata, limbic system, cerebellum and cortex. Among various possible health effects of mobile phone radiation, is the risk of inducing brain tumor leading to cancer due to radio Frequency (RF) dose from mobile phones.

4. Conclusion

In this paper, a step-by-step non-destructive dielectric measurement and modeling methods were used to determine the dielectric constant, radiation imaging,

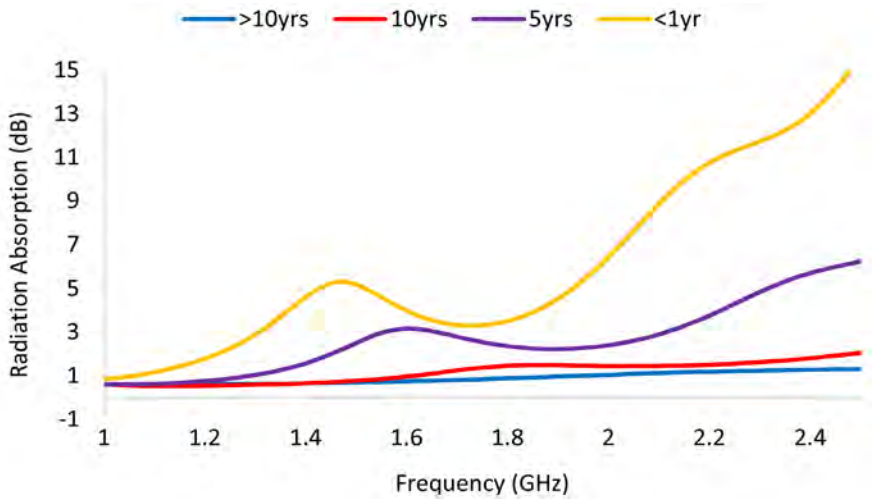

Figure 6. Radiation absorption for different bovine brain tissues at 1 - 2.4 GHz.

and absorption in brain tissue. The electromagnetic characterization of bovine brain tissue as an absorber using FEM has been carried out in the frequency range of 1 - 4 GHz band. The tissues were excited with a maximum power of 2500 mW. The E.M simulation has been carried out using the measured material properties of the heterogeneous brain tissue on COMSOL Software. The maximum absorption of radiation of more than 13 dB was observed for the less than 1-year-old brain tissue while the minimum absorption of about 1 dB was observed for the greater than 10 years old brain tissue at 2.4 GHz. It is therefore concluded that finite element method is successful in simulating radiation absorbed by brain tissue, and that radiation absorption is higher on materials with the highest permittivity value. Therefore, adolescents are prone to danger, if any, that might arise due to higher radiation absorption in brain tissues. This research method to the best of my knowledge is done for the first time in the field of electromagnetic simulation.

Acknowledgements

We thank Tertiary Education Trust (TETFund) Nigeria for the research grant and Prof. Zulkifly Abbas of the Universiti Putra Malaysia for assistance with measurements in his Laboratory.

Conflicts of Interest

The authors declare no conflicts of interest regarding the publication of this paper.

References

[1] Yakubu, A., Zulkifli, A., Nor Azowa, I. and Ahmad, F. (2015) Reduction of Electromagnetic Interference Using ZnO-PCL Nanocomposites at Microwave Frequency. *Advances in Materials Science and Engineering*, **2015**, Article ID: 132509. https://doi.org/10.1155/2015/132509

[2] Yorgancilar, E., Dasdag, S., Akdag, M.Z., Akkus, Z., Akdag, M. and Topcu, I. (2017) Does All-Day and Long-Term Exposure to Radiofrequency Radiation Emitted from Wi-Fi Affect Hearing? *Biotechnology & Biotechnological Equipment*, **31**, 1204-1209. https://doi.org/10.1080/13102818.2017.1373033

[3] Morris, R.D., Morgan, L.L. and Davis, D. (2015) Children Absorb Higher Doses of Radio Frequency Electromagnetic Radiation from Mobile Phones than Adults. *IEEE Access*, **3**, 2379-2387. https://doi.org/10.1109/ACCESS.2015.2478701

[4] Sharma, N.K., Sharma, R., Mathur, D., Sharad, S., Minhas, G., Bhatia, K., Ghosh, S.P., *et al*. (2018) Role of Ionizing Radiation in Neurodegenerative Diseases. *Frontiers in Aging Neuroscience*, **10**, 134. https://doi.org/10.3389/fnagi.2018.00134

[5] Priyadarshini, S.J. and Hemanth, D.J. (2018) Investigation and Reduction Methods of Specific Absorption Rate for Biomedical Applications: A Survey. *International Journal of RF and Microwave Computer-Aided Engineering*, **28**, e21211. https://doi.org/10.1002/mmce.21211

[6] Dasdag, S., Zulkuf, A.M., Erdal, M.E., Erdal, N., Izci, Ay.O., Ertan, Ay.M., Yilmaz, G.S., Tasdelen, B. and Yegin, K. (2015) Effects of 2.4 GHz Radiofrequency Radiation Emitted from Wi-Fi Equipment on microRNA Expression in Brain Tissue. *Interna-*

tional Journal of Radiation Biology, **91**, 555-561.
https://doi.org/10.3109/09553002.2015.1028599

[7] Moen, B.E., Møllerløkken, O.J., Bull, N., Oftedal, G. and Mild, K.H. (2013) Accidental Exposure to Electromagnetic Fields from the Radar of a Naval Ship: A Descriptive Study. *International Maritime Health*, **64**, 177-182.
https://doi.org/10.5603/IMH.2013.0001

[8] Foster, K.R. and Chou, C.K. (2016) Response to "Children Absorb Higher Doses of Radio Frequency Electromagnetic Radiation from Mobile Phones than Adults" and "Yes the Children Are More Exposed to Radiofrequency Energy from Mobile Telephones than Adults". *IEEE Access*, **4**, 5322-5326.
https://doi.org/10.1109/ACCESS.2016.2601490

[9] Federal Communications Commission (FCC) (2001) OET Bulletin 65 Supplement C. Federal Communications Commission, Washington DC.

[10] Council of the European Union (CEU) (1999) Council Recommendation of 12 July 1999 on the Limitation of Exposure of the General Public to Electromagnetic Fields (0 Hz to 300 GHz). *Journal of European Communities*, **199**, 59-70.

[11] Gultekina, D.H. and Moeller, L. (2013) NMR Imaging of Cell Phone Radiation Absorption in Brain Tissue. *PNAS*, **110**, 58-63.
https://doi.org/10.1073/pnas.1205598109

[12] Cabot, E., Stevanovic, I., Kuster, N. and Capstick, M.H. (2019) A Numerical Assessment of the Human Body Effect in the Transmission of Wireless Microphones. *Microwave and Optical Technology Letters*, **61**, 809-817.
https://doi.org/10.1002/mop.31623

[13] Kempf, S.J., Azimzadeh, O., Michael, J., Atkinson, M.J. and Tapio, S. (2012) Long-Term Effects of Ionizing Radiation on the Brain: Cause for Concern? *Radiation Environment Biophysics*, **52**, 5-16. https://doi.org/10.1007/s00411-012-0436-7

[14] Nguyen-Thoi, T., Phung-Van, P., Rabczuk, T., Nguyen-Xuan, H. and Le-Van, C. (2013) Free and Forced Vibration Analysis Using the n-Sided Polygonal Cell-Based Smoothed Finite Element Method (ncs-FEM). *International Journal of Computational Methods*, **10**, Article ID: 1340008.
https://doi.org/10.1142/S0219876213400082

[15] Pozar, D.M. (2012) Microwave Engineering. 4th Edition, John Wiley and Sons Inc., Hoboken.

[16] Jonkhout, N., Tran, J., Smith, M.A., Schonrock, N., Mattick, J.S. and Novoa, E.M. (2017) The RNA Modification Landscape in Human Disease. *RNA*, **23**, 1754-1769.
https://doi.org/10.1261/rna.063503.117

[17] Dorszewska, J., Prendecki, M., Oczkowska, A., Dezor, M. and Kozubski, W. (2016) Molecular Basis of Familial and Sporadic Alzheimer's Disease. *Current Alzheimer Research*, **13**, 952-963. https://doi.org/10.2174/1567205013666160314150501

[18] Ballard, D.H. (2015) Brain Computation as Hierarchical Abstraction. MIT Press, Cambridge. https://doi.org/10.7551/mitpress/9780262028615.001.0001

Open Journal of Biophysics, 2019, 9, 155-168
http://www.scirp.org/journal/ojbiphy
ISSN Online: 2164-5396
ISSN Print: 2164-5388

Non-Invasive Vibration-Stress of the Cirrhotic Liver of Patients Waiting for Transplantation Induces of Circulating CD133+ Stem Lymphocytes Committed Phenotypically toward the Liver

Aleksei N. Shoutko[1*], Olga A. Gerasimova[2], Vyacheslav A. Fedorov[1], Fiodor K. Zherebtsov[2]

[1]Laboratory for Improvement of the Cancer Treatment Methods, *A. M. Granov* Russian Research Center for Radiology and Surgical Technologies, Saint-Petersburg, Russia
[2]Transplantation Division, *A. M. Granov* Russian Research Center for Radiology and Surgical Technologies, Saint-Petersburg, Russia

Email: *info@rrcrst

How to cite this paper: Shoutko, A.N., Gerasimova, O.A., Fedorov, V.A. and Zherebtsov, F.K. (2019) Non-Invasive Vibration-Stress of the Cirrhotic Liver of Patients Waiting for Transplantation Induces of Circulating CD133+ Stem Lymphocytes Committed Phenotypically toward the Liver. *Open Journal of Biophysics*, **9**, 155-168.
https://doi.org/10.4236/ojbiphy.2019.93012

Received: May 3, 2019
Accepted: May 27, 2019
Published: May 30, 2019

Abstract

Background: Numerous studies of tissues' regeneration have confessed the recovery of damaged liver by hematopoietic stem cells. The cells act not only by cell replacement in the target organ but also by delivering trophic factors that support endogenous liver regeneration. A little is known of how organ-derived signals recruit such committed cells into circulation. **Objective:** We investigated the roles of noninvasive mechanical percutaneous stress of cirrhotic human liver in numbers fluctuation of trophic, liver-specific alpha-fetoprotein-positive fraction of CD133-positive hematopoietic stem cells in lymphocytes of patients waiting for liver transplantation. **Methods:** To promote in blood the number of the alpha-fetoprotein-positive fraction of CD133-positive hematopoietic stem cells, committed to liver' tissue, we activated mechanically the cirrhotic liver of patient by transcutaneous micro vibration received from skin-contacted electro-magnetic vibraphones generated mechanical pulses with amplitude 10 μm and smoothly changing frequency from 0.03 kHz to 18 kHz and back forth during one cycle duration 1 minute. The number of the alpha-fetoprotein-positive fraction of CD133-positive hematopoietic stem cells in lymphocytes of potential recipients was controlled by flow cytometry before and during daily sonication of skin area, which corresponds to liver projection on it. The 15 minutes cyclic sonication of the liver area performed daily for three weeks. **Results:** The sonication increased significantly averaged number of liver-specific alpha-fetoprotein-positive

CD133-positive blood lymphocytes in 2 - 3 times compared to a base lane. The second similar sonication, the same zone after three weeks break showed differences with baseline, but it was statistically insignificant. The result was specifically related to the liver as it showed the control sonication of the backbone's projection on the skin of a separate group of patients with cirrhotic liver from the waiting list. **Conclusion:** The stem cells committed to the liver recruit from the bone marrow into circulation, when organ mechanically stresses and secretes specific humoral signals to provoke of lymphopoiesis on host liver repair.

Keywords

Committed Stem Cells, Cirrhotic Liver, Waiting List, Mechanical Micro-Vibration, Regeneration

1. Introduction

The liver's capacity to undergo functional regeneration is mostly limited by acute mechanical injury, like partial hepatectomy or a single injection of toxic chemical substances, like carbon tetrachloride. The chronic/repeated or overwhelming injury often causes aberrant healing—the liver fibrosis that culminates in cirrhosis and hepatic failure. Both divergent processes are under control of a dynamic interplay between intrahepatic niche cells (parenchymal hepatocytes and non-parenchymal cells, including hepatic stellate cells, inflammatory cells, biliary epithelial cells, and liver sinusoidal endothelial cells) [1]. Along with intrahepatic cells, circulating hematopoietic stem/progenitor cells (HSC) derived from bone marrow (BM) can also contribute to liver regeneration by the fusion with damaged hepatocytes, or differentiation into hepatocyte-like cells, or exert a partial effect via their morphogenic and proangiogenic properties [2] [3] [4] [5]. Some agents modulated of hematopoiesis (granulocyte-colony stimulating factor: G-CSF, Plerixafor) use to mobilize HSCs into the bloodstream to reverse induced chronic liver injury, but they have standard limitations for administration to go ahead in terms of the number of cycles and the hematological toxicity [6]. Intraportal infusions of autologous HSCs from a preliminary aspirated bulk volume of BM (≈150 ml) represent another invasive approach to artificial enrichment of microenvironment of the cirrhotic liver by the HSCs trophogens [7].

Among different factors, the liver graft in cirrhotic patients can be the most natural long-term stimulus for recruitment into the peripheral blood of additional HSC [8], confirming the existence of a humoral information pathway (axis) between these two tissues. Earlier some data reported that among bulk HSCs population in the BM a small fraction of specifically liver-targeted cells preexists/resides and it may be mobilized into peripheral blood during stress and tissue injury, playing a precise role in the following reparation [9] [10] [11] [12]. Recently we showed that the orthotopic liver graft recruits the liver-specific (al-

pha-fetoprotein-positive) afp+ CD133+ HSC and some endothelial angiogenic afp+ CD31+ cells into lymphocytes (Lph) fraction of the blood [13] [14]. It remains unknown how to subvert the expected stable pro-fibrotic paracrine signals in "BM-liver" axis of those needed in orthotopic liver transplantation (OLT) into a regenerative paracrine stimulus to promote specific recruitment of morphogenic HSC committed to the rest of liver parenchymal cells. Interestingly, HSCs generated during embryonic liver development had the ability to traffic between different tissues like HSCs from adults and they both were most likely highly regulated by humoral signals to guarantee that they reached their final destinations [15].

Having the positive experience of inducible recruitment of HSC into the blood by moderate transcutaneous mechanical micro vibration of sponges bones [16] [17], we hypothesized that the direct mechanical stress of cirrhotic liver tissues might change the stagnant pro-fibrotic paracrine signals in humoral "BM-liver" axis and thus open new opportunities to influence on the specific interplay between afp+-committed morphogenic HSC and target hepatocytes.

Aim of the study was to mobilize from BM into circulation the additional number of HSC committed to the liver via the humoral signals, which provoke in the organ by its transcutaneous mechanical micro-vibrations. Here, we demonstrate the distant recruitment of liver-committed HSCs into the bloodstream of patients needed the OLT by noninvasive transcutaneous mechanical vibration of the cirrhotic liver monitoring the circulating afp+ CD133+ HSCs and afp+ CD31+ angiogenic lymphocytes number. The study allows us to confirm the possibility of an indirect and non-invasive increase the number of trophic stem cells committed to the hepatic tissues of those who are in waiting for the life-saving transplantation of a donor's organ. The long waiting time is deadly for those patients, but it is not predictable very often, because transplants are achievable by chance. The new technic proposed by us is specific and has no limit in reapplication in contrast with traumatic and non-targeted method of auto-transplantation of HSC widely used now in clinic.

2. Methods

2.1. Patients

The nine subjects within the age range of 53 - 61 years with cirrhosis listed for liver transplantation according to Model for End-Stage Liver Disease (MELD-Na) range 6 - 15 were included in this study at the Russian Research Center of Radiology and Surgical Technologies in St. Petersburg, Russia. Cirrhosis was diagnosed by clinical symptoms, biochemical indexes of liver failure, and liver histologic findings or compatible imaging findings (e.g., ultrasonography, computed tomography, or elastography). Six of nine awaiting patients received courses of mechanical vibration through skin-contacted vibraphones on the liver projection area. Other three patients received vibrations of backbones a similar contact way. The samples of peripheral blood were taken at the different time

elapsed since the start of sonication. The six healthy volunteers were involved in the investigation for the base level of blood parameters.

2.2. Equipment

The apparatus 'VITAFON-5 for vibroacoustic exposure was a serial certified source of electromechanical oscillations (GOST50444-92 and TU9444-009-23138557-2009 of RF). Standard vibraphones produced mechanical oscillations synchronously in the cyclic regime. The frequency of oscillations changed from 0.03 hertz (Hz) to 18 kilohertz (kHz) and back forth during ≈60 seconds. The amplitude of oscillations kept unchangeable about 10 μm. Mechanical micro vibrations of 8 vibraphones with a diameter of 45 mm each own achieved liver tissues percutaneously. Unit of vibraphones consisted of two rows (four in each) with the distances between the centers of rows of 75 mm and the centers of vibraphones within each row of 55 mm. Thus, the unit formed an active rectangular field of 12 × 22 cm, combined with a flat cloth frame with eight fixing sockets and adjustable soft fastenings for fixation on the human body.

2.3. Procedure/Sonication

The vibratory action usually performed once a day for 15 minutes sitting in a half/ lying position of patients. The block located on the right side of the patient so that the vibraphones tightly covers the projection region of the liver, and their lower eges coincide with the lower border of the ribs. Two main schemes of sonication of liver region were used. The scheme I of sonication included 15 minutes sonication daily, for 3 weeks (2d, 3d, and 4th). Scheme II consisted of sonication 15 minutes daily during 3 weeks, then break 3 weeks, and repeated sonication (8^{th} - 10th weeks). Scheme III served as a control for the scheme I and II. It consisted of mechanical micro vibrations from standard vibraphones with a smoothly varying frequency in the acoustic range 0.03 - 18 kHz by successive cycles of 60 seconds duration, affecting simultaneously 8 pairs of points along the entire central line of the spine with a distance between vibraphones in each pair of 0.5 cm for 15 minutes daily during 3 weeks (2d and 4th) [18].

2.4. Blood Samples

Ten ml of peripheral blood was taken once from each of six healthy volunteers at the beginning of the investigation. At schemes I, II and III such samples were taken twice during a week before sonication. At scheme I, the three samples were taken during 4th-6th weeks after the start of sonication and 12 samples during the 10th-12th weeks. At scheme II, the 15 samples were taken during 4th-6th weeks after the start of sonication and 15 samples during the 10th-12th weeks. At referent scheme III the six samples were taken during 4th-6th weeks after the start of sonication of the region of backbones projection on spine.

2.5. Preparation of Samples for Flow Cytometry

At each follow-up visit, the blood of patients examined for signs of cell's immu-

nophenotype. The goal was to identify specific features in cell parameters after sonication of liver area of a body in terms of percentages of circulating lymphocytes in synthetic phase S+, cells CD133+, CD31+, double-positive cells afp+ CD133+, afp+ CD31+, and derivate ratios (afp+ CD133+)/CD133+, (afp+ CD31+)/CD31+ and afp+ CD133+/afp+ CD31+. The mononuclear cell fraction (MNC) isolated by classical Ficoll density separation immediately after the collection of peripheral blood (10 mL), omitting the final step of magnetic cell enrichment. [19]. Viability assessed using the trypan blue exclusion test. Cells from two equal portions of the fresh MNC fraction stained for flow cytometry analysis. The nucleic acid stained by Hoechst 33342 (bis-benzimidazole fluorochrome; Sigma-Aldrich, St. Louis, MO, USA) for cell cycle analysis, which performed as described previously [20], with slight modifications. First MNCs resuspended at a density of 1067/mL in pre-warmed (37˚C) Dulbecco's Modified Eagle's Medium supplemented with 2% heat-inactivated fetal calf serum (Gibco BRL, Grand Island, NY, USA) and 10 mM HEPES (Gibco BRL). Then Hoechst 33342 added to a final concentration of 5 μg/mL, and the cells placed in a water bath at 37˚C for 120 minutes. Tubes mixed gently every 20 minutes during incubation. The cells were then centrifuged (483 relative centrifugal force for 6 minutes at 4˚C in a precooled rotor), resuspended in cold Hank's Balanced Salt Solution/2% fetal calf serum/10 mM 4-(2-hydroxyethyl)-1-piperazineethanesulfonic acid (HEPES) at a concentration of 1 - 2 × 10^7/mL, and kept at 4˚C until analysis.

The phenotypes of the circulating cells in the lymphoid part of the mononuclear cells (MNC) were evaluated using standard protocols for cell staining. MNCs prepared for conventional dual-color immunophenotyping with the fluorescence of allophycocyanin (APC)-directly conjugated anti-CD133/2 monoclonal antibodies (MoAbs), fluorescein isothiocyanate (FITC) directly conjugated anti-CD31 MoAbs, and phycoerythrin (PE)-directly conjugated anti-AFP (α-fetoprotein) MoAbs. The APC-conjugated MoAbs were from Miltenyi Biotech (Bergisch Gladbach, Germany), the FITC-conjugated MoAbs were from BD Bioscience Pharmingen (San Jose, CA, USA), and the PE-conjugated MoAbs were from R&D Systems (Minneapolis, MN, USA). Isotype-matched irrelevant MoAbs (Becton-Dickinson) used as negative controls.

2.6. Flow Cytometry

An LSR Fortessa flow cytometer (Becton-Dickinson, San Jose, CA, USA) adjusted for immunofluorescence before each measurement using the BD Cytometer Setup and Tracking Beads kits. The Lph and monocytes (Mn) fractions were separated by gating on forward (FSC) and side (SSC) light scatter dot plots, excluding cellular debris. A red laser (640 nm, 40 mW) used for the detection of CD133+ cells, a blue laser (480 nm, 50 mW) used for detection of AFP+ and CD31+ cells, and an ultraviolet (UV) laser (355 nm, 20 mW) for cells labeled with Hoechst 33342.

2.7. Flow Cytometry Analysis

All dates related to lymphocyte fraction of MNC. A minimum of 500,000 total events recorded twice for CD133+ cells detection. The percentage of positive cells calculated by subtracting the value of the appropriate isotype control. A dot plot of double (simultaneous) emission of Hoechst 33342 in blue (x-axis) and red (y-axis) wavelengths used for separation of events (G0 + G1), S, and (G2 + M) phases, as previously described. The major double (blue and red)-negative emitting population in the lower left corner of the plot represents cells in the (G0 + G1) phases of the cell cycle. The population located in the center and upper right corner of the dot plot represent the double emitting cells in the S-phase and mitotic phase (Mt) of the cell cycle respectively [19] [20].

2.8. Statistical Analyses

Single parameters were evaluated statistically with the calculation of an average (M), standard deviation (SD) and standard error (SE). The average values M were compared using t-criterion and probability p. We described the trends of the aggregate parameters before and after sonication by mathematical functions generated automatically using non-linear approximations in the Excel program. The coefficient determination R^2 used as a statistical measure of the goodness of fit of the regression line to the data. Satisfactory R^2 values were confirmed using Equation (1) for t-parameter [21]:

$$t = \sqrt{R^2} \times (n-2) \Big/ \left(1 - R^2\right) \tag{1}$$

3. Results

The data of Table 1. characterize the content of CD133-positive and CD31-positive populations in peripheral lymphocytes and their α-fetoprotein-positive (afp+) derivates (subpopulations) for volunteers.

Figure 1 shows the relative deviation of signs for patients with liver cirrhosis to corresponded signs for healthy volunteers in Table 1.

Relative decreasing of S+, CD31+ cells and a slight increase of CD133+ cells are typical for patients awaiting liver transplantation.

Figure 2 summarizes early results of sonication of the liver area according to the scheme I and II at fourth-fifth week after the start of treatment.

Table 1. Base parameters (BP) of circulating lymphocytes for healthy volunteers, percentage.

BP	CD133+	CD133+ afp+	CD31+	CD31+ afp+	s	CD133+/ CD31+	CD133+ afp+/ CD31+ afp+	CD133+ afp+/ CD133+	CD31+ afp+/ CD31+
M	0.037	0.0052	40.1	0.39	0.95	0.101*	1.64*	12.36*	0.97*
SD	0.012	0.0044	9.2	0.36	0.98	0.037	1.25	8.22	0.74
SE	0.004	0.0015	3.1	0.12	0.28	0.013	0.44	2.90	0.24
KV	0.32	0.84	0.23	0,92	1.03	0.37	0.76	0.66	0.76

*Obtained by averaging the personal ratios.

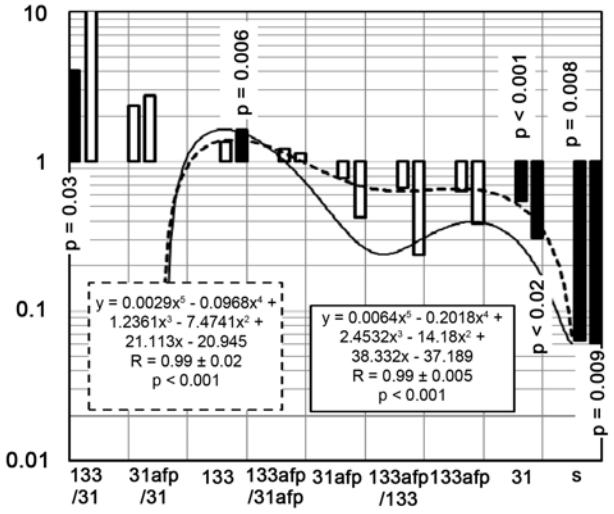

Figure 1. Relative changes of averaged cell parameters (M) at cirrhosis to those for healthy volunteers accepted as 1.0. Right columns correspond to data received before treatment according to the scheme I (solid line). Left columns correspond to data received before treatment according to scheme II and scheme III (dashed line). Statistically valid deviations are black.

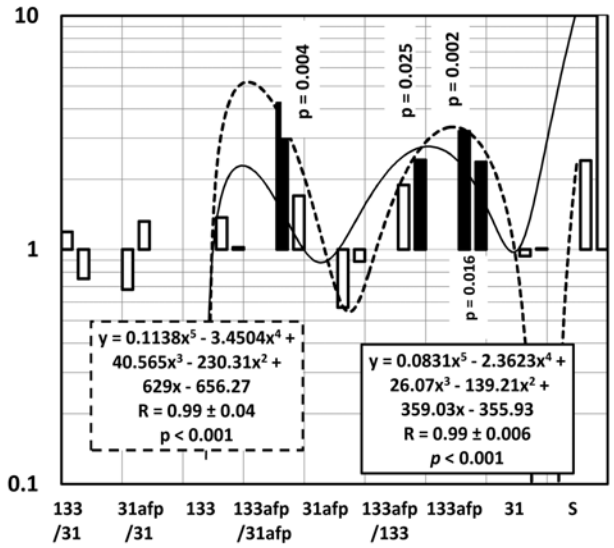

Figure 2. Relative changes of averaged cell parameters (M) after a fourth-fifth week of sonication of the liver area to those for untreated patients in Figure 1 accepted as 1.0. The right and left columns show the relative data received at 4th-6th weeks after the start of sonication according to the scheme I (solid line, right columns) and scheme II (dashed line, left columns) respectively.

The sonication normalized the preexisted abnormalities of S+, CD31+ and CD133+ cells before treatment shown in Figure 1. Moreover, it increases the number of double positive CD133+ afp+ cells, which are committed to liver tis-

sue.

The increasing of CD133+ afp+ cells in Figure 2 is specific for sonication of the liver area because the use of referent scheme III at spine area resulted in significant increasing only CD133+ population (Figure 3).

The sonication of backbones significantly increases the number of non-committed CD133+ cells in circulation not only over their number before spine treatment (Figure 3) but over the number of CD133+ cells after the first course of liver sonication, shown in Figure 2. as relative units. The real concentrations corresponded to Figure 2. Are 0.07 ± 0.022 ± 0.0125 (the scheme I) and 0.079 ± 0.037 ± 0.0099 (Scheme II). These mean values increase by backbones sonication (scheme III) 1.95fold ($p = 0.006$) and 1.75 fold ($p = 0.008$) correspondently.

There is no any specific changes registered at 10th-12th weeks after a single course of sonication according to the scheme I as it is seen in Figure 4 (right columns with solid line).

After double courses of liver area sonication according to Scheme II, all preexisted specific rise of CD133+ afp+ cells disappear at 10th-12th weeks, but they substitute by non-specific increasing of CD133+ cells. The S+ cells became elevated also compared to the corresponding data before the start of sonication shown in Figure 1 (dashed line, left columns).

Thus, the phenomenon of indirect transcutaneous mechanical mobilization of CD133+ afp+ hematopoietic stem cells committed to the targeted liver tissues arises during 4 - 6 weeks of sonication and disappears to 10^{th} - 12^{th} weeks. There was no chance to reproduce the peak of CD133+ afp+ by repeated sonication during the 8th-10th weeks at least.

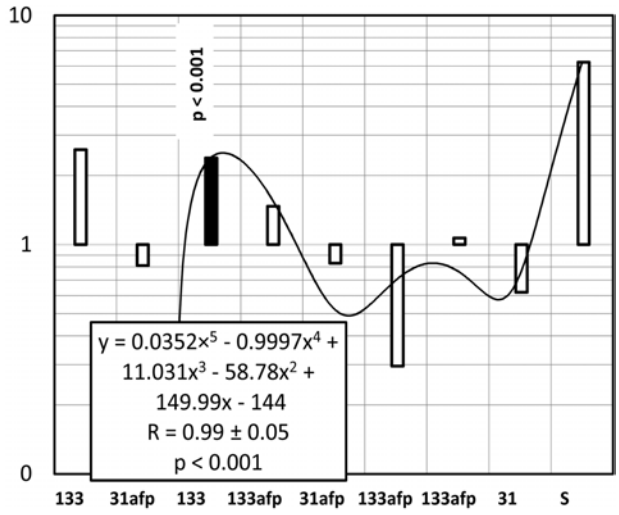

Figure 3. Relative changes of averaged cell parameters (M) after the start of sonication of the spine area to those for untreated patients in Figure 1 accepted as 1.0. The columns show the relative data received at 4th-6th weeks after the start of sonication according to Scheme III.

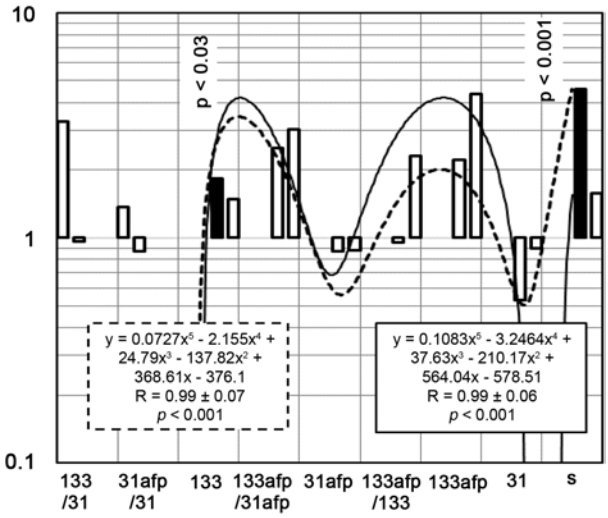

Figure 4. The relative changes of averaged cell parameters (M) during the tenth-fifteenth weeks after the start of sonication of the liver area to those for untreated patients in **Figure 1**. The columns show the relative data received at 10th-12th weeks after the start of sonication according to the scheme I (solid line, right columns) and scheme II (dashed line, left columns) respectively.

4. Discussion

It is clear that physical factors play very critical roles in biological processes. The applications of tensile strain, shear stress, electromagnetic fields, and ultrasound are among many options to enhance osteogenesis and chondrogenesis of human stem cell. Therefore, direct physical intervention is an appealing approach and should be profoundly exploited to improve clinical outcomes in tissues regeneration

There is no today medical approach for support of patients with cirrhotic liver on long and non-invasive base, apart from the prediction of optimal waiting time for liver transplantation [22]. The goal of the present article was an evaluation of the influence of the micro-vibrations on the interaction between bone marrow and liver at the level of inter-organs relation [2]. We expect that humoral signal of unknown nature from artificially stressed liver's tissues achieve the BM lymphopoietic niches and intensify either the natural production of liver committed morphogenic CD133+ afp+ lymphocytes, or their recruitment into circulations, which both suppress originally by disease. If it were true, we would receive a new approach for non-invasive and long-term targeted support of a liver function of patients waiting for a suitable transplant from a compatible donor.

Some authors found that liver exhibits mechanical resonance within registered frequencies 30 - 400 Hz, depending on odd harmonics 1 - 3 [23]. The liver itself has a frequency of around 55 - 60 MHz. The liver has also its own frequency around 55 - 60 MHz [24]. To non-invasive influence on that little-known com-

plex system, the mechanical vibrations seemed promising, as they may produce Stochastic Resonance (SR) in nonlinear biological systems, which enhance the performance of subthreshold stimuli in metabolic pathways [25] [26]. To increase the probability of the resonance process in liver tissues, we have chosen a unique source of mechanical vibrations in a wide range of frequencies [18]. The several reasons took into account in this study for using circulating lymphocytes as objects. First, lymphoid cells have most developed and flexible mechanisms of navigation toward different tissues/tropic/ and contain fractions of morphogenic/trophic cells such like CD133+, CD34+ HSC, lymphoid TdT+ cells, angiogenic CD31+ cells and other trophic unmatured cells, which usually termed as regulatory cells. Secondly, the lymphocytopoiesis is a most damaged process, and lymphoid tissue exhibits the highest loss of actual and functional mass during the life [27]. Third, the high neutrophil-to-lymphocyte ratio (NLR) is associated with a worse prognosis in various diseases of organs, including the liver [28].

In the blood of patients, we registered the deficit of naive CD31+ lymphocytes with angiogenic properties [29] [30] as well, like lymphocytes, being in the S-phase of DNA synthesis. The first course of liver or spine sonication both normalized both mentioned deficits (**Figure 2** and **Figure 3**). Thus, it is an argument against the specificity of these two effects.

On the contrary, first sonication of the liver increases of CD133+ afp+ cells, that seems quite committed (specific) to the liver tissues (**Figure 2** and **Figure 3**). We interpret the arising CD133+ afp+ cells number, as a remote result of specific paracrine stimulus originated from mechanically stressed liver parenchyma. The humoral stimulus aimed at the reproductive system of bone marrow activate and specifically recruit trophic/morphogenic marrow stem cells committed to recovering the damaged liver [31]. The signals could be either easily solved molecular substances in plasma or circulating extracellular vesicles with a size of tenths micron, recently discovered [32]. In this instance, the mechanical vibrations mimic the real damage of the liver.

Several cells of the liver might be as a target for interaction with committed CD133+ afp+ cells. Among liver, parenchymal cells is a population of CD133+ oval cells with the function of primitive, bipotent liver stem cells [33] [34], but they do not include AFP marker [35]. That is why the youngest resident hepatic stem cells (HepSCs) are hardly a target for afp+ CD31+ lymphocytes. Immature unipotent hepatoblasts, which expand during regenerative processes in the liver, have an antigenic profile, with strongly positive expression of both CD133 and the hepatic-specific AFP-marker [36] [37]. Thus, they are likely to be a target for CD133+ afp+-committed migrants [13].

Neither HepSCs nor immature unipotent hepatoblasts have at least one of the two markers AFP or CD31. [36], and we do not register any statistical proves of afp+ CD31+ lymphocytes response on the liver' sonication (**Figure 2** and **Figure 4**). This coincidence may be an additional argument for the hepatoblasts are most probable impact targets for humoral stimulus induced by liver mechanical

sonication.

Remarkable, that in terms of CD133+ afp+-committed migrants the second course of the liver area exposure (scheme II) did not change the effect of the first course. The reasons for that do not clear completely, but a limitation of lymphocytopoiesis in cirrhotic patients (**Figure 1**) and related instability/turbulence of it [13] [14] may be one of the possible causes. On the other hand, an exhausted/amortized natural ability of cirrhotic parenchyma to produce paracrine replay to mechanical stress might be the reason for that.

5. Conclusion

In conclusion, these results provide only a therapeutic roadmap to achieve long term non-invasive support of hepatic function without a traumatic transfusion of auto HSC or drugs stimulation of those awaiting the liver transplantation. Additional clinical investigations with the MELD/Na Score and the Child-Pugh Score [38] need for creating an effective and stable algorithm of employment found phenomenon.

Acknowledgements

This work was supported by the Ministry of Health in accordance with the open scientific plan of the center without any reservations regarding the open publication of the expected results.

Conflicts of Interest

The authors declare that they have no conflicts of interest.

References

[1] Ding, B.-S., Cao, Z., Lis, R., Nolan, D.J., Guo, P., Simons, M., *et al.* (2014) Divergent Angiocrine Signals from Vascular Niche Balance Liver Regeneration and Fibrosis. *Nature*, **505**, 97-102. https://doi.org/10.1038/nature12681

[2] Woo, D.H., Kim, S.K., Lim, H.J., Heo, J., Park, H.S., Kang, G.Y., *et al.* (2012) Direct and Indirect Contribution of Human Embryonic Stem Cell-Derived Hepatocyte-Like Cells to Liver Repair in Mice. *Gastroenterology*, **142**, 602-611. https://doi.org/10.1053/j.gastro.2011.11.030

[3] Ratajczak, J., Kucia, M., Mierzejewska, K., Marlicz, W., Pietrzkowski, Z., Wojakowski, W., *et al.* (2013) Paracrine Proangiopoietic Effects of Human Umbilical Cord Blood-Derived Purified CD133+ Cells—Implications for Stem Cell Therapies in Regenerative Medicine. *Stem Cells and Development*, **22**, 422-430. https://doi.org/10.1089/scd.2012.0268

[4] Liu, W.-H., Ren, L.-N., Wang, T., Navarro-Alvarez, N. and Tang, L.-J. (2016) The Involving Roles of Intrahepatic and Extrahepatic Stem/Progenitor Cells (SPCs) to Liver Regeneration. *International Journal of Biological Sciences*, **12**, 954-963. https://doi.org/10.7150/ijbs.15715

[5] Abdellatif, H. and Shiha, G. (2018) PD-L1 Expression on Circulating CD34+ Hematopoietic Stem Cells Closely Correlated with T-Cell Apoptosis in Chronic Hepatitis C Infected Patients. *International Journal of Stem Cells*, **11**, 78-86.

https://doi.org/10.15283/ijsc17047

[6] Tsolaki, E., Athanasiou, E., Gounari, E., Zogas, N., Siotou, E., Yiangou, M., *et al*. (2014) Hematopoietic Stem Cells and Liver Regeneration: Differentially Acting Hematopoietic Stem Cell Mobilization Agents Reverse Induced Chronic Liver Injury. *Blood Cells*, *Molecules*, *and Diseases*, **53**, 124-132. https://doi.org/10.1016/j.bcmd.2014.05.003

[7] Mohamadnejad, M., Vosough, M., Moossavi, S., Nikfam, S., Mardpour, S., Akhlaghpoor, S., *et al*. (2016) Intraportal Infusion of Bone Marrow Mononuclear or CD133+ Cells in Patients with Decompensated Cirrhosis: A Double-Blind Randomized Controlled Trial. *Stem Cells Translational Medicine*, **5**, 87-94. https://doi.org/10.5966/sctm.2015-0004

[8] Lemoli, R.M., Catani, L., Talarico, S., Loggi, E., Gramenzi, A., Baccarani, U., *et al*. (2007) Mobilization of Bone Marrow-Derived Hematopoietic and Endothelial Stem Cells after Orthotopic Liver Transplantation and Liver Resection. *Stem Cells*, **24**, 2817-2825. https://doi.org/10.1634/stemcells.2006-0333

[9] Kucia, M., Ratajczak, J., Reca, R., Janowska-Wieczorek, A. and Ratajczak, M.Z. (2004) Tissue-Specific Muscle, Neural and Liver Stem/Progenitor Cells Reside in the Bone Marrow, Respond to an SDF-1 Gradient and Are Mobilized into Peripheral Blood during Stress and Tissue Injury. *Blood Cells*, *Molecules and Diseases*, **32**, 52-57. https://doi.org/10.1016/j.bcmd.2003.09.025

[10] Ratajczak, M.Z., Kucia, M., Reca, R. and Majka, M. (2004) Stem Cell Plasticity Revisited: CXCR4-Positive Cells Expressing mRNA for Early Muscle, Liver and Neural Cells "Hide Out" in the Bone Marrow. *Leukemia*, **18**, 29-40. https://doi.org/10.1038/sj.leu.2403184

[11] Kucia, M., Ratajczak, J. and Ratajczak, M.Z. (2005) Bone Marrow as Source of Circulating CXCR4+ Tissue Committed Stem Cells. *Biology of the Cell*, **97**, 133-146. https://doi.org/10.1042/BC20040069

[12] Kucia, M., Reca, R., Jala, V.R., Dawn, B., Ratajczak, J. and Ratajczak, M.Z. (2005) Bone Marrow as a Home a Heterogenous Populations of Nonhematopoietic Stem Cells. *Leukemia*, **19**, 1118-1127. https://doi.org/10.1038/sj.leu.2403796

[13] Shoutko, A.N., Gerasimova, O.A., Ekimova, L.P., Zherebtsov, F.K., Mus, V.F., Granov, D.A., *et al* (2016) Long-Term Activation of Circulating Liver-Committed Mononuclear Cells after OLT. *Jacobs Journal of Regenerative Medicine*, **1**, Article ID: 011. https://jacobspublishers.com/long-term-activation-of-circulating-liver-committedmon

[14] Shoutko, A.N., Gerasimova, O.A., Ekimova, L.P., Zherebtsov, F.K., Mus, V.F., Matyurin, K.S., *et al*. (2017) Lymphocyte Reproductive Activity Normalized to Numbers of Hematopoietic Stem Cells in Blood and Rate of Death in Fatal Diseases. *International Journal of Genetics and Genomics*, **5**, 54-62. https://doi.org/10.11648/j.ijgg.20170505.12 http://www.sciencepublishinggroup.com/j/ijgg

[15] Heinig, K., Sage, F., Robin, C. and Sperandio, M. (2015) Development and Trafficking Function of Hematopoietic Stem Cells and Myeloid Cells during Fetal Ontogeny. *Cardiovascular Research*, **107**, 352-363. https://doi.org/10.1093/cvr/cvv146

[16] Karamullin, M., Baback, A., Ekimova, L., Phedorov, V., Kireeva, E., Sosukin, A., *et al*. (2008) The Blood Stem Cell's Pool Modulation in Remote Period Improved Health Status of Chernobyl Clean-Up Workers. *Radioprotection*, **43**, 89. https://doi.org/10.1051/radiopro:2008667

[17] Baback, A., Karamullin, M., Ekimova, L., Phedorov, V., Kireeva, E., Sosukin, A., *et al*. (2008) Exercise Performance vs. Growth of Haemopoietic Stem Cells Amount in CUWs Blood after Nonivasive Modulation. *Radioprotection*, **43**, 161. https://doi.org/10.1051/radiopro:2008724

[18] Shutko, A.N. and Fedorov, V.A. (2008) Sposob Obogascheniya Krovi Stvolovimi Krovetvornimi Kletkami. Patent Rossiiskoi Federacii #2166924, klass A61H23/00, BI:20/200; epab 20.07/2008. (In Russian). Http://ru-patent.info/21/65-69/2166924.html

[19] Eaker, Sh.S., Hawley, T.S., Ramezani, A. and Hawley, R.G. (2004) Detection and Enrichment of Hematopoietic Stem Cells by Side Population Phenotype. In: Hawley, T.S. and Hawley, R.G., Eds., *Methods Inmolecular Biology*: *Flow Cytometry Protocols*, 2nd Edition, Humana Press Inc., Totowa, 161-180. https://doi.org/10.1385/1-59259-773-4:161 https://flowcytometry.gwu.edu/.../flowcytometry.../fcp9.pdf

[20] Sales-Pardo, I., Avendaño, A., Martinez-Muñoz, V., García-Escarp, M., Celis, R., Whittle, P., *et al*. (2006) Flow Cytometry of the Side Population: Tips and Tricks. *Cellular Oncology*, **28**, 37-53. https://www.ncbi.nlm.nih.gov/pubmed/16675880

[21] Loveland, J.L. (2013) Mathematical Justification of Introductory Hypothesis Tests and Development of Reference Materials. All Graduate Plan B and Other Reports. Utah State University, Logan, 14. https://digitalcommons.usu.edu/gradreports/14

[22] Trieu, J.A., Bilal, M. and Hmoud, B. (2018) Factors Associated with Waiting Time on the Liver Transplant List: An Analysis of the United Network for Organ Sharing (UNOS) Database. *Annals of Gastroenterology*, **31**, 84-89. https://doi.org/10.20524/aog.2017.0217

[23] Oldenburg, A.L. and Boppart, S.A. (2010) Resonant Acoustic Spectroscopy of Soft Tissues Using Embedded Magnetomotive Nanotransducers and Optical Coherence Tomography. *Physics in Medicine & Biology*, **55**, 1189-1201. https://doi.org/10.1088/0031-9155/55/4/019

[24] Sharma, A. and Maurya, A.K. (2017) Aggregate Frequencies of Body Organs. *International Journal of Electrical*, *Electronics and Data Communication*, **5**, 94-98. http://iraj.in

[25] Arredondo, L.T. and Perez, C.A. (2017) Spatially Coincident Vibrotactile Noise Improves Subthreshold Stimulus Detection. *PLoS ONE*, **12**, e0186932. https://doi.org/10.1371/journal.pone.0186932

[26] Milanese, C., Cavedon, V., Sandri, M., Tam, E., Piscitelli, F., Boschi, *et al*. (2018) Metabolic Effect of Bodyweight Whole-Body Vibration in a 20-min Exercise Session: A Crossover Study Using Verified Vibration Stimulus. *PLoS ONE*, **13**, e0192046. https://doi.org/10.1371/journal.pone.0192046

[27] Richardson, R.B., Allan, D.S. and Lea, Y. (2014) Greater Organ Involution in Highly Proliferative Tissues Associated with the Early Onset and Acceleration of Ageing in Humans. *Experimental Gerontology*, **55**, 80-91. https://doi.org/10.1016/j.exger.2014.03.015

[28] Agiasotelli, D., Alexopoulou, A., Vasilieva, L., Kalpakou, G., Papadaki, S. and Dourakis, S.P. (2016) Evaluation of Neutrophil/Leukocyte Ratio and Organ Failure Score as Predictors of Reversibility and Survival Following an Acute-On-Chronic Liver Failure Event. *Hepatology Research*, **46**, 514-520. https://doi.org/10.1111/hepr.12582

[29] Ashman, L.K. and Aylett, G.W. (1991) Expression of CD31 Epitopes on Human Lymphocytes: CD31 Monoclonal Antibodies Differentiate between Naive

(CD45RA+) and Memory (CD45RA-) CD4-Positive T Cells. *Tissue Antigens*, **38**, 208-212. https://doi.org/10.1111/j.1399-0039.1991.tb01899.x

[30] Hur, J., Yang, H.-M., Yoon, Ch.-H., Lee, Ch.-S., Park, K.-W., Kim, J.-H., *et al.* (2007) Identification of a Novel Role of T Cells in Postnatal Vasculogenesis. Characterization of Endothelial Progenitor Cell Colonies. *Circulation*, **116**, 1671-1682. https://doi.org/10.1161/CIRCULATIONAHA.107.694778

[31] Huch, M. and Dolle, L. (2016) The Plastic Cellular States of Liver Cells: Are EpCAM and Lgr5 Fit for Purpose? *Hepatology*, **64**, 652-662. https://doi.org/10.1002/hep.28469

[32] Teixeira, J.H., Silva, A.M., Almeida, M.I., Barbosa, M.A. and Santos, S.G. (2016) Circulating Extracellular Vesicles: Their Role in Tissue Repair and Regeneration. *Transfusion and Apheresis Science*, **55**, 53-61. https://doi.org/10.1016/j.transci.2016.07.015

[33] Rountree, C.B., Barsky, L., Ge, S.H., Zhu, J., Senadheera, S.H. and Crooks, G.M. (2007) A CD133-Expressing Murine Liver Oval Cell Population with Bilineage Potential. *Stem Cells*, **25**, 2419-2429. https://doi.org/10.1634/stemcells.2007-0176

[34] Corbeila, D., Fargeasa, C.A. and Jászaib, J. (2014) CD133 Might Be a Pan Marker of Epithelial Cells with Dedifferentiation Capacity. *PNAS*, **111**, E1451-E1452. https://doi.org/10.1073/pnas.1400195111

[35] Turner, R., Lozoya, O., Wang, Y., Cardinale, V., Gaudio, E., Alpini, G., *et al.* (2011) Human Hepatic Stem Cell and Maturation Liver Lineage Biology. *Hepatology*, **53**, 1035-1045. https://doi.org/10.1002/hep.24157

[36] Haruna, Y., Saito, K., Spaulding, S., Nalesnik, M.A. and Gerber, M.A. (1996) Identification of Bipotential Progenitor Cells in Human Liver Development. *Hepatology*, **23**, 476-481. https://doi.org/10.1002/hep.510230312

[37] Liang, O.D., Korff, T., Eckhardt, J., Rifaat, J., Baal, N., Herr, F.T., *et al.* (2004) Oncodevelopmental Alphafetoprotein Acts as a Selective Proangiogenic Factor on Endothelial Cell From the Fetomaternal Unit. *The Journal of Clinical Endocrinology & Metabolism*, **89**, 1415-1422. https://doi.org/10.1210/jc.2003-031721

[38] Puentes, J.C.P., Rocha, H., Nicolau, S. and Ferrão, G. (2018) Effectiveness of the MELD/Na Score and the Child-Pugh Score for the Identification of Palliative Care Needs in Patients with Cirrhosis of the Liver. *Indian Journal of Palliative Care*, **24**, 526-528. https://www.ncbi.nlm.nih.gov/pubmed/30410269 https://doi.org/10.4103/IJPC.IJPC_97_18

Scientific Research Publishing

Open Journal of Biophysics, 2019, 9, 169-197
http://www.scirp.org/journal/ojbiphy
ISSN Online: 2164-5396
ISSN Print: 2164-5388

DNA Sequencing: Current State and Prospects of Development

Lusine Gasparyan[1,2], Ilya Mazo[1], Vahan Simonyan[3], Ferdinand Gasparyan[1,2]

[1]Argentys Informatics, LLC, Gaithersburg MD, USA
[2]Yerevan State University, Yerevan, Armenia
[3]The Department of Biochemistry & Molecular Medicine, The School of Medicine and Health Sciences, The George Washington University, Washington, DC, USA
Email: fgaspar@ysu.am

How to cite this paper: Gasparyan, L., Mazo, I., Simonyan, V. and Gasparyan, F. (2019) DNA Sequencing: Current State and Prospects of Development. *Open Journal of Biophysics*, **9**, 169-197.
https://doi.org/10.4236/ojbiphy.2019.93013

Received: May 5, 2019
Accepted: July 14, 2019
Published: July 17, 2019

Abstract

In this review, we collected and classified the stages of development of DNA sequencing methods and described its peculiarities. We pay attention mostly on solid-stead nanopore sequencing methods. Detailed discussion of the peculiarity and feasibility of the electrical methods of DNA sequencing is discussed. The detail analyses of the literature data, some critical considerations and the potential ways of optimization of DNA nanopore sequencing were presented.

Keywords

DNA Sequencing, ISFET Sensor, EIS Sensor, Solid-Stead Nanopore

1. Introduction

Since the discovery of the double-helix structure of the Deoxyribose Nucleic Acid (DNA) [1], the research on DNA sensors has grown drastically. Biosensors, especially DNA-biosensors are utilized to study DNA-related phenomena. The process of DNA sequencing is a precise determination of the amount and distribution of the nucleotides (A-adenine, T-thymine, C-cytosine, and G-guanine) in DNA molecules. Quick improvements in the cost and speed of DNA sequencing are having a strong influence on comprehensive genome research. Genomic information has many applications beside human medicine, for example, in security (DNA identification, pathogens detection, consumables authentication), insurance (individual polices, risk assessment), biotech (microbial engineering, GMO, livestock breeding, agriculture), health care (diagnosis, disease prevention, pharmacogenetics, gene therapy, vaccines, transplant programs),

defense, and evolutionary biology. However, the costs of sequencing are still too high for routine application. As noted in [2] [3] single-molecule genome sequencer using solid-state nanopore devices is one of the most promising candidates for a realization of $1000 personal genome-sequencing.

During its development DNA sequencing has some stages. Evolution of first, second, third and fourth generation of sequencing platforms and their applications detailed are presented in [3] [4] [5] [6]. One of the challenges for next-generation DNA sequencing is the creation of reliable, stable, reproducible, and cheap nanoscale structures-devices. Several nanoscale electronic methods have been proposed for high-throughput single-molecule nucleic acid sequence identification. DNA bases can be identified statistically in nanopore translocation events. Under the influence of an electric field, the negatively charged polynucleotides can be captured and drawn through the channel in a process termed "translocation".

In this review, we collected and classified the stages of development of DNA sequencing methods and described its peculiarities. We pay attention mostly on solid-stead nanopore sequencing methods. Detailed discussion of the peculiarity and feasibility of the electrical methods of DNA sequencing is discussed. The detail analyses of the literature data, some critical considerations and the potential ways of optimization of DNA nanopore sequencing were presented. In the contrast of other reviews in this field, we try to more critically discuss the "weak points" of some works (see Part 4).

2. DNA Sequencing Methods

DNA sequencing methods are:

✓ Basic DNA sequencing

- Sanger method (chain termination). Sanger sequencing is a method DNA sequencing first commercialized by Applied Bio systems, based on the selective incorporation of chain-terminating dideoxynucleosides by DNA polymerase during *vitro* DNA replication [7] [8].
- Maxam-Gilbert method (chemical termination). This method is based on nucleobase-specific partial chemical modification of DNA and subsequent cleavage of the DNA backbone at sites adjacent to the modified nucleotides [9].

✓ Advanced DNA sequencing

- Shotgun method. Shotgun sequencing is a method used for sequencing long DNA strands [10].

✓ Next generation DNA sequencing

- Illumina sequencing method. This sequencing method is based on reversible dye-terminators that enable the identification of single bases as they are introduced into DNA strands [11].
- Pyrosequencing method. Pyrosequencing is a method of DNA sequencing based on the "sequencing by synthesis" principle, in which the sequencing is

performed by detecting the nucleotide incorporated by a DNA polymerase [12].

✓ Solid-state (and biological) sequencing method [13].

Further our main attention will be focusing in last solid-state (and biological) nanopore sequencing method.

Although sequencing methods using nanopores have been studied in some detail, nevertheless, new perceptual architectures are emerging that are intended for the next generation of biosensors. In recent years many types of architectures have been proposed for new approaches to biomolecular sensing using nanoelectronics, including also the appearance of molecular (tunneling) junctions as a platform for perception.

In the past decade, the single-nanometer-scale pores demonstrated great capability for the detection, identification, and characterization of a variety of analytes, such as biomolecules like bacteria [14], protein [15] [16] [17] [18] [19], antibody [20] [21], nucleic acid [22] [23], DNA [24] [25], RNA (Ribonucleic acid) [26] [27].

Now the bio-, graphene, nanoribbon, nanotube, solid-state and hybrid nanopores are used successfully.

A large number of researches have been reported on DNA sequencing with solid-state nanopores based on different substrates, such as silicon oxide (SiO_2) [28] [29], silicon nitride (SiN_x) [30] [31] [32] [33], aluminum oxide (Al_2O_3) [34] [35], molybdenum sulfide (MoS_2) [34] [36] [37] [38] [39] [40], boron nitride (BN) [41] [42] [43], graphene [20] [37] [38] [44]-[52], carbon nanotube [53] [54] [55] [56] [57], nanochannel [40] [58] [59] [60] and polymers [61] [62] [63] [64] [65].

Solid-state nanopores exhibited remarkable chemical, thermal, and mechanical stability and extraordinary versatility in terms of the size, shape, and surface properties, as well as structural robustness. Different types of nanopores and typical technologies applied in the field of solid-state nanopore-based DNA sequencing have been detailed analyzed and reviewed in [4] [61] [66]. Nanopore sequencing is a label-free and amplification-free single-molecule approach, in which DNA molecules are driven through channels, producing signals that allow researchers to identify the corresponding sequences [62] [63] [67]-[76].

Nanopore-based DNA sequencing has led to fast and high-resolution recognition and detection of DNA bases. Solid-state and biological nanopores have low signal-to noise ratio (SNR) (<10) and are generally too thick (>5 nm) to be able to read at single-base resolution. A nanopore in graphene has a SNR of ~3 under DNA ionic current. Using atomistic and quantum simulations, it is found that a single-layer MoS_2 is an extraordinary material (SNR > 15) for DNA sequencing by two competing technologies (nanopore and nanochannel) [40]. To increase both SNR and dwell time in a conventional silicon-substrate nanopore, are added nano-well of 100 - 150 nm in diameter [77]. A MoS_2 nanopore shows four distinct ionic current signals for single-nucleobase detection with low noise level. In addition, a single-layer MoS_2 shows a characteristic change in the total

density of states for each base. The direct band gap of MoS_2 (1.88 eV [78]) is significantly changed when bases are placed on top of the pristine MoS_2 and armchair MoS_2 nanoribbon, thus making MoS_2 a promising material for base detection *via* transverse current tunneling measurements [36] [40]. Molecular dynamics simulations protein transport a nanopore in a quasi-2D heterostructure stacked together by graphene and MoS_2 nanosheets proposed in [37] [38]. In the case of a weak signal current, there is a need of its amplification. To increase the measured signal current in various complex systems, the movement of DNA must be slowed down. To do this, one suggests using a protein nanopore [24] for example, in combination with solid-state nanopores. It is shown that a protein nanopore with a covalently attached adapter molecule can continuously identify unlabeled nucleoside 5'-monophosphate molecules with accuracies averaging 99.8% [19].

The data [79] show that near-infrared SERS (surface-enhanced Raman scattering) on colloidal silver clusters also is an effective method of detecting single molecules. It is applicable to a wide range of molecules, including "colorless" biomolecules, for example, nucleotides in DNA sequencing.

The technique of reproducible conductivity measurements on single nucleotides with limited conformation and an improved algorithmic approach for isolating nucleotide bases is proposed in the [80]. The method of quantum point contact single-nucleotide conductance sequencing uses combed and electrostatically connected single DNA and RNA nucleotides on a self-assembled monolayer of cysteamine molecules. It is shown that by changing the applied bias and the pH condition, it is possible to turn on and turn off the molecular conductivity, which leads to a reversible nucleotide perturbation for electronic recognition. In [80], the potential of using simple surface modifications and existing biochemical fragments in individual nucleotide bases for reliable, direct, single-molecular nanoelectronics DNA and a method for identifying nucleotides of RNA for sequencing is demonstrated.

Drawing attention to the timely need for standardization of reliable nanosize devices for cheap, fast and scalable DNA detection, in [44] the nanoscale formed by the side heterostructure of graphene and hexagonal boron nitride is considered as a potential architecture. It is noted that blocks of DNA structure, nucleotide groups unambiguously associated with nano-gang states and emerging induced states, can be attributed as leaving a DNA sequence impression in the calculated current-voltage characteristic. Two offset windows are advanced: lower (1 - 1.2 V) and higher (2.7 - 3 V), where it is possible to uniquely identify all four bases from the current traces, although a higher sensitivity is obtained in the higher voltage window. Ways to improve the sensitivity of the DNA-nucleotide base using functionalized graphene nanogap as a solid-state device was analyzed in [45]. The appropriate translocation rate of the base molecule provides a time-dependent function of interaction change inside of interaction interval of each individual base with graphene nanopore. The forces between bases and graphene nanopore are calculated as interaction characteristics

of bases [47]. Molecular dynamics method is used for the DNA base and graphene nanopore calculations. The time-dependent in-plane for graphene transient force signal resolution for different bases is probed. Possibility of base identification by combination of transient in-plane force taken as orientation averaged signal is studied. The nucleobases are inserted into a pore in a graphene nanoribbon, and the electrical current and conductance spectra are calculated as functions of voltage applied across the nanoribbon. The conductance spectra and charge densities are analyzed in the presence of each nucleobase in the graphene nanopore. The results indicate that due to significant differences in the conductance spectra the proposed device has adequate sensitivity to discriminate between different nucleotides. Moreover, it is shown that the nucleotide conductance spectrum is affected little by its orientation inside the graphene nanopore.

Since DNA bases are different from each other in atomic scale, it is essential to collect base-specific information at atomic level to correspond to the DNA sequence with the measured signals. The amount of current which can pass through the nanopore at any given moment therefore varies depending on whether the nanopore is bonded by an A, a C, a G or T nucleotides. The change in the current through the nanopore as the DNA molecule passes through the nanopore represents a direct reading of the DNA sequence. In this case, four separate reading would be used, each one responsible for identifying one of the four DNA bases. The transient characteristics of the individual bases can be used for identification of the bases.

According to the different types of the signals, the DNA detection methods can be roughly classified into two categories [81]:

- the electrical detection methods, and
- the optical readout methods.

The optical detection methods require excitation irradiation source and photo-detector that transforms fluorescence light into measurable electrical signal, and optoelectronic connection to the reaction chamber. Therefore, the optical systems are often relatively large and expensive to be used in hand-held point-of-care devices [82].

In this review, optical detection methods will not be considered.

3. Electrical Detection Methods

Electrical detection methods for nanopore-based DNA sequencing are:

- Method Based on Ionic Blockade Current [83] [84] [85] [86] [87];
- Method Based on Tunneling Current [35] [82] [88] [89] [90] [91];
- Method Based on Capacitance Variation [92] [93] [94];
- Method Based on Electric Potential Change [95] [96].

3.1. Ionic Blockade Current Method

The current blockades are found to be sensitive to the properties of the nucleo-

tide composition, sizes, and secondary structure, and to physical parameters such as the driving field intensity, temperature, and ionic strength of the bio-liquid. These blockades are therefore a rich and powerful source of information regarding the dynamics of polynucleotides in the pore. The process of translocation occurs in two main stages (**Figure 1**):

- nucleotide "capture" in which one of the nucleotide's ends is threaded a small distance through the channel, and
- nucleotide sliding through the channel.

During translocation, the ionic current flowing through the channel is mostly blocked, indicating the presence of the polymer/molecule inside the channel.

In 1996, Kasianowicz *et al.* opened a whole new field when they reported the first ionic current blockades caused by the translocation of single-stranded RNA and DNA homopolymers through a 1.4 nm wide, 10 nm long, channel-forming α-hemolysin (α-HL) in an artificial lipid bilayer [97].

The experimental and theoretical efforts to elucidate polymer capture and the transport dynamics of biopolymers in nanosized pores are detailed reviewed in [65]. The initial concept for nanopore sequencing involved threading an individual single-stranded DNA (ssDNA) molecule through the staphylococcal α-HL protein pore under an applied potential while recording modulations of the ionic current passing through the pore. Each base will be registered, in sequence, by a characteristic decrease in current amplitude [87] [97] [99] [100] [101]. It has been demonstrated that an individual nucleobase can be identified on a static strand in a nanopore [102]; however, the rate of DNA translocation under a potential is too high for the necessary current resolution in a moving strand unless the bases are subjected to chemical modification with bulky groups [103]. The main technical problems required for the monophosphatization of high-resolution nucleosides are presented in [19]. It is shown that the robustness of lipid-bilayers is very sensitive to external and experimental conditions, to pH value, salt composition, temperature and mechanical stress, which can make the supporting membrane very unstable.

When the pore is empty the path of the ions in bio-liquid is not blocked and relatively large ion current flows through membrane, when the polymer/DNA

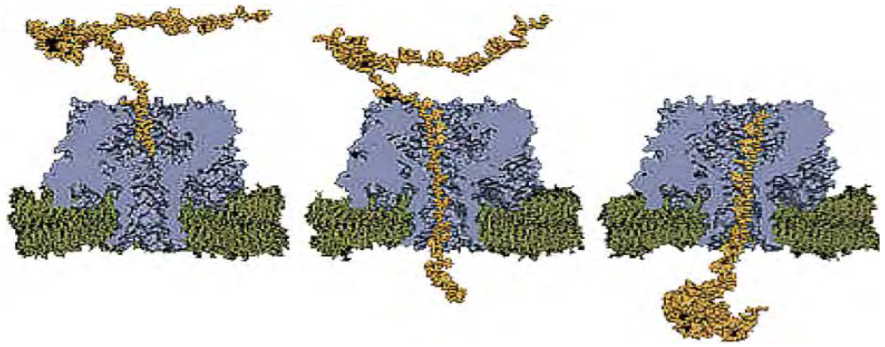

Figure 1. Molecular dynamic simulation of a ssDNA molecule translocating from one side of the membrane (pore) to the other. Adapted from Dekker's review [98].

enters the pore, it partially blocks the path of the ions, resulting in a significant decrease in current (Figure 2). When a molecule is translocate through a nanopore that partially blocks and prevents ions from freely flowing from one side to the other, and thus modifies the ionic transport. Despite that DNA also carries a charge through the pore, its relative speed compared to translocation of ions is very slow and this translates into a "blockade event", during which the ionic current briefly exhibits a lowered value. These translocation events give rise to spikes, also named pulses, in the ionic current baseline that can be characterized by their frequency, dwell time, and drop amplitude. The polymer/DNA makes many attempts to cross the pore; the unsuccessful attempts result in current blockades of very short durations (t_0 in Figure 2).

The modulation of current flowing through a nanowire by DNA molecules has been proposed as high throughput sequencing techniques. Xie *et al.* successfully detected the translocation of DNA molecules through a nanopore drilled at the edge of a silicon nanowire connected with electrodes [104]. Using such a nanowire-nanopore field-effect transistor (FET) sensor, they demonstrated that localized changes in the electrical potential during DNA translocations are responsible for FET conductance decreases (modulation) that correlated with the ionic current blockades.

The full details of the current blockade phenomenon are extremely complex: the involved variables are the pore size, pore geometry, DNA dynamics, homogeneity of the bio-liquid, chemical associations and charge condensations on the pore, ionic conditions on both sides of the separating membrane (including the ionic cloud that may condense around the pore), concentration of the macromolecules in the solution, ionic condensation on the macromolecules, voltage difference across the pore and temperature.

In general the translocation process can be viewed as a process controlled by following main factors:

- external driving forces (gravity, electrophoretic and drag forces),

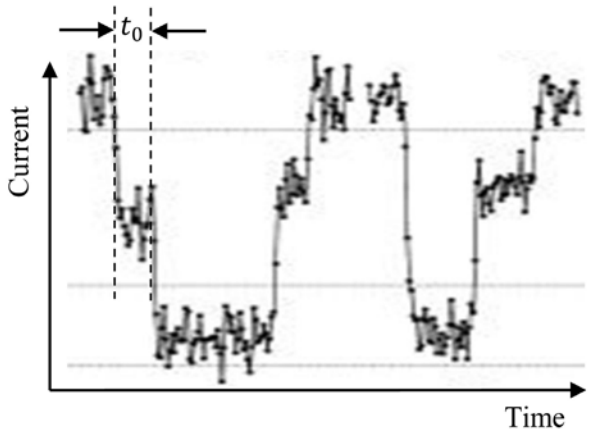

Figure 2. Example of ionic current traces illustrating the substrate structure of polynucleotide-induced current blockade events [87].

- applied potentials to lateral electrodes,
- polymer dynamics in the aqueous solution,
- type, concentration and orientation of nucleotides,
- pore or channel architecture (form, sizes), and
- molecule–pore interactions in atomic scale.

The main part of stages of translocation dynamics through the pore are detailed analyzed in [64]. It is provided a combined theory-experiment progress report on the understanding of (bio)polymer translocation.

For ionic conductance G of a cylindrical nanopore the following expression is commonly used in the literature [105]:

$$G = \sigma\left(\frac{4l}{\pi d^2} + \frac{1}{d}\right)^{-1}.$$

Here σ is the bulk conductivity, l is the length (the membrane thickness) and d is the diameter of the nanopore.

The capture radius r_c is the distance at which the electrophoretic force overwhelms the free thermodynamic diffusion and makes unlikely a molecule to escape the electric field forced diffusion (**Figure 3**). Once within the capture radius, single molecules are eventually captured and translocate to the other side. Molecules are captured by open bonds of hydrogen, nitrogen or carbon atoms of nucleotides (usually weak bonds) and move under the action of electroosmotic forces in the electrolyte.

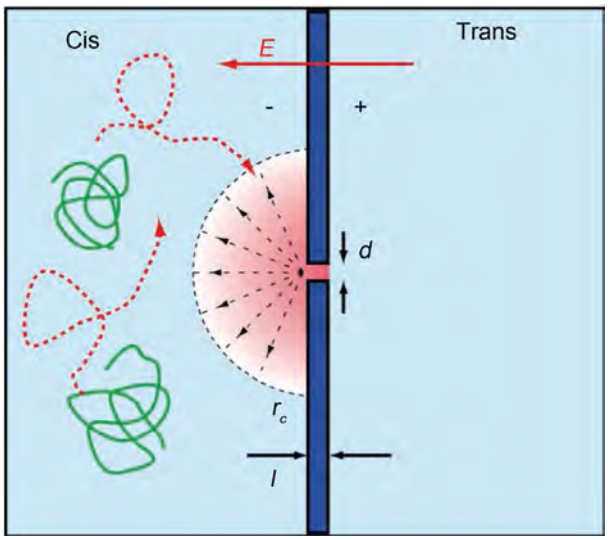

Figure 3. Scheme of capture of biopolymer in a nanopore. When an electric field is applied across a membrane, the potential drop mainly occurs at the nanopore, forming a funneling field driving the molecule toward the pore aperture. Outside of the capturing radius r_c, the electric field plays a marginal role and the molecules freely diffuse. Picture adapted from [3]. "Cis" indicates that the functional groups are on the same side of the carbon chain, while "Trans" conveys that functional groups are of opposing sides of the carbon chain.

3.2. Tunnel Current Method

As one of potential future techniques mentioned in [6] is DNA sequencing by tunneling currents. Besides the measurement of the changes in the ionic current, as the DNA passes through the pore, there are efforts to measure tunnel current flow through each base of DNA molecule (in a technique called Tunneling Currents DNA Sequencing) as it traverses the pore or channel. The expectations are that each base will show sufficiently different tunneling current and the base sequence will be deduced from the differences in the tunneling currents amplitude. This technique could have the potential to sequence orders of magnitude faster than the ionic current methods [6]. As noted yet the graphene nanogaps and nanopores also show potential for electrical DNA sequencing [46]. The change in the electric tunnel current is determined as a function of the applied bias and the coupled differential conductivity is analyzed at a voltage that seems to be suitable for distinguishing four nucleotides. A negative effect of differential resistance for one of the nucleotides (deoxyguanosine monophosphate) is predicted. It has been proposed that single molecules of DNA could be sequenced by measuring the physical properties of the bases as they pass through a nanopore [100]. Theoretical calculations suggest that electron tunneling can identify bases in ssDNA without enzymatic processing [106] [107], and it was experimentally shown that tunneling can sense individual nucleotides [108] and nucleosides [109], short DNA oligomers [110]. The use of graphene nanoribbons for transverse current modulation by DNA in two-terminal devices presented in **Figure 4**, develops in [49]. Usage of the carbon nanotubes (CNT) as tunneling tips presented in **Figure 5**.

An approach for reading the sequence of a DNA molecule passing between electrodes on a nanopore using tunneling signals associated with a hydrogen bond is proposed in [88]. Interaction with the base electrode is modeled using a scanning tunneling microscope (STM) probe with a nucleobase that is detached from the nucleoside monolayer.

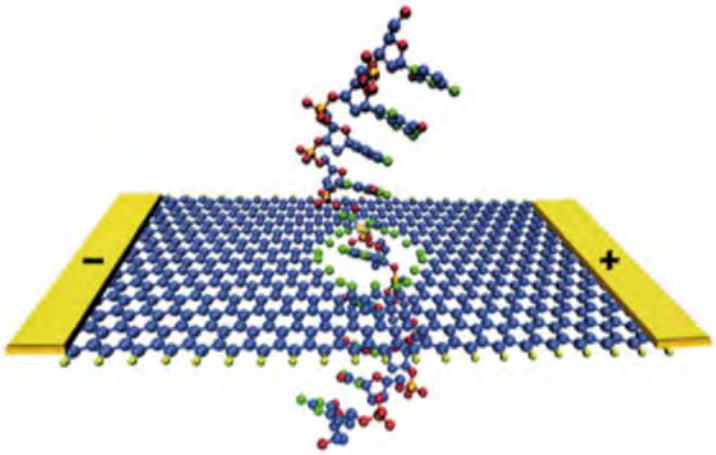

Figure 4. The use of graphene nanoribbons for transverse current modulation by DNA in two-terminal devices [49].

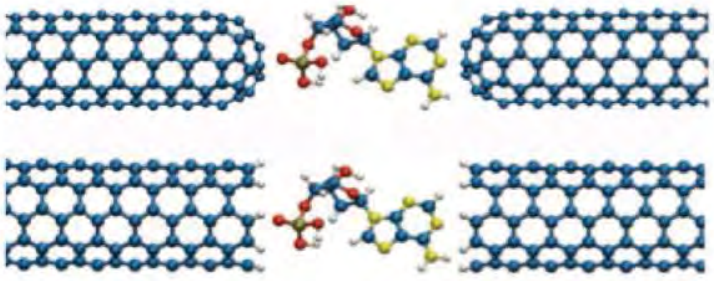

Figure 5. Carbon nanotubes as transverse tunneling electrodes. Two configurations are shown, depending if whether the tips are capped or open (carbon and hydrogen atoms respectively are shown in blue and white). In addition to ideal aspect ratios and unique electronic properties, CNTs may help orient nucleotides in the nanopore through specific π-stacking interactions. Adapted from [3].

An advantage of transverse tunneling electronic current over ionic current measurements is the fact that the current is measured in the range of **nano-ampere**, meaning that the translocation speed of DNA is less of a problem than if it is measured at higher frequencies compared to the **pico-ampere** ionic current of small-diameter nanopores.

Method of mechanically controllable break junction (MCBJ) is successfully used by several authors to investigate translocation behavior of DNA molecules [91] [108] [111]. Schematic of a nanofabricated nano-MCBJ shown on **Figure 6**. Tsutsui *et al.* first used sub-2 nm gold nanoelectrodes made from MCBJ technique to detect individual nucleotides in distilled water [108]. With suspended nanogap electrodes in solution, they showed that electron transport occurs by tunneling through nucleotides when freely diffusing individual bases get trapped between the tunneling tips. In such an event, characteristic current pulses are recorded, and they show that the electrical conductance of the bases was significantly different to open the way to individual bases differentiation, with current modulation due to individual bases of about 10 pA. In a microchannel, they could similarly detect freely diffusing mononucleotides and short DNA oligomers of up to 22 bases by tunneling measurements.

Method of mechanically controllable break junction (MCBJ) is successfully used by several authors to investigate translocation behavior of DNA molecules [91] [108] [111]. Schematic picture of a nanofabricated nano-MCBJ shown on **Figure 6**. Tsutsui *et al.* first used sub-2 nm gold nanoelectrodes made from MCBJ technique to detect individual nucleotides in distilled water [108]. With suspended nanogap electrodes in solution, they showed that electron transport occurs by tunneling through nucleotides when freely diffusing individual bases get trapped between the tunneling tips. In such an event, characteristic current pulses are recorded, and they show that the electrical conductance of the bases was significantly different to open the way to individual bases differentiation, with current modulation due to individual bases of about 10 pA. In a microchannel, they could similarly detect freely diffusing mononucleotides and short

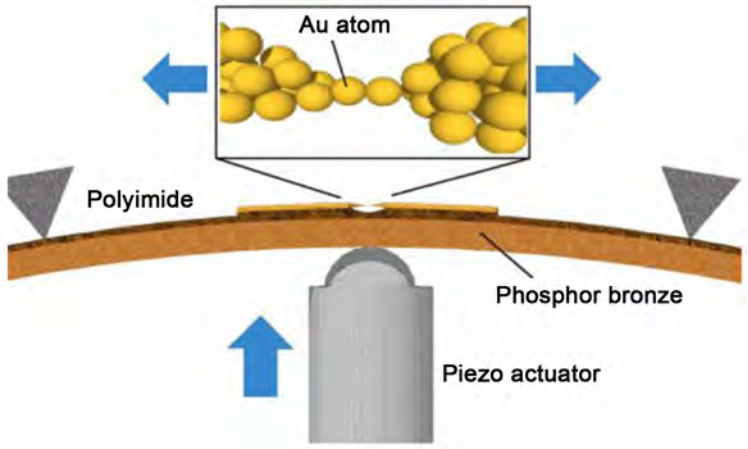

Figure 6. Schematic of a nanofabricated mechanically controllable break junction (MCBJ). Adapted from [91].

DNA oligomers of up to 22 bases by tunneling measurements.

Tunnel current arises in molecular junction created between metallic electrodes and individual nucleobase during passing of the single-nucleobase through nanopore (**Figure 7**). The change in the electric tunnel current (quantum conductance) is determined as a function of the applied bias and the coupled differential conductivity. As the nucleobase have comparatively high electrical resistance metallic electrodes and nucleobase create a nanosized metal-"dielectric"-metal nanostructure ("instant" molecular junction). Value of tunneling current depends on the length of binding single-nucleobase and characterized it. The appropriate translocation rate of the base molecule provides a time-dependent function of interaction change inside of interaction interval of each individual base with junction electrodes. Issues such as unreliable metal–molecule junction formation, variation of nucleotide conformations, insufficient differences between the molecular orbitals HOMO and LUMO (HOMO—high occupied molecular orbital, LUMO—low unoccupied molecular orbital) are responsible for single-nucleotide conduction lead to overlapping nanoelectronic measurements and poor nucleotide discrimination, especially at low coverage on single molecules. The transient characteristics of the individual bases (*i.e.* amplitude of the current through junction) can be used for identification of the bases.

Using nano-MCBJ the conductance-time profiles DNA/RNA oligomers are investigated in [111]. Based on the differences in the conductance-time profiles, authors sequentially identified the base-type in the oligonucleotide just passing through the sensing electrode, resulting in the determination of partial sequence. It is proposed a tunneling current based identification as a single-molecule DNA/RNA sequencing. In [91] a single molecule technology that measures the tunneling currents conducted through single base molecules of DNA and RNA passing between two nanoelectrodes of the nano-MCBJ is developed. Nanopores with diameter ~2 nm are formed on a Si substrate covered with a thin Si_3N_4 film.

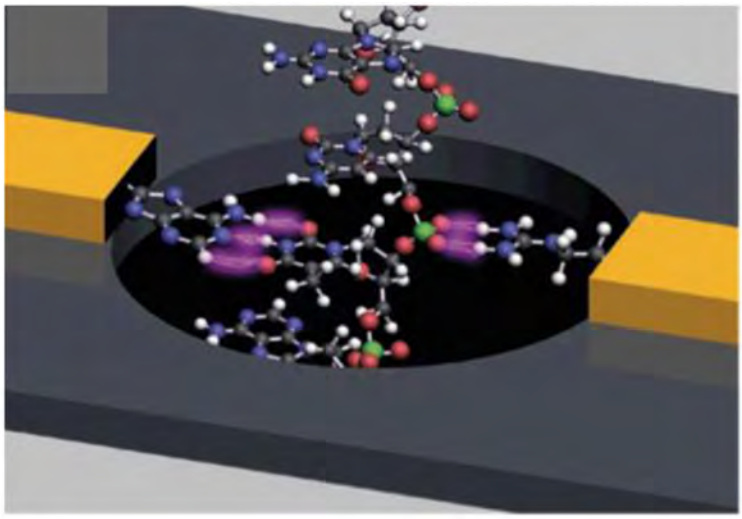

Figure 7. Transverse nanopore electrodes for tunneling current measurements of the DNA backbone with a nanopore. Picture adapted from [100].

To reduce electrical noise, electrodes are covered with a thin SiO_2 film. This nanostructure detects molecules passing through the nanopore with the changes in the electric current flowing between the nanogap electrodes, not with the changes in the ionic current flowing parallel to the nanopore. This current between the nanoelectrodes is sourced from a tunneling current conducted via molecules passing through the membrane. Four bases of DNA are distinguishable by their different electrical resistances.

Note that understanding the adsorption properties of DNA bases on electrode (metal) surfaces is fundamental for the rational control of surface functionalization leading to the realization of biocompatible devices for biosensing applications. Investigations of molecule-metal surface interactions that govern the structural and electronic properties of the molecular nanostructures formed upon adsorption are relevant, not only to control surface functionalization for biosensor applications [112] [113] [114] [115], but also to understand the complex biomolecule-surface interactions in general [112] [116].

Tunnel current extremely sensitive to thermal fluctuation in aqueous solution composition and molecule sizes.

Benefits of tunneling readout are:

- direct reads of epigenetic marking, which can be carried out by direct measurement of the pulses of tunnel currents;
- no consumables—purely physical reads;
- simple control of the speed of the molecule, which can be done by selecting the potential of the reference electrode (gate), taking into account the other forces that determine the movement of the molecule in the electrolyte (gravity and drag force).

3.3. Capacitance Variation Method

A new design of the sensor forms a flat-plate capacitor with the locally sus-

pended monolayer MoS2 nanoribbon that functionalized by cytosine molecules, which are complementary to guanine was proposed in [39]. In such a setup the subject to measurement is the modification of capacitance caused by the temporary deflection of the nanoribbon.

The change in capacitance in response to deviations of the tape and the resulting electrical signal is measured using existing integrated circuits without using microscopy techniques. An aqueous functionalized nano-containing MoS_2 suspended on a solid electrode as a capacitive displacement sensor is designed to determine the DNA sequence proposed in [39]. The observed sequencing events arise from the combination of the basic Watson-Crick pairing, one of the most basic mechanisms of binding to the key and the key of nature, with the ability of atomically thin membranes of the appropriate size to flex essentially in response to subnanoatomic forces.

DNA sequencing can be done also by the capacitance variation method using ion-sensitive field-effect transistors (ISFET), electrolyte-insulator-semiconductor (EIS) based bio-chemical sensors [117]-[122], and light-addressable potentiometric sensors (LAPS) [123] (**Figure 8**). In the case of ISFET the threshold voltage changes vs. pH concentration in bio-liquid or drain current changes vs. gate voltage, for the case EIS the capacitance changes vs. bias voltage, and for the case of LAPS the photocurrent changes vs. bias voltage.

The **ISFET** (**Figure 8(a)**) is one of the most popular electrical biosensors. Much attention has been paid to silicon-based biosensors in the field of bio-analytical applications due to their favorable characteristics, which include sensitivity, greater SNR, speed, miniaturization, and low cost. The ISFET, conventionally referred to as a pH sensor, has been used to measure H^+ or OH^- ions concentration in an aqueous solution, causing an interface potential on the gate insulator (SiO_2 layer in **Figure 8**). Many different biosensors have been developed based on pH sensors since various biomolecular interactions produce protons. The operating principle of the ISFET is simple. Specific molecules are selectively taken into a probe layer on the FET channel, which detects the molecular

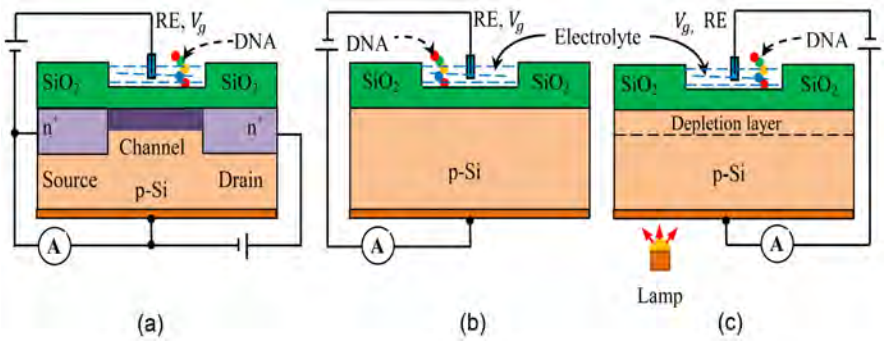

Figure 8. Schematic illustration of the nanosized bio-chemical sensor structures: (a) ISFET—ion sensitive field effect transistor; (b) EIS—electrolyte-insulator-semiconductor; (c) LAPS—light addressable potentiometric sensor. RE—reference electrode; V_g is the gate voltage.

charge in the probe layer. This charge accumulation shifts the flat band voltage of the field-effect transistor. Effect conditioned with channel conductivity modulation. In the case of DNA detection, the probe is ssDNA with a known sequence, immobilized on the substrate. Since the DNA backbone has intrinsic negative charge, the change in surface charge conditions lead to a change in the FET channel conductance, which can be measured using electrochemical cell consisting of a FET gate as the working electrode together with a reference electrode immersed into a solution. In the case of an ISFET biosensor, the amount of the current flow will be determined by the charges of biomolecules interacting on the gate dielectric. An attractive feature of such FETs is that it is possible to detect biomolecular interactions in a label-free manner through a direct change in conductance or a related electrical property.

A related approach utilizes the changes in the conductance of the semiconductor material, which is attached to the nanopore, when DNA molecules translocate through the channel. This method based on the ISFET biosensors made on nanotubes, nanowires and nanoribons [104] [124]. Those sensors have not long life time because non stability and non-reliability of thin insulator layer (usually SiO_2, Si_3N_4 or Ta_2O_5) covered semiconductor material (usually silicon) in aqueous solution. Biological or chemical molecules, adsorbed on the surface of the current channel, create a strong chemical bonding.

The **EIS** capacitor (**Figure 8(b)**) is one of these modified designs and has been broadly applied for bio-sensing. The EIS structure is identical to that of a metal-oxide-semiconductor (MOS) capacitor but the gate electrode is replaced by an electrolyte medium and a reference electrode. The insulator, commonly an oxide, is thus directly exposed to the electrolyte so changes in the aqueous solution can affect the oxide surface potential and modulate the response of the device.

Estrela *et al.* employed MOS capacitors consisting of $Au/SiO_2/Si$ and poly-Si thin film transistors with a gold metal gate as ISFET biosensor for label-free electrical detection of DNA hybridization [125]. When probe DNA bind to its complementary DNA, changes in electric potential in the electric double layer occur, leading to a shift in the C-V (capacitance-voltage) or I-V (current-voltage) characteristics.

When the target ssDNA is supplied, hybridization occurs if the target DNA is complementary to the probe DNA. With or without specific hybridization can be detected by the difference in charge since a nucleotide has a negative charge on the phosphate group.

In the [122] summarizes the FET-based DNA sensors strategies.

The **LAPS** (**Figure 8(c)**) is a kind of the ISFET, which has an EIS structure. By illuminating parts of the sensor surface with infrared light, a photocurrent flow of which the amplitude depends on the local surface potential or local pH value. In this way, the surface potential distribution can be obtained by scanning the light pointer across the surface of LAPS.

3.4. Electric Potential Change

The detection of electric potential change based on an ISFET [126] has shown excellent sensitivity for ion concentration [127], penicillin [128], glucose [129], urease [130], neuronal activity [131], extracellular recording [132], and specific DNA sequence including single nucleotide polymorphisms [1] [87] [133], and so on.

Basic mechanisms of potential generation for electrochemical sensors are [134]:

- pH or ion-concentration change,
- enzymatic reactions,
- affinity binding of molecules (antigen-antibody affinity reaction, or DNA hybridization),
- potential changes that are coming from living biological systems as a result of more sophisticated biochemical processes (action potential of nerve cells, dipole potentials, etc.).

Detail review of advances and developments in the bio-analytical use of ISFET-based biosensors presented in [118] [135]. An electrochemical sensor for detection of unlabeled ssDNA using peptide nucleic acid (PNA) probes coupled to the FET gate is demonstrated in [136]. An application of ISFET technology for the detection of single nucleotide polymorphisms suggested in [137]. In this study authors developed a useful procedure for sequencing one base via the detection of single-base mismatch in DNA. When DNA strands bind to the gate surface of ISFETs, changes in surface potential of semiconductor occur due to the negative charge of DNA, thereby allowing excellent performance of in DNA sensing. Therefore, the capacitance of the system electrolyte-insulator-semiconductor depletion layer will be changed. Then conductivity of the semiconductor depletion layer will be modulated, and source-drain signal current will be changed. For identification and quantification of individual analytes antibodies are the most commonly used capture agents. Note that for biomolecular recognition in ISFET based sensors it is necessary that biological sensing should take place within the Debye screening length λ_D. In electrolytes, the Debye length is a measure of a charge carrier's net electrostatic effect in a solution and how far its electrostatic effect persists. In an electrolyte or a colloidal suspension, the Debye length for a monovalent electrolyte is [138]

$$\lambda_D = \sqrt{\frac{\varepsilon_0 \varepsilon_r k_B T}{2 \times 10^3 e^2 N_A J}}.$$

Here ε_0 is the permittivity of free space, ε_r is the dielectric constant, k_B is the Boltzmann constant, T is the absolute temperature, e is the electron charge, N_A is the Avogadro number, J is the ionic strength of the electrolyte in molar units.

The binding of a charged biomolecule result depletion or accumulation of carriers in semiconductor surface layer and cause change of electric charges on

the gate electrode. In FET biosensors the electric field generating from the binding of a charged biomolecule to the gate is analogous to applying a voltage to a gate. Source-drain current of ISFET can be presented as follows:

$$I_{ds} \propto \mu C \frac{W}{L} V_{GS}^2,$$

where μ is the charge carrier's mobility in the current channel, W and L sizes of the current channel, V_{GS} is the gate voltage, and

$$C = \frac{\varepsilon_0 \varepsilon_i}{t_i}$$

is the gate capacitance per unit area, t_i is the thickness of the insulator layer; ε_i is the dielectric constant of insulator, respectively.

Note that the sequencing mechanisms of sensors based on ISFETs can be used only for detecting nucleic acid using pH sensitivity and amplifying the useful signal in real time.

ISFET biosensors have the following applications: DNA-based ISFETs, ISFETs for electro-immunological sensing, enzyme based-ISFETs, ISFETs for monitoring living cell responses.

4. Some Notes (Criticism) and Conclusion

The challenges for next generation DNA sequencing are to have robust, stable and reproducible nanosized sensor-devices. One major challenge of nanopore-based DNA sequencing technologies is to find an efficient way to reduce DNA translocation speed so that each nucleotide can reside long enough in the pore for reading and forming "long"-time and accurate recognition. The existing methods of DNA sequencing are still not well optimized from the point of view of cost and DNA translocation speed. Detailed analyses show that the main problems of electrical detection methods for nanopore-based DNA sequencing are:

- high translocation speed of molecules through the pore (in bases/s: 1000 [139], 9600 [140], 55,000 [135] [141], 70,000,000 [39]);
- low level of desired electrical signal (of the order of pA for ionic blockade currents [87] [97]-[104] and of the order of nA for tunnel currents [19] [65] [87] [142] [143]);
- low value of the signal-to-noise ratio (for biological and graphene nanopores <10 [40]).
- etc.

In the other hand to achieve high-quality sequencing performance, solid-state nanopores should have the following characteristics:

- the size of the nanopores should be comparable to the DNA molecule diameter (~1 nm for ssDNA and ~2 nm for dsDNA);
- the effective length/thickness of the nanopore should be no more than the distance between two adjacent bases (~0.5 nm for ssDNA) to realize sin-

gle-base sequencing precision.

Note that all of the biological and synthetic nanopores have barrels of ~5 nm (which is considerably longer than the base-to-base distance of 3.4 Å) in thickness and accommodate ~10 - 15 nucleotides at a time. It is, therefore, impossible to achieve single-base resolution using blockage current measurements. In addition, the average rate at which a polymer typically translocates through a nanopore is on the order of 1 nucleotide/μs (*i.e.*, on the order of MHz detection), which is too fast to resolve. The time distribution of two processes (capture, entry, and translocation) is non-Poisson and often differs by an order of magnitude. This means that two molecules pass through a nanopore at considerably different rates and the slower one could be missed or misinterpreted.

Analysis conducted above revealed the following.

1) Case of Ionic Current Blockade

It is well known that ionic current I is carried out by mass transfer

$$m = kIt_0,$$

where k is the electrochemical equivalent, t_0 is the current passing time (see **Figure 2**). By connecting electrons from the cathode, the protons in aqueous solution are converted into hydrogen atoms, which are converted into a hydrogen molecule. The latter must be removed from the electrolyte near the cathode. The movement of hydrogen molecules will create some fluctuation around the cathode in the aqueous solution. As a result, the solution homogeneity will be disturbed, which will lead to increased current noise and decreased signal-to-noise ratio. Other ions which are in solution can come closer the corresponding electrodes take or give away electrons and turn into neutral atoms. Some of these atoms can be deposited on the electrodes, some at the bottom of the chamber. The process of atoms deposition on the electrodes is the random process and will repeat many times when pore is empty. Such process will inevitably lead to a reduction in pore size. Then pore will be closed for the following DNA molecules. To restore the sensor, it will be necessary to open a new pore. This means that the re-productivity of the DNA sensing and reading process will be very low. On the other hand, the ionic current has a very low value (of the order of picoamperes), and therefore it will be very sensitive to any fluctuations (solution homogeneity, pore diameter, etc.). So, the noise level will be high, and the SNR value will be low.

2) Case of Tunnel Current

Note following. In the case of the single layer graphene nanopore sequencing effective thickness (the covalent diameter of carbon) is equal to 0.15 nm [144] and for the effective sequencing will be used at least 3 - 5 layered graphene nanoribbon. Let us turn more detail to the case shown in **Figure 4** (adapted from [49]), which is very common in the literature (see also [52]). There presented usage of graphene nanoribbons for transverse current modulation by DNA in two-terminal devices. In [49] we read: "*Unlike other recent biosensors based on transverse electronic transport through translocated DNA, which utilize small*

(*of the order of pA*) *tunneling current across a nanogap or a nanopore yielding a poor signal-to-noise ratio, our device concept relies on the fact that in ZGNRs* (*zigzag nanoribbon*) *local current density is peaked around the edges so that drilling a nanopore away from the edges will not diminish the conductance. Inserting a nucleobase into the nanopore affects the charge density in the surrounding area, thereby modulating edge conduction currents* …". In [52] we read: "*The nucleobases were inserted into a pore in a graphene nanoribbon, and the electrical current and conductance spectra were calculated as function of voltage applied across the nanoribbon.*"

In this regard, it is necessary to note the following.

The total current between the electrodes is equal to the sum of the conduction current of the continuous layer near the pores and the tunneling current through nucleobase (compare **Figure 4** and **Figure 9**). It is known that the conductivity of graphene in continuous regions is much greater than the conductivity of the nucleobases of the DNA molecule in the pore. Note that at room temperature, graphene has slightly better conductivity than silver. Electron and hole mobilities of up to 200,000 $cm^2/V{\cdot}s$ and high maximum current densities of ~2 mA/μm in width, or 6×10^9 A/cm^2 have been measured in graphene [145]. On the other hand, the conductivity of organic molecules (including nucleobases) is much smaller (electrical resistances are usually on the order of Mom) and they are closer to dielectrics than conductors. With such parameters, the conduction current through a continuous layer of graphene will be much greater than the tunneling current. This means that the measured current, both in the absence and in the presence of DNA in the pore, will be exactly the conduction current and its fluctuation will be very insignificant.

At the transverse nanopore electrodes presented in **Figure 7** the capture cross section area of the electrodes for the DNA molecule is very small and the conductive bridge can be created only with the appropriate orientation of the molecule. The probability of the molecule capture will be low.

Note also that comparing with the ionic blockade current level of the tunnel

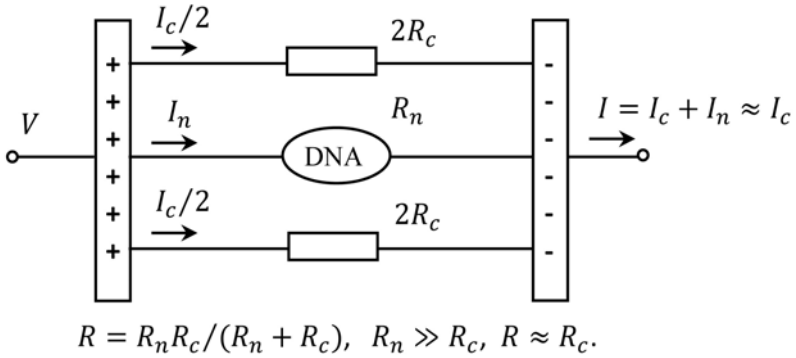

Figure 9. Equivalent scheme of two-terminal device for transverse current modulation made on graphene nanoribbons (see Ref. [49]). R_n and R_c are resistances of nucleobase and continuous region of graphene, I_c, I_n are currents through continuous region and nucleobase, I is the total current.

current is higher and it is not more sensitive to any fluctuations (for example solution homogeneity).

3) Case of the change in capacitance

For the case of a design of the sensor forms a flat-plate capacitor with the locally suspended monolayer MoS2 nanoribbon proposed in [39] where the subject to measurement is the modification of capacitance caused by the temporary deflection of the nanoribbon note following. The change in capacitance in response to deviations of the tape and the measured resulting electrical signal must be very low and therefore they will be hard measurable and very sensitive to any fluctuations. Note that average deflection was ~(0.1 - 0.2) Å or (0.01 - 0.02) nm (**Figure 2** [39]).

4) Case ISFET and EIS sensors

Sequencing mechanisms of sensors based on ISFETs can actually be used only for detecting nucleic acid using pH sensitivity and amplifying the useful signal in real time. For the ISFET and capacitive EIS biosensors we can note:

- non-stability and non-reliability of work because of thin insulator layer (6 - 8 nm),
- random character of the capture of molecules on the sensing layer,
- etc.

To realize more correct, precise and more measurable (comparatively high currents), low noisy DNA sequencing it is necessary to use new, more optimal architecture of nanopore and as an information signal use tunnel current through metal-nucleotide-metal junctions. One variant of the optimal architecture developed by us presented in [146].

Conflicts of Interest

The authors declare no conflicts of interest regarding the publication of this paper.

References

[1] Watson, J.D. and. Crick F.H.C. (1953) Molecular Structure of Nucleic Acids: A Structure for Deoxyribose Nucleic Acid. *Nature*, **171**, 737-738. https://doi.org/10.1038/171737a0

[2] Service, R.F. (2006) The Race for the $1000 Genome. *Science*, **311**, 1544-1546. https://doi.org/10.1126/science.311.5767.1544

[3] Fanget, A. (2013) Towards Tunneling Electrodes for Nanopore-Based DNA Sequencing. Thèse No 5700. Ecole Polytechnique Fèdèrale de Lausanne, Suisse.

[4] Raza, S. and Ameen, A. (2017) Nano Pore Sequencing Technology: A Review. *International Journal of Advances in Scientific Research*, **3**, 90-95. https://doi.org/10.7439/ijasr.v3i8.4333

[5] Pillai, S., Gopalan, V. and Lam, A.K.-Y. (2017) Review of Sequencing Platforms and Their Applications in Phaeochromocytoma and Paragangliomas. *Critical Reviews in Oncology/Hematology*, **116**, 58-67.

[6] Ansorge, W.J. (2016) Next Generation DNA Sequencing (II): Techniques, Applica-

tions. *Journal of Next Generation Sequencing and Applications*, No. S1, 5.

[7] Sanger, F. and Coulson, A.R. (1975) A Rapid Method for Determining Sequences in DNA by Primed Synthesis with DNA Polymerase. *Journal of Molecular Biology*, **94**, 441-446. https://doi.org/10.1016/0022-2836(75)90213-2

[8] Sanger, F., Nicklen, S. and Coulson, A.R. (1977) DNA Sequencing with Chain-Terminating Inhibitors. *Proceedings of the National Academy of Sciences of the United States of America*, **74**, 5463-5467. https://doi.org/10.1073/pnas.74.12.5463

[9] Maxam, A.M. and Gilbert, W. (1977) A New Method for Sequencing DNA. *Proceedings of the National Academy of Sciences of the United States of America*, **74**, 560-564. https://doi.org/10.1073/pnas.74.2.560

[10] Anderson, S. (1981) Article Navigation Shotgun DNA Sequencing Using Cloned DNase I-Generated Fragments. *Nucleic Acids Research*, **9**, 3015-3027. https://doi.org/10.1093/nar/9.13.3015

[11] Canard, B. and Sarfati, R.S. (1994) DNA Polymerase Fluorescent Substrates with Reversible 3'-Tags. *Gene*, **148**, 1-6. https://doi.org/10.1016/0378-1119(94)90226-7

[12] Nyren, P., Petersson, B. and Uhlen, M. (1993) Solid Phase DNA Minisequencing by an Enzymatic Luminometric Inorganic Pyrophosphate Detection Assay. *Analytical Biochemistry*, **208**, 171-175.

[13] Hultman, S., Stahl, S., Homes, E. and Uhlén, M. (1989) Direct Solid Phase Sequencing of Genomic and Plasmid DNA Using Magnetic Beads as Solid Support. *Nucleic Acids Research*, **17**, 4937-4946. https://doi.org/10.1093/nar/17.13.4937

[14] Loman, N.J., Quick, J. and Simpson, J.T. (2015) A Complete Bacterial Genome Assembled *de Novo* Using Only Nanopore Sequencing Data. *Nature Methods*, **12**, 733-735. https://doi.org/10.1038/nmeth.3444

[15] Lin, X., Ivanov, A.P. and Edel, J.B. (2017) Selective Single Molecule Nanopore Sensing of Proteins Using DNA Aptamer-Functionalised Gold Nanoparticles. *Chem. Sci.*, **8**, 3905-3912. https://doi.org/10.1039/C7SC00415J

[16] Wloka, C., Van Meervelt, V., Van Gelder, D., Danda, N., Jager, N., Williams, C.P. and Maglia, G. (2017) Label-Free and Real-Time Detection of Protein Ubiquitination with a Biological Nanopore. *ACS Nano*, **11**, 4387-4394. https://doi.org/10.1021/acsnano.6b07760

[17] Kennedy, E., Dong, Z., Tennant, C. and Timp, G. (2016) Reading the Primary Structure of a Protein with 0.07 nm^3 Resolution Using a Subnanometre-Diameter Pore. *Nature Nanotechnology*, **11**, 968-976. https://doi.org/10.1038/nnano.2016.120

[18] Plesa, C., Ruitenberg, J.W., Witteveen, M.J. and Dekker, C. (2015) Detection of Individual Proteins Bound along DNA Using Solid-State Nanopores. *Nano Letters*, **15**, 3153-3158. https://doi.org/10.1021/acs.nanolett.5b00249

[19] Clarke, J., Wu, H.-C., Jayasinghe, L., Patel, A., Reid, S. and Bayley, H. (2009) Continuous Base Identification for Single-Molecule Nanopore DNA Sequencing. *Nature Nanotechnology*, **4**, 265-270. https://doi.org/10.1038/nnano.2009.12

[20] Farimani, A.B., Heiranian, M., Min, K. and Aluru, N.R. (2017) Antibody Subclass Detection Using Graphene Nanopores. *The Journal of Physical Chemistry Letters*, **8**, 1670-1676. https://doi.org/10.1021/acs.jpclett.7b00385

[21] Wang, S., Haque, F., Rychahou, P.G., Evers, B.M. and Guo, P. (2013) Engineered Nanopore of Phi29 DNA-Packaging Motor for Real-Time Detection of Single Colon Cancer Specific Antibody in Serum. *ACS Nano*, **7**, 9814-9822.

https://doi.org/10.1021/nn404435v

[22] Shi, J., Hou, J. and Fang, Y. (2016) Recent Advances in Nanopore-Based Nucleic Acid Analysis and Sequencing. *Microchimica Acta*, **183**, 925-939. https://doi.org/10.1007/s00604-015-1503-y

[23] Ying, Y.-L., Zhang, J., Gao, R. and Long, Y.-T. (2013) Nanopore-Based Sequencing and Detection of Nucleic Acids. *Angewandte Chemie International Edition*, **52**, 13154-13161. https://doi.org/10.1002/anie.201303529

[24] Rincon-Restrepo, M., Mikhailova, E., Bayley, H. and Maglia, G. (2011) Controlled Translocation of Individual DNA Molecules through Protein Nanopores with Engineered Molecular Brakes. *Nano Letters*, **11**, 746-750. https://doi.org/10.1021/nl1038874

[25] Howorka, S., Cheley, S. and Bayley, H. (2001) Sequence-Specific Detection of Individual DNA Strands Using Engineered Nanopores. *Nature Biotechnology*, **19**, 636-639. https://doi.org/10.1038/90236

[26] Zahid, O.K., Wang, F., Ruzicka, J.A., Taylor, E.W. and Hall, A.R. (2016) Sequence-Specific Recognition of MicroRNAs and Other Short Nucleic Acids with Solid-State Nanopores. *Nano Letters*, **16**, 2033-2039. https://doi.org/10.1021/acs.nanolett.6b00001

[27] Clamer, M., Höfler, L., Mikhailova, E., Viero, G. and Bayley, H. (2014) Detection of 3'-End RNA Uridylation with a Protein Nanopore. *ACS Nano*, **8**, 1364-1374. https://doi.org/10.1021/nn4050479

[28] Bulushev, R.D., Marion, S. and Radenovic, A. (2015) Relevance of the Drag Force during Controlled Translocation of a DNA-Protein Complex through a Glass Nanocapillary. *Nano Letters*, **15**, 7118-7125. https://doi.org/10.1021/acs.nanolett.5b03264

[29] He, H., Xu, X., Wang, P., Chen, L. and Jin, Y. (2015) The Facile Surface Chemical Modification of a Single Glass Nanopore and Its Use in the Nonenzymatic Detection of Uric Acid. *Chemical Communications*, **51**, 1914-1917. https://doi.org/10.1039/C4CC09185J

[30] Yin, B., Xie, W., Liang, L., Deng, Y., He, S., He, F., Zhou, D., Tlili, C. and Wang, D. (2017) Covalent Modification of Silicon Nitride Nanopore by Amphoteric Polylysine for Short DNA Detection. *ACS Omega*, **2**, 7127-7135. https://doi.org/10.1021/acsomega.7b01245

[31] Shekar, S., Niedzwiecki, D.J., Chien, C.C., Ong, P., Fleischer, D.A., Lin, J., Rosenstein, J.K., Drndic, M. and Shepard, K.L. (2016) Measurement of DNA Translocation Dynamics in a Solid-State Nanopore at 100 ns Temporal Resolution. *Nano Letters*, **16**, 4483-4489. https://doi.org/10.1021/acs.nanolett.6b01661

[32] Liang, Z., Tang, Z., Li, J., Hu, R., Yu, D. and Zhao, Q. (2015) Interaction Prolonged DNA Translocation through Solid-State Nanopores. *Nanoscale*, **7**, 10752-10759. https://doi.org/10.1039/C5NR01954K

[33] Montagne, F., Blondiaux, N., Bojko, A. and Pugin, R. (2012) Molecular Transport through Nanoporous Silicon Nitride Membranes Produced from Self-Assembling Block Copolymers. *Nanoscale*, **4**, 5880-5886. https://doi.org/10.1039/c2nr31498c

[34] Venkatesan, B.M., Shah, A.B., Zuo, J.-M. and Bashir, R. (2010) DNA Sensing Using Nanocrystalline Surface-Enhanced Al_2O_3 Nanopore Sensors. *Advanced Functional Materials*, **20**, 1266-1275. https://doi.org/10.1002/adfm.200902128

[35] Zwolak, M. and Di Ventra, M. (2005) Electronic Signature of DNA Nucleotides via Transverse Transport. *Nano Letters*, **5**, 421-424.

https://doi.org/10.1021/nl048289w

[36] Yin, K., Huang, S., Chen, X., Wang, X., Kong, J., Chen, Y. and Xue, J. (2018) Generating Sub-Nanometer Pores in Single-Layer MoS_2 by Heavy-Ion Bombardment for Gas Separation: A Theoretical Perspective. *ACS Applied Materials & Interfaces*, **10**, 28909-28917. https://doi.org/10.1021/acsami.8b10569

[37] Luan, B. and Zhou, R. (2018) Single-File Protein Translocations through Graphene—MoS_2 Heterostructure Nanopores. *The Journal of Physical Chemistry Letters*, **9**, 3409-3415. https://doi.org/10.1021/acs.jpclett.8b01340

[38] Luan, B. and Zhou, R. (2018) Spontaneous Transport of Single-Stranded DNA through Graphene—MoS_2 Heterostructure Nanopores. *ACS Nano*, **12**, 3886-3891. https://doi.org/10.1021/acsnano.8b01297

[39] Smolyanitsky, A., Yakobson, B.I., Wassenaar, T.A., Paulechka, E. and Kroenlein, K. (2016) A MoS_2-Based Capacitive Displacement Sensor for DNA Sequencing. *ACS Nano*, **10**, 9009-9016. https://doi.org/10.1021/acsnano.6b05274

[40] Farimani, A.B., Min, K. and Aluru, N.R. (2014) DNA Base Detection Using a Single-Layer MoS_2. *ACS Nano*, **8**, 7914-7922. https://doi.org/10.1021/nn5029295

[41] De Souza, F.A.L., Amorim, R.G., Scopel, W.L. and Scheicher, R.H. (2017) Electrical Detection of Nucleotides via Nanopores in a Hybrid Graphene/h-BN Sheet. *Nanoscale*, **9**, 2207-2212. https://doi.org/10.1039/C6NR07154F

[42] Gu, Z., Zhang, Y., Luan, B. and Zhou, R. (2016) DNA Translocation through Single-Layer Boron Nitride Nanopores. *Soft Matter*, **12**, 817-823. https://doi.org/10.1039/C5SM02197A

[43] Zhang, L. and Wang, X. (2016) DNA Sequencing by Hexagonal Boron Nitride Nanopore: A Computational Study. *Nanomaterials*, **6**, 111-121. https://doi.org/10.3390/nano6060111

[44] Shukla, V., Jena, N.K., Grigoriev, A. and Ahuja, R. (2017) Prospects of Graphene–hBN Heterostructure Nanogap for DNA Sequencing. *ACS Applied Materials & Interfaces*, **9**, 39945-39952. https://doi.org/10.1021/acsami.7b06827

[45] Amorim, R.G., Rocha, A.R. and Scheicher, R.H. (2016) Boosting DNA Recognition Sensitivity of Graphene Nanogaps through Nitrogen Edge Functionalization. *Journal of Physical Chemistry C*, **120**, 19384-19388. https://doi.org/10.1021/acs.jpcc.6b04683

[46] Prasongkit, J., Grigoriev, A., Pathak, B., Ahuja, R. and Scheicher, R.H. (2013) Theoretical Study of Electronic Transport through DNA Nucleotides in a Double-Functionalized Graphene Nanogap. *Journal of Physical Chemistry C*, **117**, 15421-15428. https://doi.org/10.1021/jp4048743

[47] Takeuchi, K. and Zolotoukhina, T. (2013) Individual DNA Base Identification at the Transport through Graphene Nanopore. *ASME* 11*th International Conference on Nanochannels, Microchannels, and Minichannels*, Sapporo, Japan, 16-19 June 2013, V001T10A003.

[48] Traversi, F., Raillon, C., Benameur, S.M., *et al*. (2013) Detecting the Translocation of DNA through a Nanopore Using Graphene Nanoribbons. *Nature Nanotechnology*, **8**, 939-945. https://doi.org/10.1038/nnano.2013.240

[49] Saha, K.K., Drndić, M. and Nikolić, B.K. (2012) DNA Base-Specific Modulation of Microampere Transverse Edge Currents through a Metallic Graphene Nanoribbon with a Nanopore. *Nano Letters*, **12**, 50-55. https://doi.org/10.1021/nl202870y

[50] Merchant, C.A., Healy, K., Wanunu, M., Ray, V., Peterman, N., Bartel, J., Fischbein, M.D., Venta, K., Luo, Z., Johnson, A.T.C. and Drndić, M. (2010) DNA Transloca-

tion through Graphene Nanopores. *Nano Letters*, **10**, 2915-2921. https://doi.org/10.1021/nl101046t

[51] Schneider, G.F., Kowalczyk, S.W., Calado, V.E., Pandraud, G., Zandbergen, H.W., Vandersypen, L.M.K. and Dekker, C. (2010) DNA Translocation through Graphene Nanopores. *Nano Letters*, **10**, 3163-3167. https://doi.org/10.1021/nl102069z

[52] Nelson, T., Zhang, B. and Prezhdo, O.V. (2010) Detection of Nucleic Acids with Graphene Nanopores: *Ab Initio* Characterization of a Novel Sequencing Device. *Nano Letters*, **10**, 3237-3242. https://doi.org/10.1021/nl9035934

[53] Yang, N. and Jiang, X. (2017) Nanocarbons for DNA Sequencing: A Review. *Carbon*, **115**, 293-311. https://doi.org/10.1016/j.carbon.2017.01.012

[54] Liu, L., Xie, J., Li, T. and Wu, H.-C. (2015) Fabrication of Nanopores with Ultrashort Single-Walled Carbon Nanotubes Inserted in a Lipid Bilayer. *Nature Protocols*, **10**, 1670-1678. https://doi.org/10.1038/nprot.2015.112

[55] Zhang, S., Wang, X., Li, T., Liu, L., Wu, H.C., Luo, M. and Li, J. (2015) Sensitive Detection of a Modified Base in Single-Stranded DNA by a Single-Walled Carbon Nanotube. *Langmuir*, **31**, 10094-10099. https://doi.org/10.1021/acs.langmuir.5b01272

[56] Kim, H.S., Lee, S.J. and Kim, Y.-H. (2014) Distinct Mechanisms of DNA Sensing Based on N‐Doped Carbon Nanotubes with Enhanced Conductance and Chemical Selectivity. *Small*, **10**, 774-781. https://doi.org/10.1002/smll.201301225

[57] Liu, L., Yang, C., Zhao, K., Li, J. and Wu, H.C. (2013) Ultrashort Single-Walled Carbon Nanotubes in a Lipid Bilayer as a New Nanopore Sensor. *Nature Communications*, **4**, Article No. 2989. https://doi.org/10.1038/ncomms3989

[58] Göpfrich, K., Li, C.-Y., Mames, I., Bhamidimarri, S.P., Ricci, M., Yoo, J., Mames, A., Ohmann, A., Winterhalter, M., Stulz, E., Aksimentiev, A. and Keyser, U.F. (2016) Ion Channels Made from a Single Membrane-Spanning DNA Duplex. *Nano Letters*, **16**, 4665-4669. https://doi.org/10.1021/acs.nanolett.6b02039

[59] Di Ventra, M. and Taniguchi, M. (2016) Decoding DNA, RNA and Peptides with Quantum Tunneling. *Nature Nanotechnology*, **11**, 117-126. https://doi.org/10.1038/nnano.2015.320

[60] Gao, H.L., Wang, M., Wu, Z.Q., Wang, C., Wang, K. and Xia, X.H. (2015) Morpholino-Functionalized Nanochannel Array for Label-Free Single Nucleotide Polymorphisms Detection. *Analytical Chemistry*, **87**, 3936-3941. https://doi.org/10.1021/ac504830e

[61] Agah, S., Zheng, M., Pasquali, M. and Kolomeisky, A.B. (2016) DNA Sequencing by Nanopores: Advances and Challenges. *Journal of Physics D: Applied Physics*, **49**, Article ID: 413001. https://doi.org/10.1088/0022-3727/49/41/413001

[62] Laszlo, A., Derrington, I., Ross, B., Brinkerhoff, H., Adey, A., Nova, I., Craig, J., Langford, K., Samson, J.M., Daza, R., Doering, K., Shendure, J. and Gundlach, J. (2014) Decoding Long Nanopore Sequencing Reads of Natural DNA. *Nature Biotechnology*, **32**, 829-833. https://doi.org/10.1038/nbt.2950

[63] Venkatesan, B.M. and Bashir, R. (2011) Nanopore Sensors for Nucleic Acid Analysis. *Nature Nanotechnology*, **6**, 615-624. https://doi.org/10.1038/nnano.2011.129

[64] Panja, D., Barkema, G.T. and Kolomeisky, A.B. (2013) Through the Eye of the Needle: Recent Advances in Understanding Biopolymer Translocation. *Journal of Physics: Condensed Matter*, **25**, Article ID: 413101. https://doi.org/10.1088/0953-8984/25/41/413101

[65] Meller, A. (2003) Dynamics of Polynucleotide Transport through Nanometre-Scale

Pores. *Journal of Physics*: *Condensed Matter*, **15**, R581-R607.

[66] Liu, Z., Wang, Y., Deng, T. and Chen, Q. (2016) Solid-State Nanopore-Based DNA Sequencing Technology. *Journal of Nanomaterials*, 2**016**, Article ID: 5284786. https://doi.org/10.1155/2016/5284786

[67] Timp, W., Mirsaidov, U.M., Wang, D., Comer, J., Aksimentiev, A. and Timp, G. (2010) Nanopore Sequencing: Electrical Measurements of the Code of Life. *IEEE Transactions on Nanotechnology*, **9**, 281-294. https://doi.org/10.1109/TNANO.2010.2044418

[68] Shi, W., Friedman, A.K. and Baker, L.A. (2017) Nanopore Sensing. *Analytical Chemistry*, **89**, 157-188. https://doi.org/10.1021/acs.analchem.6b04260

[69] Garrido-Cardenas, J., Garcia-Maroto, F., Alvarez-Bermejo, J. and Manzano-Agugliaro, F. (2017) DNA Sequencing Sensors: An Overview. *Sensors*, **17**, 588-602. https://doi.org/10.3390/s17030588

[70] Liu, L. and Wu, H.C. (2016) DNA-Based Nanopore Sensing. *Angewandte Chemie International Edition*, **55**, 15216-15222. https://doi.org/10.1002/anie.201604405

[71] Deamer, D., Akeson, M. and Branton, D. (2016) Three Decades of Nanopore Sequencing. *Nature Biotechnology*, **34**, 518-524. https://doi.org/10.1038/nbt.3423

[72] Goodwin, S., McPherson, J.D. and McCombie, W.R. (2016) Coming of Age: Ten Years of Next-Generation Sequencing Technologies. *Nature Reviews Genetics*, **17**, 333-351. https://doi.org/10.1038/nrg.2016.49

[73] Marx, V. (2015) Nanopores: A Sequencer in Your Backpack. *Nature Methods*, **12**, 1015-1018. https://doi.org/10.1038/nmeth.3625

[74] Shendure, J.A., Porreca, G.J., Church, G.M., Gardner, A.F., Hendrickson, C., Kieleczawa, J. and Slatko, B.E. (2011) Overview of DNA Sequencing Strategies. In: *Current Protocols in Molecular Biology*, Chapter 7, Unit 7.1., 1-23.

[75] Linnarsson, S. (2010) Recent Advances in DNA Sequencing Methods—General Principles of Sample Preparation. *Experimental Cell Research*, **316**, 1339-1343. https://doi.org/10.1016/j.yexcr.2010.02.036

[76] Carson, S. and Wanunu, M. (2015) Challenges in DNA Motion Control and Sequence Readout Using Nanopore Devices. *Nanotechnology*, **26**, Article ID: 074004.

[77] Lee, K., Lee, H., Lee, S.-H., Kim, H.-M., Kim, K.-B. and Kim, S.J. (2017) Enhancing the Sensitivity of DNA Detection by Structurally Modified Solid-State Nanopore. *Nanoscale*, **9**, 18012-18021. https://doi.org/10.1039/C7NR05840C

[78] Gusakova, J., Wang, X., Shiau, L.L., Krivosheeva, A., Shaposhnikov, V., Borisenko, V., Gusakov, V. and Tay, B.K. (2017) Electronic Properties of Bulk and Monolayer TMDs: Theoretical Study within DFT Framework (GVJ-2e Method). *Physica Status Solidi* (*a*), **214**, Article ID: 1700218. https://doi.org/10.1002/pssa.201700218

[79] Kneipp, K., Kneipp, H., Kartha, V.B., Manoharan, R., Deinum, G., Itzkan, I., Dasari, R.R. and Feld, M.S. (1998) Detection and Identification of a Single DNA Base Molecule Using Surface-Enhanced Raman Scattering (SERS). *Physical Review E*, **57**, R6281(R). https://doi.org/10.1103/PhysRevE.57.R6281

[80] Afsari, S., Korshoj, L.E., Abel Jr., G.R., Khan, S., Chatterjee, A. and Nagpal, P. (2017) Quantum Point Contact Single-Nucleotide Conductance for DNA and RNA Sequence Identification. *ACS Nano*, **11**, 11169-11181. https://doi.org/10.1021/acsnano.7b05500

[81] Soni, G.V. and Meller, A. (2007) Progress toward Ultrafast DNA Sequencing Using Solid-State Nanopores. *Clinical Chemistry*, **53**, 1996-2001. https://doi.org/10.1373/clinchem.2007.091231

[82] United States Food and Drug Administration (2016) Nucleic Acid Based Tests. http://www.fda.gov/MedicalDevices/ProductsandMedicalProcedures/InVitroDiagnostics/ucm330711.htm

[83] Chen, K., Juhasz, M., Gularek, F., Weinhold, E., Tian, Y., Keyser, U.F. and Bell, N.A.W. (2017) Ionic Current-Based Mapping of Short Sequence Motifs in Single DNA Molecules Using Solid-State Nanopores. *Nano Lett*ers, **17**, 5199-5205. https://doi.org/10.1021/acs.nanolett.7b01009

[84] Larkin, J., Henley, R., Bell, D.C., Cohen-Karni, T., Rosenstein, J.K. and Wanunu, M. (2013) Slow DNA Transport through Nanopores in Hafnium Oxide Membranes. *ACS Nano*, **7**, 10121-10128. https://doi.org/10.1021/nn404326f

[85] Moretti, M., Di Fabrizio, E., Cabrini, S.R., De Angelis, F. and Firrao, G. (2008) An ON/OFF Biosensor Based on Blockade of Ionic Current Passing through a Solid-State Nanopore. *Biosensors and Bioelectronics*, **24**, 141-147. https://doi.org/10.1016/j.bios.2008.03.047

[86] Shendure, J., Balasubramanian, S., Church, G.M., Gilbert, W., Rogers, J., Schloss, A.J. and Waterston, R.H. (2017) DNA Sequencing at 40: Past, Present and Future. *Nature*, **550**, 345-353. https://www.nature.com/articles/nature24286 https://doi.org/10.1038/nature24286

[87] Butler, T.Z., Gundlach, J.H. and Troll, M. (2007) Ionic Current Blockades from DNA and RNA Molecules in the *α*-Hemolysin Nanopore. *Biophysical Journal*, **93**, 3229-3240. https://doi.org/10.1529/biophysj.107.107003

[88] He, J., Lin, L., Zhang, P. and Lindsay, S. (2007) Identification of DNA Basepairing via Tunnel-Current Decay. *Nano Letters*, **7**, 3854-3858. https://doi.org/10.1021/nl0726205

[89] Zwolak, M. and Di Ventra, M. (2008) *Colloquium*: Physical Approaches to DNA Sequencing and Detection. *Reviews of Modern Physics*, **80**, 141-165. https://doi.org/10.1103/RevModPhys.80.141

[90] Xu, M., Endres, R.G. and Arakawa, Y. (2007) The Electronic Properties of DNA Bases. *Small*, **3**, 1539-1543. https://doi.org/10.1002/smll.200600732

[91] Taniguchi, M. (2014) Single-Molecule Sequencing Technologies of Biomolecules via Electric Currents. 18*th International Conference on Miniaturized Systems for Chemistry and Life Sciences*, San Antonio, TX, 26-30 October 2014, 199-204.

[92] Gracheva, M.E., Xiong, A.L., Aksimentiev, A., Schulten, K., Timp, G. and Leburton, J.-P. (2006) Simulation of the Electric Response of DNA Translocation through a Semiconductor Nanopore-Capacitor. *Nanotechnology*, **17**, 622-633. https://doi.org/10.1088/0957-4484/17/3/002

[93] Gracheva, M.E., Aksimentiev, A. and Leburton, J.-P. (2006) Electrical Signatures of Single-Stranded DNA with Single Base Mutations in a Nanopore Capacitor. *Nanotechnology*, **17**, 3160-3165. https://doi.org/10.1088/0957-4484/17/13/014

[94] Heng, J.B., Aksimentiev, A., Ho, C., Dimitrov, V., Sorsch, T., Miner, J., Mansfield, W., Schulten K. and Timp, G. (2005) Beyond the Gene Chip. *Bell LabsTechnical Journal*, **10**, 5-22. https://doi.org/10.1002/bltj.20102

[95] Milgrew, M.J. and Cumming, D.R.S. (2008) Matching the Transconductance Characteristics of CMOS ISFET Arrays by Removing Trapped Charge. *IEEE Transactions on Electron Devices*, **55**, 1074-1079. https://doi.org/10.1109/TED.2008.916680

[96] Maruyama, Y., Terao, S. and Sawada, K. (2009) Label Free CMOS DNA Image Sensor Based on the Charge Transfer Technique. *Biosensors and Bioelectronics*, **24**, 3108-3112. https://doi.org/10.1016/j.bios.2009.03.031

[97] Kasianowicz, J.J., Brandin, E., Branton, D. and Deamer, D.W. (1996) Characterization of Individual Polynucleotide Molecules Using a Membrane Channel. *Proceedings of the National Academy of Sciences of the United States of America*, **93**, 13770-13773. https://doi.org/10.1073/pnas.93.24.13770

[98] Dekker, C. (2007) Solid-State Nanopores. *Nature Nanotechnology*, **2**, 209-215. https://doi.org/10.1038/nnano.2007.27

[99] Deamer, D.W. and Branton, D. (2002) Characterization of Nucleic Acids by Nanopore Analysis. *Accounts of Chemical Research*, **35**, 817-825. https://doi.org/10.1021/ar000138m

[100] Branton, D., Deamer, D.W., Marziali, A., Bayley, H., Benner, S.A., Butler, T., Di Ventra, M., Garaj, S., Hibbs, A., Huang, X., Jovanovich, S.B., Krstic, P.S., Lindsay, S., Ling, X.S., Mastrangelo, C.H., Meller, A., Oliver, J.S., Pershin, Y.V., Ramsey, J.M., Riehn, R., Soni, G.V., Tabard-Cossa, V., Wanunu, M., Wiggin, M. and Schloss, J.A. (2008) The Potential and Challenges of Nanopore Sequencing. *Nature Biotechnology*, **26**, 1146-1153. https://doi.org/10.1038/nbt.1495

[101] Bayley, H. (2006) Sequencing Single Molecules of DNA. *Current Opinion in Chemical Biology*, **10**, 628-637. https://doi.org/10.1016/j.cbpa.2006.10.040

[102] Ashkenasy, N., Sanchez-Quesada, J., Bayley, H. and Ghadiri, M.R. (2005) Recognizing a Single Base in an Individual DNA Strand: A Step Toward DNA Sequencing in Nanopores. *Angewandte Chemie International Edition*, **44**, 1401-1404. https://doi.org/10.1002/anie.200462114

[103] Mitchell, N. and Howorka, S. (2008) Chemical Tags Facilitate the Sensing of Individual DNA Strands with Nanopores. *Angewandte Chemie International Edition*, **47**, 5565-5568. https://doi.org/10.1002/anie.200800183

[104] Xie, P., Xiong, Q., Fang, Y., Qing, Q. and Lieber, C.M. (2012) Local Electrical Potential Detection of DNA by Nanowire-Nanopore Sensors. *Nature Nanotechnology*, **7**, 119-125. https://doi.org/10.1038/nnano.2011.217

[105] Stefan, W.K., Alexander, Y.G., Yitzhak, R. and Cees, D. (2011) Modeling the Conductance and DNA Blockade of Solid-State Nanopores. *Nanotechnology*, **22**, Article ID: 315101. https://doi.org/10.1088/0957-4484/22/31/315101

[106] Lagerqvist, J., Zwolak, M., and Di Ventra, M. (2007) Influence of the Environment and Probes on Rapid DNA Sequencing via Transverse Electronic Transport. *Biophysical Journal*, **93**, 2384-2390. https://doi.org/10.1529/biophysj.106.102269

[107] Krstic, P.S., Wells, J.C., Fuentes-Cabrera, M., Xu, D. and Lee, J.W. (2007) Toward Electronic Conductance Characterization of DNA Nucleotide Bases. *Solid State Phenomena*, **121-123**, 1387-1390. https://doi.org/10.4028/www.scientific.net/SSP.121-123.1387

[108] Tsutsui, M., Taniguchi, M., Yokota, K. and Kawai, T. (2010) Identifying Single Nucleotides by Tunnelling Current. *Nature Nanotechnology*, **5**, 286-290. https://doi.org/10.1038/nnano.2010.42

[109] Chang, S., Huang, S., He, J., Liang, F., Zhang, P., Li, S., Chen, X., Sankey, O. and Lindsay, S. (2010) Electronic Signatures of all Four DNA Nucleosides in a Tunneling Gap. *Nano Letters*, **10**, 1070-1075. https://doi.org/10.1021/nl1001185

[110] Huang, S., He, J., Chang, S., Zhang, P., Liang, F., Li, S., Tuchband, M., Fuhrmann, A., Ros, R. and Lindsay, S. (2010) Identifying Single Bases in a DNA Oligomer with Electron Tunneling. *Nature Nanotechnology*, **5**, 868-873. https://doi.org/10.1038/nnano.2010.213

[111] Ohshiro, T., Tsutsui, M., Matsubara, K., Furuhashi, M., Taniguchi, M. and Kawai,

T. (2012) Single-Molecule Tunnel-Current Based Identification of DNA/RNA Towards Sequencing by Using Nano-MCBJ. 16*th International Conference on Miniaturized Systems for Chemistry and Life Sciences*, Okinawa, Japan, 28 October-1 November 2012, 204-206.

[112] Cheng, L. (2016) Role of Hydrogen Bonding in the Formation of Adenine Chains on Cu(110) Surfaces. *Materials*, **9**, 1016-1027. https://doi.org/10.3390/ma9121016

[113] Kestell, J., Boscoboinik, J.A., Cheng, L., Garvey, M., Bennett, D.W. and Tysoe, W.T. (2015) Structural Changes in Self-Catalyzed Adsorption of Carbon Monoxide on 1,4-Phenylene Diisocyanide Modified Au(111). *Journal of Physical Chemistry C*, **119**, 18317-18325. https://doi.org/10.1021/acs.jpcc.5b04783

[114] Nelson, B.P., Grimsrud, T.E., Liles, M.R., Goodman, R.M. and Corn, R.M. (2000) Surface Plasmon Resonance Imaging Measurements of DNA and RNA Hybridization Adsorption onto DNA Microarrays. *Analytical Chemistry*, **73**, 1-7. https://doi.org/10.1021/ac0010431

[115] Xu, W. (2008) Adsorption of Organic Molecules on Solid Surfaces. A Scanning Tunneling Microscopy Study. PhD Thesis, Interdisciplinary Nanoscience Center (iNANO) and Department of Physics and Astronomy University of Aarhus, Denmark.

[116] Sowerby, S.J., Edelwirth, M. and Heckl, W.M. (1998) Self-Assembly at the Prebiotic Solid−Liquid Interface: Structures of Self-Assembled Monolayers of Adenine and Guanine Bases Formed on Inorganic Surfaces. *The Journal of Physical Chemistry B*, **102**, 5914-5922. https://doi.org/10.1021/jp980684l

[117] Schöning, M. and Poghossian, A. (2006) Bio FEDs (Field-Effect Devices): State-of-the-Art and New Directions. *Electroanalysis*, **18**, 1893-1900. https://doi.org/10.1002/elan.200603609

[118] Lee, C.-S., Kim, S.K. and Kim, M. (2009) Ion-Sensitive Field-Effect Transistor for Biological Sensing. *Sensors*, **9**, 7111-7131. https://doi.org/10.3390/s90907111

[119] Pijanowska, D.G. and Torbicz, W. (2005) Biosensors for Bioanalytical Applications. *Bulletin of the Polish Academy of Sciences*: *Technical Sciences*, **53**, 251-260.

[120] Kimura, J., Ito, N., Kuriyama, T., Kikuchi, M., Arai, T., Negishi, N. and Tomita, Y. (1989) *J. Electrochem. Soc.*, **136**, 1744-1747.

[121] Bergveld, P. (1970) Development of an Ion-Sensitive Solid-State Device for Neurophysiological Measurements. *IEEE Transactions on Biomedical Engineering*, **BME-17**, 70-71. https://doi.org/10.1109/TBME.1970.4502688

[122] Veigas, B., Fortunato, E. and Baptista, P.V. (2015) Field Effect Sensors for Nucleic Acid Detection: Recent Advances and Future Perspectives. *Sensors*, **15**, 10380-10398. https://doi.org/10.3390/s150510380

[123] Hafeman, D.G., Parce, J.W. and McConnel, H.M. (1988) Light-Addressable Potentiometric Sensor for Biochemical Systems. *Science*, **240**, 1182-1185. https://doi.org/10.1126/science.3375810

[124] Gasparyan, F., Zadorozhny, I., Khondkaryan, H., Arakelyan, A. and Vitusevich, S. (2018) Photoconductivity, pH Sensitivity, Noise, and Channel Length Effects in Si Nanowire FET Sensors. *Nanoscale Research Letters*, **13**, 87-96. https://doi.org/10.1186/s11671-018-2494-5

[125] Estrela, P., Stewart, A., Yan, F. and Migliorato, P. (2005) Field Effect Detection of Biomolecular Interactions. *Electrochimica Acta*, **50**, 4995-5000. https://doi.org/10.1016/j.electacta.2005.02.075

[126] Khan, M.I., Khan, A.M., Nouman, A., Azhar, M.I. and Saleem, M.K. (2012) pH

Sensing Materials for MEMS Sensors and Detection Techniques. *Int. Conf. on Solid-State and Integrated Circuit* (*ICSIC* 2012) *IPCSIT*, Vol. 32, IACSIT Press, Singapore, 18-23. http://www.ipcsit.com/vol32/004-ICSIC2012-D0022.pdf

[127] Bergveld, P. (2003) Thirty Years of ISFETOLOGY: What Happened in the Past 30 Years and What May Happen in the Next 30 Years. *Sensors and Actuators B*: *Chemical*, **88**, 1-20. https://doi.org/10.1016/S0925-4005(02)00301-5

[128] Caras, S. and Janata, J. (1980) Field Effect Transistor Sensitive to Penicillin. *Analytical Chemistry*, **52**, 1935-1937. https://doi.org/10.1021/ac50062a035

[129] Lee, C.H., Seo, H.I., Lee, Y.C., Cho, B.W., Jeong, H. and Dohn, B.K. (2000) All Solid Type ISFET Glucose Sensor with Fast Response and High Sensitivity Characteristics. *Sensors and Actuators B*: *Chemical*, **64**, 37-41. https://doi.org/10.1016/S0925-4005(99)00480-3

[130] Sekiguchi, T., Nakamura, M., Kato, M., Nishikawa, K., Hokari, K., Sugiyama, T. and Asaka, M. (2000) Immunological *Helicobacter pylori* Urease Analyzer Based on Ion-Sensitive Field Effect Transistor. *Sensors and Actuators B*: *Chemical*, **67**, 265-269. https://doi.org/10.1016/S0925-4005(00)00522-0

[131] Offenhäusser, A., Sprössler, C., Matsuzawa, M. and Knoll, W. (1997) Field-Effect Transistor Array for Monitoring Electrical Activity from Mammalian Neurons in Culture. *Biosensors and Bioelectronics*, **12**, 819-826. https://doi.org/10.1016/S0956-5663(97)00047-X

[132] Meyburg, S., Goryll, M., Moers, J., Ingebrandt, S., Böcker-Meffert, S., Lüth, H. and Offenhäusser, A. (2006) N-Channel Field-Effect Transistors with Floating Gates for Extracellular Recordings. *Biosensors and Bioelectronics*, **21**, 1037-1044. https://doi.org/10.1016/j.bios.2005.03.010

[133] Chang, J.C. and Kan, Y.W. (1979) Beta 0 Thalassemia, a Nonsense Mutation in Man. *Proceedings of the National Academy of Sciences of the USA*, **76**, 2886-2889. https://doi.org/10.1073/pnas.76.6.2886

[134] Schöning, M.J. and Poghossian, A. (2002) Recent Advances in Biologically Sensitive Field-Effect Transistors (BioFETs). *Analyst*, **127**, 1137-1151. https://doi.org/10.1039/B204444G

[135] Hu, Y. (2015) Advanced Sensing and Processing Methodologies for ISFET Based DNA Sequencing. A Report Submitted for the Degree of Doctor of Philosophy of Imperial College London, London.

[136] Kaisti, M., Kerko, A., Aarikka, E., Saviranta, P., Boeva, Z., Soukka, T. and Lehmusvuori, A. (2017) Real-Time Wash-Free Detection of Unlabeled PNA-DNA Hybridization Using Discrete FET Sensor. *Scientific Rpeorts*, **7**, Article No. 15734. https://doi.org/10.1038/s41598-017-16028-7

[137] Purushothaman, S., Toumazou, C. and Ou, C.-P. (2006) Protons and Single Nucleotide Polymorphism Detection: A Simple Use for the Ion Sensitive Field Effect Transistor. *Sensors and Actuators B*: *Chemical*, **114**, 964-968. https://doi.org/10.1016/j.snb.2005.06.069

[138] Russel, W.B., Saville, D.A. and Schowalter, W.R. (1989) Colloidal Dispersions. Cambridge University Press, Cambridge. https://doi.org/10.1017/CBO9780511608810

[139] Fologea, D., Uplinger, J., Thomas, B., McNabb, D.S. and Li, J. (2005) Slowing DNA Translocation in a Solid-State Nanopore. *Nano Letters*, **5**, 1734-1737. https://doi.org/10.1021/nl051063o

[140] Peng, H.B. and Ling, X.S.S. (2009) Reverse DNA Translocation through a Sol-

id-State Nanopore by Magnetic Tweezers. *Nanotechnology*, **20**, Article ID: 185101. https://doi.org/10.1088/0957-4484/20/18/185101

[141] He, Y., Tsutsui, M., Fan, C., Taniguchi, M. and Kawai, T. (2011) Controlling DNA Translocation through Gate Modulation of Nanopore Wall Surface Charges. *ACS Nano*, **5**, 5509-5518. https://doi.org/10.1021/nn201883b

[142] Akenson, M., Branton, D., Kasianowicz, J.J., Brandin, E. and Deamer, D.W. (1999) Microsecond Time-Scale Discrimination Among Polycytidylic Acid, Polyadenylic Acid, and Polyuridylic Acid as Homopolymers or as Segments Within Single RNA Molecules. *Biophysical Journal*, **77**, 3227-3233. https://doi.org/10.1016/S0006-3495(99)77153-5

[143] Maitra, R.D., Kim, J. and Dunbar, W.B. (2012) Recent Advances in Nanopore Sequencing. *Electrophoresis*, **33**, 3418-3428. https://doi.org/10.1002/elps.201200272

[144] Pyykkö, P. and Atsumi, M. (2009) Molecular Double-Bond Covalent Radii for Elements Li-E112. *Chemistry*: *A European Journal*, **15**, 12770-12779. https://doi.org/10.1002/chem.200901472

[145] Han, M.Y. (2010) Electronic Transport in Graphene Nanoribbons. Columbia University Press, New York.

[146] Gasparyan, L., Mazo, I., Simonyan, V. and Gasparyan, F. (2019) Modified DNA Sequencing Method through Effective Regulation of the DNA Translocation Speed in Aqueous Solution. *Proceedings of International Conference on Advances in Functional Materials*, The George Washington University, Washington DC, 22-24 July 2019, in Press.

Scientific Research Publishing

Open Journal of Biophysics, 2019, 9, 198-203
http://www.scirp.org/journal/ojbiphy
ISSN Online: 2164-5396
ISSN Print: 2164-5388

Electrostatic Mechanism for Depolymerization-Based Poleward Force Generation at Kinetochores

L. John Gagliardi[1], Daniel H. Shain[2]

[1]Department of Physics, Rutgers The State University of New Jersey, Camden, NJ, USA
[2]Department of Biology, Rutgers The State University of New Jersey, Camden, NJ, USA.
Email: gagliard@scarletmail.rutgers.edu, dshain@camden.rutgers.edu

How to cite this paper: Gagliardi, L.J. and Shain, D.H. (2019) Electrostatic Mechanism for Depolymerization-Based Poleward Force Generation at Kinetochores. *Open Journal of Biophysics*, **9**, 198-203.
https://doi.org/10.4236/ojbiphy.2019.93014

Received: June 1, 2019
Accepted: July 22, 2019
Published: July 25, 2019

Abstract

Experiments implicating bound volume positive charge at kinetochores interacting with negative charge at microtubule free ends have prompted our calculation of the force at kinetochores for chromosome poleward motility during mitosis. We present here a corroborating force calculation between positively charged Hec1 tails in kinetochores and negatively charged C-termini at microtubule free ends. Based on experimentally-known charge magnitudes on Hec1 tails and C-termini at microtubule free ends, an *ab initio* calculation of poleward (tension) force per microtubule that falls within the experimental range is demonstrated. Due to the locations of C-termini charges on concave sides of splaying microtubules, this attractive force between subsets of low curvature splaying microtubule protofilaments C-termini eventually fails for subsets of protofilaments with more pronounced curvature, thus generating poleward force as microtubules depolymerize in a dynamic coupling, as observed experimentally. The mechanism by which kinetochores establish and maintain a dynamic coupling to microtubules for force production during the complex motions of mitosis remains elusive, and force generation at kinetochores has emerged as a signature problem in chromosome motility. In agreement with experiment, two separate calculations show that attractive electrostatic interactions over nanometer distances account for poleward chromosome forces at kinetochores.

Keywords

Mitosis, Chromosome, Motility, Force, Electrostatics

1. Background

Force generation at kinetochores has emerged as one of the signature problems

in mitotic movements. Consistent with theoretical predictions made over a decade ago [1] [2], electrostatic interactions at kinetochores between negatively charged microtubule plus ends and positive charge at kinetochores have more recently been proposed for chromosome motility during mitosis [3]. A number of currently advanced models involve interactions that are fundamentally electrostatic, including mechanisms for chromosome movements based on protofilament-end splaying. A brief review of current models for force production at kinetochores is given elsewhere [4], where we support the experimental work of Miller *et al.* [3] with an *ab initio* calculation of the force between bound volume positive charge distributions at kinetochores interacting electrostatically with bound negative charge at free ends of microtubules.

Our purpose here is to mathematically corroborate that calculation with one that is based on direct interactions between positively charged unstructured Ndc80Hec1 tails in kinetochores and negatively charged C-termini at the free ends of microtubules, supporting an electrostatic-based model that explains poleward force generation.

Miller *et al.* [3], advances Ndc80/Hec1 as responsible for electrostatics-based force production at kinetochores. They propose that the force-producing interaction is electrostatic since an unstructured positively charged Hec1 tail cannot bind microtubules lacking negatively charged C-termini, concluding that "… the highest affinity interactions between kinetochores and microtubules are ionic attractions between two unstructured domains". Our approach supports the role of Hec1 as bound volume charge distributions—"positively charged Hec1 tails" [3]—at kinetochores, interacting electrostatically with bound negative charge at and near the free ends of microtubules—"ionic attractions between two unstructured domains" [3].

Chromosomes can move toward a proximal pole only when their kinetochores are connected to microtubules coming from that pole [5]. Microtubule polymerization and depolymerization follow a pattern characterized as "dynamic instability." This means that at any given time, some of the microtubules are growing, while others are undergoing rapid breakdown. The rate at which microtubules undergo net assembly, or disassembly (depolymerization), varies with mitotic stage [6]. In the present context, depolymerization-based electrostatic attractions are responsible for poleward force generation at kinetochores; electrostatic interactions for poleward force production at centrosomes are treated elsewhere [7].

The electrostatic properties of tubulin have been well-studied [8] [9] [10] [11]. Large-scale computer calculations have determined the dipole moment to be as large as 1800 Debye [9] [12]. Tubulin has a large overall charge of −20 (electron charges) at pH 7, and up to 40% of the charge resides on C-termini [13]. This large net charge on C-termini is integral to electrostatics-based force production at kinetochores (see below).

2. Results

In the context of force generation for chromosome motility at kinetochores,

Miller *et al.* [3] state that "… our data argue strongly that the Hec1 tail is the critical attachment for deploymerization-coupled movements of chromosomes"; and conclude "… the highest affinity interactions between kinetochores and microtubules are ionic attractions between two unstructured domains." This essentially proposes that bound, oppositely charged distributions are the underlying cause for poleward chromosome motions. As mentioned above, we recently published a force calculation between Hec1 charges, modeled as an experimentally known bound volume positive charge—"unstructured" positive charge—at kinetochores, and experimentally known negative charge at kinetochore microtubule free plus ends that agrees with experimental measurements of the poleward force for chromosome motility [4]. Here we provide a force calculation between positively charged Hec1 tails in kinetochores and negatively charged C-termini at and near microtubule free ends that confirms our previous proposal.

Since the lengths of Hec1 tails are much longer than the location volumes of C-termini charge distributions, Hec1 tails will be modeled as very long linear charges, with a linear charge density λ C/m (Coulombs/meter). A simple application of Gauss's law [14] for an infinitely long line charge distribution gives the electric field magnitude at a distance r from the line charge as

$$E = \lambda/2\pi\varepsilon r \tag{1}$$

where ε ($=k\varepsilon_0$) is the kinetochore permittivity, ε_0 = 8.85 pF/m (picoFarads/meter), and k is the kinetochore dielectric constant. Note that the relatively small contributions from edge effects near the ends of the Hec1 tails are neglected in this calculation.

The N-terminal tail of Hec1 contains an equivalent positive charge Q of 10 (electron charges, e) [3], distributed over a distance l of 55 nm [15], giving a linear charge density $\lambda = Q/l$ of 10 e/55 nm = 29 pC/m (picoCoulombs per meter). The force generating interaction is between positively charged Hec1 tails and negatively charged C-termini on concave sides of splaying protofilaments.

For the force per protofilament, we have:

$$F_{pf} = qE = ne\lambda/2\pi\varepsilon r \tag{2}$$

where $q = ne$ is the charge of n electrons on C-termini of a protofilament interacting with a Hec1 tail. Consistent with their open structures, a cytosol-saturated kinetochore is expected to have a dielectric constant midway between the kinetochore *dry* value and cytoplasmic water [16]. Since most condensed-matter (dry) dielectric constants are between 1 and 5, the value for cytoplasmic water dominates, and a conservative midpoint value k = 45 ((80 + 10)/2) will be assumed [4]. Substituting this value in (2), with λ = 29 pC/m, and the distance of the effective charge centers of C-termini charges, r = 3 nm, we have F_{pf} = 0.6n pN/pf (picoNewtons per protofilament).

Kinetochores generally number at least 8 Hec1 proteins per microtubule [17], and there are 13 protofilaments per microtubule. It will therefore be conserva-

tively assumed that four protofilaments in a microtubule are interacting with a Hec1 tail at any given moment. These subsets would be constantly changing among the microtubules penetrating a kinetochore. Thus, the total force per microtubule $F = 4(0.62)\ n = 2.5\ n$ pN/MT (picoNewtons per microtubule). Equating this to the experimental range 1 - 5 pN/MT [18], we find that $n = 0.4$ - 2.5 electron charges. This result, like that of the previous calculation [4], falls well within the observed experimental range [9] [13] [19], and the agreement represents a successful *ab initio* theoretical derivation of this force magnitude.

Since microtubule C-termini are on the concave sides of progressively splaying microtubules, increasing protofilament curvature will lead to a separation of the charges on Hec1 tails and C-termini. Subsets of low curvature splaying protofilaments produce poleward force, while other subsets of protofilaments with more pronounced curvature in later stages of depolymerization fail to bind. Accordingly, poleward forces are generated as microtubules depolymerize, in agreement with observation.

3. Discussion

Electrostatic fields within the cytosol are subject to strong attenuation due to screening by oppositely charged ions (counterion screening), decreasing exponentially to much smaller values over a distance of several *Debye lengths*. The Debye length within cells is typically given to be of order 1 nm [20], and since cells have much larger dimensions, one is tempted to conclude that electrostatic force could not be a major factor in providing the cause for chromosome motility in biological cells. However the presence of microtubules challenges that notion. Microtubules can be thought of as intermediaries that extend the reach of the electrostatic interaction over cellular distances, making the second most powerful force in nature available to cells in spite of their ionic nature.

Cellular electrostatics is also strongly influenced by reduced counterion screening due to layered water adhering to charged molecules. Such water layering – with consequent reduction or elimination of Debye screening – at charged proteins has long been theorized [21] [22], and has been confirmed by experiment [23]. Additionally, water between sufficiently close (up to 3 nm) charged proteins has a dielectric permittivity that is considerably reduced from the *bulk* value far from charged surfaces [24] [25] [26]. The combination of these effects (or conditions)—water layering and reduced dielectric constant—can significantly influence cellular electrostatics in a number of important ways. This is especially true in relation to mitosis [26].

4. Conclusion

Given positive charge at kinetochores and negative charge on plus ends of microtubules, it is difficult to conceptualize there not being an attractive electrostatic poleward-directed force between these structures. A direct calculation of the electrostatic force between positively charged Hec1 tails and negatively

charged C-termini at and near the free ends of microtubules supports an electrostatic force generating mechanism for poleward chromosome motions during mitosis. A singular strength of the present calculation is that the disassembly rate of microtubules at kinetochores is explicitly shown to be correlated with force production at kinetochores. In a broader context, understanding the underlying forces and mechanisms that dictate chromosome movements through mitosis will be critical to the development of approaches to circumvent anomalous cell divisions (e.g., cancer).

Authors' Contributions

LJG conceptualized the theoretical aspects of this article and DHS provided intellectual contributions. Both authors read and approved the final manuscript.

Conflicts of Interest

The authors declare they have no competing interests.

References

[1] Gagliardi, L.J. (2002) Electrostatic Force in Prometaphase, Metaphase, and Anaphase-A Chromosome Motions. *Physical Review E*, **66**, Article ID: 011901. https://doi.org/10.1103/PhysRevE.66.011901

[2] Gagliardi, L.J. (2005) Electrostatic Force Generation in Chromosome Motions during Mitosis. *Journal of Electrostatics*, **63**, 309-327. https://doi.org/10.1016/j.elstat.2004.09.007

[3] Miller, S.A., Johnson, M.L. and Stukenberg, P.T. (2008) Kinetochore Attachments Require an Interaction between Unstructured Tails on Microtubules and Ndc80/Hec1. *Current Biology*, **18**, 1785-1791. https://doi.org/10.1016/j.cub.2008.11.007

[4] Gagliardi, L.J. and Shain, D.H. (2016) Electrostatic Forces Drive Poleward Chromosome Motions at Kinetochores. *Cell Division*, **11**, 14. https://doi.org/10.1186/s13008-016-0026-1

[5] Nicklas, R.B. and Kubai, D.F. (1985) Microtubules, Chromosome Movement, and Reorientation after Chromosomes Are Detached from the Spindle by Micromanipulation. *Chromosoma*, **92**, 313-324. https://doi.org/10.1007/BF00329815

[6] Alberts, B., *et al.* (1994) Molecular Biology of the Cell. 3rd Edition, Garland, New York, 920.

[7] Gagliardi, L.J. and Shain, D.H. (2014) Polar Electrostatic Forces Drive Poleward Chromosome Motions. *Cell Division*, **9**, 5. https://doi.org/10.1186/s13008-014-0005-3

[8] Sataric, M.V., Tuszynski, J.A. and Zakula, R.B. (1993) Kinklike Excitations as an Energy Transfer Mechanism. *Physical Review E*, **48**, 589-597. https://doi.org/10.1103/PhysRevE.48.589

[9] Brown, J.A. and Tuszynski, J.A. (1997) Dipole Interactions in Axonal Microtubules as a Mechanism of Signal Propagation. *Physical Review E*, **56**, 5834-5840. https://doi.org/10.1103/PhysRevE.56.5834

[10] Baker, N.A., *et al.* (2001) Electrostatics of Nanosystems: Applications to Microtubules and the Ribosome. *Proceedings of the National Academy of Sciences*, **98**, 10037-10041. https://doi.org/10.1073/pnas.181342398

[11] Tuszynski, J.A., Brown, J.A. and Hawrylak, P. (1998) Dielectric Polarization, Electrical Conduction, Information Processing and Quantum Computation in Microtubules: Are They Plausible? *Philosophical Transactions of the Royal Society of London. Series A*, **356**, 1897-1926. https://doi.org/10.1098/rsta.1998.0255

[12] Tuszynski, J.A., *et al.* (1995) Ferroelectric Behavior in Microtubule Dipole Lattices: Implications for Information Processing, Signaling and Assembly/Disassembly. *Journal of Theoretical Biology*, **174**, 371-380. https://doi.org/10.1006/jtbi.1995.0105

[13] Tuszynski, J.A., *et al.* (2002) Electrostatic Properties of Tubulin and Microtubules. In: Crowley, J.M., Zaretsky, M. and Kazkaz, G., Eds., *Proceedings of the Electrostatics Society of America and Institute of Electrostatics—Japan*, Laplacian Press, Morgan Hill, 41-50.

[14] Halliday, D. and Resnick, R. (1962) Physics. Vol. 2, John Wiley & Sons, New York, 698.

[15] Wilson-Kubalek, E.M., *et al.* (2008) Orientation and Structure of the Ndc80 Complex on the Microtubule Lattice. *The Journal of Cell Biology*, **182**, 1055-1061. https://doi.org/10.1083/jcb.200804170

[16] Schelkunoff, S.A. (1963) Electromagnetic Fields. Blaisdell, New York, 29.

[17] Joglekar, A.P., *et al.* (2006) Molecular Architecture of a Kinetochore-Microtubule Attachment Site. *Nature Cell Biology*, **8**, 581-598. https://doi.org/10.1038/ncb1414

[18] Grishchuk, E.L., *et al.* (2005) Force Production by Disassembling Microtubules. *Nature*, **438**, 384-388. https://doi.org/10.1038/nature04132

[19] Stracke, R., *et al.* (2002) Analysis of the Migration Behavior of Single Microtubules in Electric Fields. *Biochemical and Biophysical Research Communications*, **293**, 602-609. https://doi.org/10.1016/S0006-291X(02)00251-6

[20] Benedek, G.B. and Villars, F.M.H. (2000) Physics: With Illustrative Examples from Medicine and Biology: Electricity and Magnetism. Springer-Verlag, New York, 403. https://doi.org/10.1007/978-1-4612-1240-9

[21] Jordan-Lloyd, D. and Shore, A. (1938) The Chemistry of Proteins. JA Churchill Publishing Company, London. https://doi.org/10.1021/ja01220a017

[22] Pauling, L. (1945) The Adsorption of Water by Proteins. *Journal of the American Chemical Society*, **67**, 555-557.

[23] Toney, M.F., *et al.* (1994) Voltage-Dependent Ordering of Water Molecules at an Electrode-Electrolyte Interface. *Nature*, **368**, 444-446. https://doi.org/10.1038/368444a0

[24] Bockris, J.O. and Reddy, A.K.N. (1977) Modern Electrochemistry. Plenum, New York.

[25] Teschke, O., Ceotto, G. and De Souza, E.F. (2001) Interfacial Water Dielectric Permittivity-Profile Measurements Using Atomic Force Spectroscopy. *Physical Review E*, **64**, Article ID: 011605. https://doi.org/10.1103/PhysRevE.64.011605

[26] Gagliardi, L.J. (2009) Electrostatic Considerations in Mitosis. iUniverse Publishers, Bloomington, IN.

Scientific Research Publishing

Open Journal of Biophysics, 2019, 9, 204-217
http://www.scirp.org/journal/ojbiphy
ISSN Online: 2164-5396
ISSN Print: 2164-5388

Evaluation of the Knowledge of CT Scan Prescribers on Patients' Radioprotection in Senegal

Serigne Moussa Badiane[1*], Pape Ibrahima Sane[2], Coumba Ndoffene Ndiaye[2], Kalidou Gueye[2], Oumar Ndoye[2], Kuassi M. Amoussou-Guenou[3], Mamadou Mbodji[2]

[1]Biophysics and Nuclear Medicine, Gaston Berger University, Saint-Louis, Senegal
[2]Biophysics and Nuclear Medicine, Cheikh Anta DIOP University, Dakar, Senegal
[3]Biophysics and Nuclear Medicine, Abomey-Clavi, Benin University, Benin
Email: *drmoussabadiane@gmail.com

How to cite this paper: Badiane, S.M., Sane, P.I., Ndiaye, C.N., Gueye, K., Ndoye, O., Amoussou-Guenou, K.M. and Mbodji, M. (2019) Evaluation of the Knowledge of CT Scan Prescribers on Patients' Radioprotection in Senegal. *Open Journal of Biophysics*, **9**, 204-217.
https://doi.org/10.4236/ojbiphy.2019.93015

Received: April 30, 2019
Accepted: July 23, 2019
Published: July 26, 2019

Abstract

Medical imaging has enabled major improvements in the medical care of the patient. However, some of these tests have the disadvantage of using ionizing radiation at low doses. Although the CT scan is a powerful diagnostic tool, it remains a highly radiant imaging modality. In addition, the risk of radiation-induced cancer associated with low X-ray doses is established by the American Phase 2 study BEIR VII, and preventive measures require a good level of knowledge on radioprotection by imaging test prescribers. In our study, we evaluated the knowledge of CT scan prescribers in Senegal regarding patient radioprotection. These prescribers consisted of physicians and surgeons without distinction of specialty. Our objective was to have the required data for optimizing CT prescriptions in compliance with the principles of radioprotection. Our work focused on a descriptive analytical study of 107 doctors who prescribed CT scan in public health institutions in Senegal. Our results revealed poor knowledge of doctors prescribing CT scan on induced radio risks, even though the majority of them stated that they took those risks into account. Our data were not isolated, they were applicable to similar studies conducted outside Senegal. In summary, our study led on the one hand to recommendations on initial and continuing training and on the other hand on organizational and regulatory considerations.

Keywords

Radioprotection, Risk of Radiation-Induced Cancer, CT Scan Prescribers, Health Institutions in Senegal

1. Introduction

The medical use of ionizing radiation has become the most important source of irradiation in the world. On the one hand, the knowledge and skills of professionals using this radiation determine the implementation of radioprotection measures recommended by international and national organizations. On the other hand, the situation in African countries is worrying due to the absence and/or non-compliance with radioprotection laws and regulations. In Senegal, CT scanning equipment is on the rise and CT scans are regularly prescribed in hospitals. Although the CT scan is a powerful diagnostic tool, it remains a highly radiant imaging modality. In addition, the risk of radiation-induced cancer associated with low X-ray doses is established by the American Phase 2 study BEIR VII [1]. However, compliance with the principles of justification, optimization and limitation requires a good level of knowledge by prescribers regarding patient radioprotection. We evaluated the knowledge of CT scan prescribers in Senegal following the model of the study by Gervaise *et al.* [2] conducted in 2011 in France to assess the level of knowledge of CT scan prescribers about patient radioprotection. Our objective is to have sufficient data to optimize CT prescriptions in compliance with the principles of radioprotection. Our study involved 107 doctors, including senior and junior doctors.

2. Materials and Methods

The study involved prescribers from 10 hospitals in Senegal.

This was a descriptive and analytical cross-sectional study of 107 doctors, including senior and junior doctors (trainees and junior registrars who prescribe CT scan.

- Criteriaof inclusion

All the doctors prescribing CT scan and who agreed to answer to the questions were included.

- Criteria of non-inclusion

All medical imaging specialists and CT scan practitioners even if they are also prescribers.

- Data collection

The data were collected using a questionnaire (see **Appendix**).

The questionnaire was submitted to the prescribers and then retrieved after a minimum period of 24 hours. The data were collected by second-year-medical students further to their course on radioprotection.

The data collected were verified, recorded and analyzed using Excel software.

- Data collected

The data collected concerned mainly the following parameters:

The status of senior or junior doctors.

Their unit.

The management of the benefit-risk ratio when prescribing a CT scan.

The level of irradiation during a CT scan.

The risk of radiation-induced cancer.

Whether or not they have received training on radioprotection.

Whether or not they have read a handbook on the proper use of imaging tests at least once (See the survey sheet).

- Ethical consideration

The free and informed consent of the interviewees was obtained in advance and confidentiality was guaranteed.

3. Results

107 Questionnaires were submitted to the doctors and among them 102 responded (Table 1). This distribution corresponds to 49% of doctors in training and 51% of senior doctors (Diagram 1).

Question 1. Do you prescribe CT scan?

To this question, 96% of juniors and 94.4% of respondents said they prescribe CT scan (Table 2).

Question 2. When prescribing a CT scan, have you ever considered the benefit/risk ratio of X-rays?

In this question, 57% of the prescribers affirmed to take into account the benefit-risk ratio against 43% (Table 3 and Diagram 2).

Among those who take into account the benefit-risk ratio 60% are seniors compared to 40% of juniors (Figure 1).

Question 3. When prescribing a CT scan, have you already informed the patient about the risks associated with x-rays and the resulting benefit/risk ratio features?

Table 1. Number of questionnaires submitted to doctors.

Number of questionnaires submitted to doctors: 107 (see diagram number 1)		
Number of questionnaires treated = 102		
Number of unanswered questionnaires = 05		
Status	Junior doctors	Seniors
Total	50	52

Table 2. Frequency of prescription of CT scan.

Status	Junior doctors		seniors	
Answers	yes	no	yes	no
Total	50	2	52	3
Percentage of prescribers	96%		94.4%	

Table 3. Benefit-risk consideration.

Status	Junior doctors		seniors	
Answers	yes	no	yes	no
Total	23	27	35	17

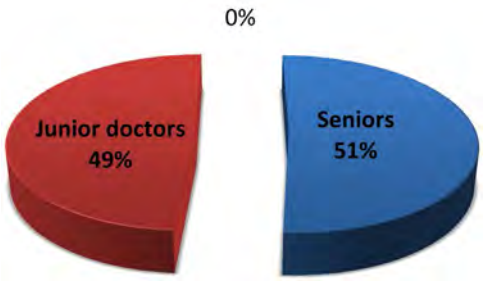

Diagram 1. Distribution of prescribers by status.

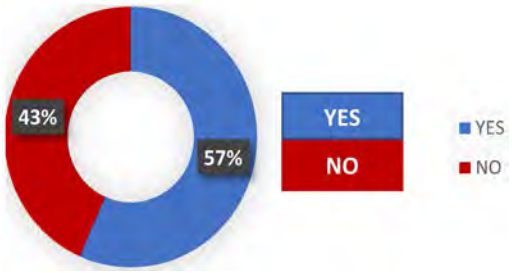

Diagram 2. frequency of prescribers that take into account the benefit/risk ratio.

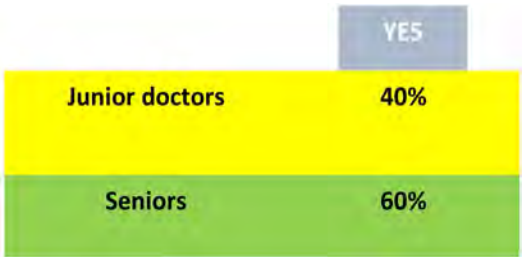

Figure 1. Statutes of the prescribers considering the benefit/risk ratio.

In this question, 25% of the prescribers affirmed informing their patients of the benefit-risk ratio against 75% (Table 4 and Diagram 3).

Among those who claim to inform their patients, there were 44% of junior prescribers and 56% of senior (Figure 2).

Question 4. In your opinion, and compared to the dose delivered for a chest X-ray (RT), the average dose delivered during a standard abdominal CT scan is equivalent to:

0.5% of participants gave the right answer (Table 5 and Diagram 4).

Expected correct response: Compared to the dose delivered for chest X-ray (RT), the average dose delivered during a standard abdominal CT scan is equivalent to 100 RT < CT < 250 RT.

Question 5. Knowing that the natural irradiation is about 2.5 msv/year, how much do you estimate the average dose delivered during an abdominopelvic CT scan?

0.4% of participants gave the right answer.

Table 4. Patient information on the benefit-risk ratio.

Status	Junior doctors		seniors	
Answers	yes	no	yes	no
Total	11	39	14	38

Table 5. Knowledge of the radiation dose level of an abdominopelvic CT compared to a chest X-ray.

Characteristics	CT < RT	RT < CT < 10 RT	10 RT < CT < 100 RT	100 RT < CT < 250 RT	250 RT < CT	Do not know
Answers	26	24	11	5	3	33

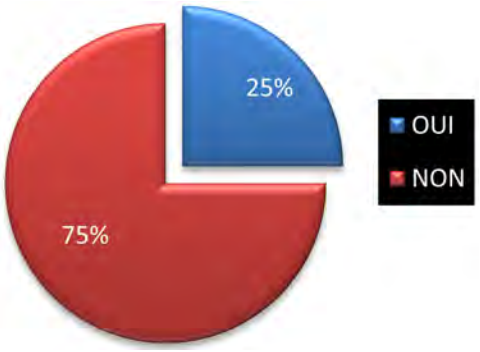

Diagram 3. Frequency of prescribers who inform their patients about the benefit/risk ratio.

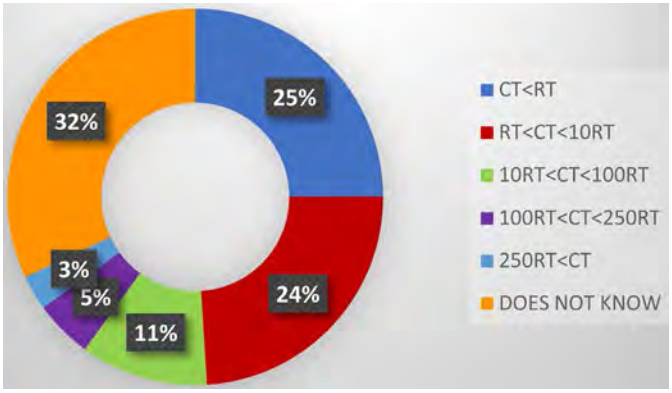

Diagram 4. Frequency of prescribers who know the radiation dose level of an abdominopelvic CT compared to a chest X-ray.

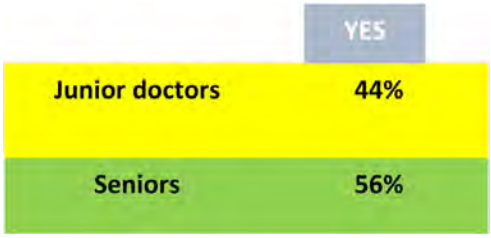

Figure 2. Statutes of the prescribers informing about the benefit/risk ratio.

Expected correct response: The average dose delivered during an abdominal pelvic CT scan is estimated between 5 to 20 mSv (Table 6 and Diagram 5).

Question 6. According to the latest consensus conferences, there is a risk of developing radiation-induced cancer due to the dose delivered during a single standard abdominal-pelvic CT scan. If yes, how high do you estimate this risk?

17% of the participants gave the right answer.

Expected correct answer: A risk of developing radiation-induced cancer due to the dose delivered during a single standard abdominal-pelvic CT scan is estimated at 1/1000 (Table 7 and Diagram 6).

Table 6. Comparison of natural irradiation versus an abdominopelvic CT scan.

Characteristics	<5 mSv	5 to 20 mSv	<20 mSv	Do not know
Answers	19	4	16	63

Table 7. Risk of radio cancer induced at low doses.

Characteristics	None	1/1000	1/50,000	1/100,000	1/500,000	Do not know
Answers	43	17	4	13	8	17

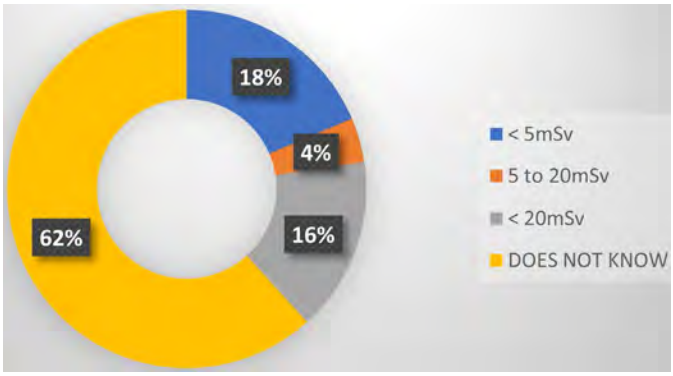

Diagram 5. Frequency of prescribers who know the radiation dose level of an abdominopelvic CT compared to natural irradiation.

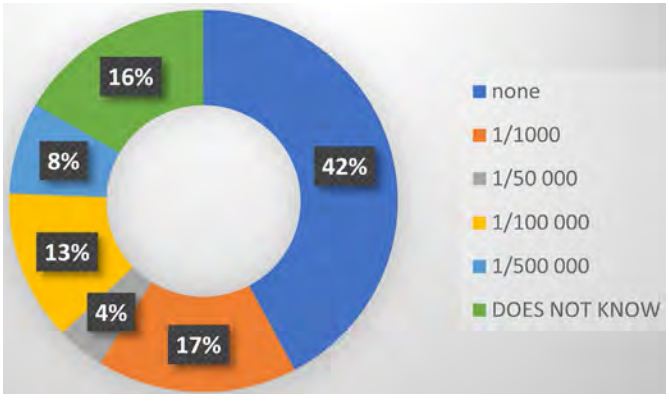

Diagram 6. Frequency of prescribers who know the level of risk of radiation-induced cancer based on the latest consensus conferences.

Question 7. Have you ever been trained on patient radioprotection?

9% of prescribers claim to have received radiation protection training (Table 8 and Diagram 7). The proportion of prescribers claiming to have been trained is 55.6% for junior versus 44.4% for seniors (Figure 3).

Question 8. Have you ever read a handbook on the proper use of medical imaging tests?

To this question, 23% of prescribers stated that they had already consulted a guide (see Table 9, Diagram 8). Of those, 43.5% were junior and 56.5% were

Table 8. Radiation protection training.

Characteristics	Junior doctors		Seniors	
Answers	yes	no	yes	no
Staff	5	45	4	48

Table 9. Prescribers claiming to have already consulted a guide to the correct use of médical imaging exams.

Characteristics	Junior doctors		Seniors	
Answers	yes	no	yes	no
Staff	10	40	13	39

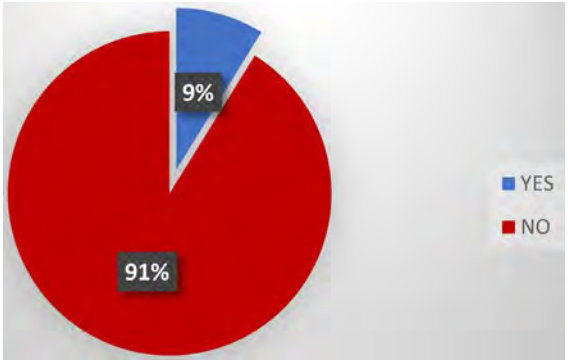

Diagram 7. Frequency of prescribers who have received radiation protection training.

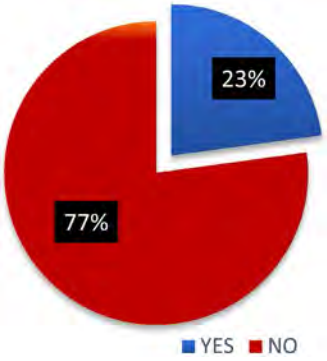

Diagram 8. Frequency of prescribers who have already consulted a guide to the correct use of imaging screens.

Figure 3. Statutes of prescribers informing about the benefit/risk ratio.

Figure 4. Statutes of the prescribers claiming to have already consulted a guide of good use in imagery.

seniors (**Figure 4**).

4. Discussion

4.1. Analytical Interpretation of the Survey Results

Medical science uses various sources of ionizing radiation, produced either by electric generators or by radionuclides. While their medical interest and usefulness have been established, these techniques contribute significantly to the population's exposure to ionizing radiation. After natural exposure, they represent the second most important source of exposure for the population and the first source of artificial origin. The current state of knowledge on the dangers and risks associated with ionizing radiation has led the international community to set health objectives for radioprotection aiming at avoiding the appearance of so-called tissue or deterministic reactions but also at reducing the probability of radiation-induced cancers [3]. The interest of knowing the risk of radiation-induced cancer is an element of radioprotection.

To this end, studies focusing on good imaging practices and compliance with handbooks for the prescription of irradiating imaging tests are arousing growing interest within the scientific community. The choice amongst imaging modalities is therefore in favour of non-irradiating techniques and, failing that, the lowest doses possible.

Our study shows that prescribers' knowledge on patient radioprotection is unsatisfactory, with a significant underestimation of the level of radiation doses delivered to patients and the potential risks of radiation-induced cancer that result from them. However, this observation is not only limited to the prescribing doctors in our study, but is consistent with the results of numerous studies con-

ducted on populations of hospital practitioners [2] [4] and also on a population of radiologists, although to a lesser extent [5].

For example, for Lee *et al.* in a study conducted in 2004 [6], only 9% of paramedics reported that they thought there was an increased risk of radiation-induced cancer due to the use of a CT while only 22% of them had informed the patient. The dose ratio between a CT scan and a frontal chest X-ray was also significantly underestimated.

In another similar study, conducted in 2004 [7] Jacob *et al.* found a higher correct response rate among the group of doctors who had previously received patient radioprotection training compared to the group who had never received such training.

The course on radioprotection in the medical program is only delivered during the first cycle of medical study without any particular focus, thus at the end of the training curriculum the doctor keeps only vague memories of the concepts of radioprotection. Furthermore, the availability and distribution of prescription handbooks for imaging tests is an issue.

Therefore, the training of practitioners on radioprotection seems to play a key role. However, although the interest of such training is highlighted by organizations such as Euratom, [4] it seems to be neglected in medical programs. Such training would allow a better knowledge and consideration of the potential risk of radiation-induced cancer associated with low X-ray doses by prescribers. This could then lead to a better justification for irradiating imaging tests and also help the patient get the right information.

Moreover, with the current availability of publications, the patient can already find a lot of information on the Internet or in the newspapers that the prescriber must be able to comment on and sometimes qualify. However, in some circumstances, this information which the doctor should provide to the patient becomes a must. This is particularly the case for pregnant women or young patients with chronic pathologies requiring repeated CT scan.

The limited knowledge of prescribing doctors about patient radioprotection challenges the "quality" of their medical care. Quality in the provision of medical care takes into account the availability of protocols, information for practitioners and patients [6]. Improving the quality of medical care in our contexts of operation will require CT prescribers to be aware of the concepts of radioprotection, justification, optimization and limitation of the risk of radiation exposure.

We have found that prescribing doctors do not feel comfortable with radioprotection and are not involved in this practice. Krille *et al.* [8] in their 2010 literature review assessed doctors' knowledge of the doses and risk of CT scan. Thus, despite the methodological differences of the 14 studies included, this article concludes that doctors' risk awareness should increase. This lack of professional involvement is more prevalent in the medical field than in other fields using ionizing radiation [9]. In the February 2008 publication of the journal "Bulletin and Memoirs of the Belgian Royal Academy of Medicine", Dr. Smeesters compares the radiological risk awareness and radioprotection knowledge of

medical staff (diagnostic and therapeutic) with the knowledge of professionals using ionizing radiation in an industrial setting. According to the author, radioprotection culture and risk awareness are less widespread in the medical field than in other sectors using ionizing radiation [10]. The first concern of doctors is to establish a diagnosis and treat effectively, so radioprotection logically takes a back seat [4]. This attitude would not be related to negligence or opposition to radioprotection strategies, but rather to ignorance. They are also unanimous in recognizing a risk to the repeated use of ionizing tests, even if this assessment is uncertain and presents a strong inter-individual variability. However, an article in the Swiss Doctors' newsletter reports that doctors feel uncomfortable when informing patients about the radiological risk [10].

4.2. Statistical Approach

We chose a descriptive approach to provide a detailed picture of the knowledge of CT prescribers about patient radioprotection.

Two variables should be noted:

- an independent variable that is the status of prescribing doctors.
- a dependent variable which is the level of knowledge about patient radioprotection.

In our sampling, we had sought an approach that was fairly representative of the population of CT prescribers in Senegal.

This sample was non-probabilistic because we did not find it relevant to submit our questionnaire to radiology or nuclear medicine practitioners who are also potential prescribers.

Following our network, we have been able to move widely from University Hospital Centers to Regional Hospital Centers. This has resulted in a fairly representative sample of CT scan prescribers in Senegal. The small sample size of 107 participants is a potential source of sampling bias. Nevertheless, data saturation was achieved on a sample of maximum variables that seems to have been well conducted because if we look at the sociological characteristics of the doctors in the study, we have 52 senior doctors and 50 junior doctors. Demographically, the majority of the study is made up of urban doctors. However, despite practice and culture that may differ, the initial medical training is the same. Data collection was done using a questionnaire based on the Gervais *et al.* [2] model. In order to encourage the participant in the study, we avoided submitting a questionnaire that at first glance could appear complex and interfere with the desire to answer. Therefore, the first questions were accessible and we also guaranteed the anonymity of the participants and any other identification data. Our approach was cost-effective because out of 107 questions submitted, 105 doctors answered.

Depending on the participant's availability, almost all of them gave us a time slot to answer our questionnaire, while others gave us an appointment the next day to retrieve the completed questionnaires.

4.3. Strengths and Weaknesses

The qualitative nature of this study reflects both the conscious opinion of prescribing doctors on radioprotection and its unconscious representation, compared to a quantitative study. Qualitative studies go beyond rationality and open up a window on what the subject "really" thinks. This allows us to see the different positions that prescribing doctors may have on the subject. The number of interviews conducted resulted in the collection of a significant amount of ideas.

For reasons of convenience and adherence, the majority of interviews were conducted at the interviewee's worksite. During the interviews, doctors were sometimes interrupted in their reasoning by the telephone or patients knocking on the door. Several interviews were conducted at the end of the day.

4.4. Challenges of the Study

We did not encounter any major difficulties in carrying out this work, except for the risks associated with travel.

4.5. Major Orientations

The purpose of studies such as ours is to improve the control of ionizing radiation risk in the sectors concerned (radiology, nuclear medicine, radiotherapy, dental surgery) and to improve the safety of patients subjected to diagnostic or curative radiation, by prioritizing the dissemination and application of the regulatory framework and its translation into national institutional and professional procedures and recommendations.

This is based on several axes, including raising awareness among all the professionals concerned (radiologists and prescribers, radio-pharmacists, medical physicists, handlers, dental surgeons) on the need to take radioprotection into account for any prescription and/or use of ionizing radiation, particularly around the principles of justification and optimization of the various modalities. But also the facilitation of the adherence and appropriation of professionals to the approaches for the analysis of practices, as proposed by the High Authority for Health in France (HAS), as a lever for the quality and safety of care [7] by involving them widely in the implementation of radioprotection procedures and measures.

However, these steps require the implementation of practical orientation training during initial and continuing medical training.

Education and training on radioprotection require strong action in some countries by the Ministry of Higher Education and Health to ensure that medical education programs better integrate the physical and biological bases of the effects of ionizing radiation, their various applications and radioprotection.

The relevant training topics would be structured around:

- the national and international regulatory legislative and institutional framework,

- staff and patient safety requirements,
- quality control of equipment,
- employers' obligations regarding workplace safety standards, monitoring and follow-up of staff.

These steps should lead to the design of information systems on patients' doses of exposure under the supervision of the various actors and bodies concerned and the improvement of mandatory quality control for new and existing installations through measures informing about the quantity of radiation emitted during irradiation examination procedures.

In addition, it would be useful in our conditions to set up an information and advice system for doctors and patients confronted with a problem of exposure to ionizing radiation to verify the relevance of radiological examinations requested either at the level of insurance providers or even public authorities and this should be mandatory for the radiology department through a systematic welcoming of the patient by the radiologist before any imaging test. In our opinion, the radiologist should not just consider the patient and their pathology as an image to read. This robotic method of management is a strainer that reduces the chances of the patient and the quality of their medical care.

In the same line, we encourage the promotion of national expertise in radioprotection by setting up a powerful, transparent and pluralist scientific monitoring system to follow-up the evolution and critical analysis of new scientific data likely to have an impact on radioprotection in the short and long terms. The major orientation would be a vigilant and responsible radioprotection with an emphasis on the reduction of doses received by the public, patients and professionals.

These proposals comply with the report of the commission headed by Professor Constantin VROUSOS submitted to the Director General of Nuclear Safety and Radioprotection in France on 2nd March 2004 [11].

5. Conclusion

The observation of low level of knowledge of CT prescribers in patient radiation protection challenges the public health authorities and learned societies on the need to train health professionals. The current upgrading of the imaging technical platforms of the main national hospitals as well as regional hospitals is turning training needs into a real emergency. The lack of continuous training of medical staff and patients on radioprotection is a disadvantage and a potentially serious risk due to the diverse profile of the staff and equipment installed in health services. In summary, our work resulted in recommendations focused on initial and ongoing training to be developed, as well as organizational and regulatory aspects to be improved.

Conflicts of Interest

The authors declare no conflicts of interest regarding the publication of this paper.

References

[1] National Research Council, *et al.* (2006) Health Risks from Exposure to Low Levels of Ionizing Radiation: BEIR VII Phase 2. National Academies Press, Washington DC.

[2] Gervaise, A., Esperabe-Vignau, F., Pernin, M., *et al.* (2011) Evaluation des connaissances des prescripteurs de scanner en matière de radioprotection des patients. *Journal de Radiologie*, **92**, 681-687. https://doi.org/10.1016/j.jradio.2011.03.023

[3] (2000) Sfrnet.org en ligne paris France. Société Française de Radiologie. http://www.sfrnet.org/sfr/professionnels/5-referentiels-bonnes-pratiques/directive-euratom/index.phtml

[4] has-sante.fr en ligne Paris (France) (2012) Haute autorité de santé. https://www.has-sante.fr/portail/upload/docs/application/pdf/2013-07/radioprotection_du_patient_et_analyse_des_pratiques_dpc_et_certification_des_etablissements_de_sante_format2clics.pdf

[5] Azria, E., Bétrémieux, P., Caeymaex, L., *et al.* (2007) L'information dans le contexte du soin périnatal: Aspects éthiques. *Archives de Pédiatrie*, **14**, 1231-1239. https://doi.org/10.1016/j.arcped.2007.07.005

[6] Krille, L., Hammer, G.P., Merzenich, H. and Zeeb, H. (2010) Systematic Review on Physician's Knowledge about Radiation Doses and Radiation Risks of Computed Tomography. *European Journal of Radiology*, **76**, 36-41. https://doi.org/10.1016/j.ejrad.2010.08.025

[7] Wong, C.S., *et al.* (2012) A Questionnaire Study Assessing Local Physicians, Radiologists and Interns' Knowledge and Practice Pertaining to Radiation Exposure Related to Radiological Imaging. *European Journal of Radiology*, **81**, 264-268. https://doi.org/10.1016/j.ejrad.2011.02.022

[8] Lefebvre, G., Smeesters, P. and Van Bladel, L. (2006) Contrôle et évaluation de la radioprotection des patients en Belgique: Organisation, bilan et perspectives. *Contrôle*, **172**, 12-16.

[9] asn.fr en ligne Paris (France): Autorité de Sureté Nucléaire 2016. https://www.asn.fr/Informer/Publications/Rapports-de-l-ASN

[10] Smeesters, P., Firket, H., Smeesters, P., Frühling, J., Smeesters, P., Behar, A., Vanderhaeghen, J.-J., *et al.* (2008) Radioprotection et pratique médicale: Progrès, défis et menaces. *Bulletin et mémoires de l'Académie Royale de Médecine de Belgique*, **163**, 145-160.

[11] la documentationfrancaise.fr. Rapport de la commission VROUSOS. Priorites en radioprotection en ligne Paris (France): La Documentation française 2004. https://www.ladocumentationfrancaise.fr/var/storage/rapports-publics/044000102.pdf

Appendix

Survey sheet.

Evaluation of the knowledge of CT scan prescribers on patient radioprotection in Senegal

QUESTIONNAIRE

(Tick the answers that you think are correct)

Junior doctor/Senior (years of experience since the MD)…….. Years

Unit: ……..

Hospital: ……..

Do you prescribe CT scan? (Even occasionally) Yes ☐ No ☐

Which organ CT scan do you prescribe the most?.....

When prescribing an CT scan, have you ever taken into account the benefit/risk ratio related to x-rays? Yes ☐ No ☐

When prescribing a CT scan, have you already informed the patient about the risks associated with x-rays and the resulting benefit/risk ratio? Yes ☐ No ☐

In your opinion, compared to the dose delivered for a chest X-ray (RT), the average dose delivered during an abdominal pelvic is equivalent to:

☐ CT < RT

☐ 10 RT > CT > RT

☐ 100 RT > CT > 10 RT

☐ 250 RT > CT > 100 RT

☐ CT > 250 RT

Knowing that the natural irradiation is about 2.5 mSv *per year, how much do you estimate the average dose delivered during an abdominal pelvic CT scan*? …….. mSv

In your opinion and according to the latest consensus conferences, is there a risk of developing radiation-induced cancer due to the dose delivered during a single standard abdominal CT scan and if so, how high do you estimate this risk?

☐ None (= no risk of radiation-induced cancer for a single abdominal-pelvic CTscan)

☐ 1 per 1000 (= 1 in 1000 patients at risk of developing cancer due to the dose received by having a single abdominal and pelvic CT scan)

☐ 1 per 50,000

☐ 1 per 100,000

☐ 1 per 500,000

Have you ever been trained on patient radioprotection? Yes ☐ No ☐

Have you once read a handbook on the proper use of medical imaging tests? Yes ☐ No ☐

NB-Junior doctor = specialization in progress

Scientific Research Publishing

Open Journal of Biophysics, 2019, 9, 218-237
http://www.scirp.org/journal/ojbiphy
ISSN Online: 2164-5396
ISSN Print: 2164-5388

Aging Leads to Over-Expression of Na^+/K^+ Pump Units in Liver and Na^+/Ca^{2+} Exchangers in Brain Cortex

Anna Nikoghosyan, Armenuhi Heqimyan, Sinerik Ayrapetyan*

Life Sciences International Postgraduate Educational Center, UNESCO Chair in Life Sciences, Yerevan, Armenia
Email: *info@biophys.am

How to cite this paper: Nikoghosyan, A., Heqimyan, A. and Ayrapetyan, S. (2019) Aging Leads to Over-Expression of Na^+/K^+ Pump Units in Liver and Na^+/Ca^{2+} Exchangers in Brain Cortex. *Open Journal of Biophysics*, **9**, 218-237.
https://doi.org/10.4236/ojbiphy.2019.93016

Received: May 8, 2019
Accepted: July 26, 2019
Published: July 29, 2019

Abstract

The metabolic controlling of tissue hydration is the fundamental parameter determining cell functional activity and its dysfunction is the common consequence of any cell pathology, including aging. The aim of the present study is to reveal the differences of age-dependent metabolic controlling of cell hydration of excitable tissue such as brain cortex and non-excitable tissues such as liver and spleen. For this purpose, the age-dependent sensitivity of cell hydration in excitable and non-excitablet issues is studied through depressing metabolic activity by cooling and its activation by supplying animals with distilled water, by inactivation of Na^+/K^+ pump and activation of Na^+/Ca^{2+} exchange in the reverse mode. The obtained data bring us to the conclusion that the metabolic regulation of cell hydration in excitable tissue is realized by the activation of electrogenic Na^+/K^+ pump and Na^+/Ca^{2+} exchange in the cell membrane and the formation of endogen water by mitochondrial activity, while the regulation of cell hydration in non-excitable tissue is carried out only by the activity of mitochondrial function. Aging leads to an over-expression of Na^+/K^+ pump units in liver and Na^+/Ca^{2+} exchanger in brain cortex of rats.

Keywords

Rat, Hydration, Brain Cortex, Liver, Spleen, [^{3}H]-Ouabain

1. Introduction

Intracellular water, being the dominant component of cell and the common medium for intracellular metabolic reactions, has a determined role in the regulation of cell activity realizing by surface-dependent changes in the number of

functional active proteins in the membrane having enzyme, receptor, ionic channel properties [1] and hydration-dependent stimulation of intracellular macromolecules' activity [2]. Therefore, the dysfunction of metabolic controlling of cell hydration can be considered a common consequence of cell pathology, including aging. It is known that aging-induced dehydration of excitable tissues (ET), like brain cortex and heart muscle, leads to cell apoptosis or necrosis [3]. Although the non-excitable tissues (NET) such as liver and spleen are dehydrated in aging the dysfunction of their metabolic activity very often brings to over-hydration and increase of cell proliferation [4] [5]. It is also known that the membrane of NET cells is highly permeable for water molecules than for ions and has more pronounced volume of recovering mechanism than that in ET cells [5] [6].

Our previous study has shown that the metabolic water efflux from the cells serves as the key mechanism for controlling the low permeability of inward ionic currents through the membrane [7]. The dysfunction of Na^+/K^+ pump, being the common consequence of cell pathology, including aging can be considered as the main reason for age-dependent tissue dehydration. It is known that Na^+/K^+ pump generating Na^+ gradient on the membrane serves as the energy source for Na^+/Ca^{2+} and Na^+/H^+ exchangers in the membrane. As the cell membrane of NET is highly permeable for water as well as for H^+, the electrogenic properties of the Na^+/K^+ pump and Na^+/Ca^{2+} exchange are shunted by H^+ influx. So, it is suggested that Na^+/K^+ pump and Na^+/Ca^{2+} exchange are unable to generate the osmotic gradients on NET cells of the membrane, while in ET cell membrane they generate these gradients. Therefore, it is predicted that in the regulation of cell volume in ET cells involve the electrogenic ionic transporting mechanisms in the membrane and mitochondrial processes generating the water molecule release in cytoplasm. To check this hypothesis in the present work, the comparative study of the role of the membrane ion transporting mechanisms and the intracellular oxidative processes in age-dependent impairment of metabolic controlling of cell hydration in ET and NET in *in vivo* and in *in vitro* experiments are performed using different experimental conditions.

2. Materials and Methods

2.1. Animals

All procedures performed on animals were carried out following the protocols approved by Animal Care and Use Committee of Life Sciences International Postgraduate Educational Centre (LSIPEC, Yerevan, Armenia).

The experiments were performed on healthy young (6 weeks old, weighting ~35 g) and old (18 months old, weighting ~250 g) albino rats. They were regularly examined, kept under control of the veterinarians in LSIPEC and reserved in a specific pathogen-free animal room under optimum conditions of 12 h light/dark cycles, at temperature of 22˚C ± 2˚C, with a relative humidity of 50% and were fed *ad libitum* on a standard lab chow and water.

2.2. Chemicals

Tyrode's physiological solution (PS) containing (in mM) 137 NaCl, 5.4 KCl, 1.8 $CaCl_2$, 1.05 $MgCl_2$, 5 $C_6H_{12}O_6$, 11.9 $NaHCO_3$, and 0.42 NaH_2PO_4 and adjusted to pH 7.4 was used. PS with 50% of NaCl was received by replacing 68.5 mM of NaCl from 137 mM NaCl with 2 M mannitol dissolved in PS for maintaining the osmolarity of the solution. These two types of PS in corresponding figures named as 100% Na and 50% Na. All chemicals were obtained from "Medisar" Industrial Chemical Importation Company (Yerevan, Armenia). The distilled water (DW) was received in laboratory by means of corresponding apparatus. The [^{3}H]-ouabain with specific activity 25.34 Ci/mM (PerkinElmer, Massachusetts, USA) at 10^{-4}M, 10^{-9}M and cold (non-radioactive) ouabain at 10^{-4}M, 10^{-9}M were used for incubation and intraperitoneal (i/p) injections. The volume of injected solutions was adjusted according to the weight of animals (0.02 ml/g).

2.3. Tissue Preparation

The experimental data were received in *in vivo* and in *in vitro* conditions. The tissue samples from each experiment were investigated after decapitation. Since the anesthetics with different chemical and pharmacological profiles significantly affect the metabolic processes in tissues [8], [9] in our experiments the animals were sharply immobilized by freezing method [10] and decapitated. Full absence of somatic reflexes was recorded after this procedure. The brain cortex, liver, spleen tissues were isolated and dissected according to the corresponding experiments.

2.4. Experimental Design

The experiments of the first, second and third series were carried out in *in vivo* conditions. In each animal group (young and old) 6 rats were taken in all series of experiments. In the first series of experiments the animals of both young (n = 6) and old (n = 6) subgroups were i/p injected by PS (as a control). After 30 min the animals were decapitated and 5 samples were taken from each animal's brain cortex, liver and spleen tissues. Thus, from each tissue were received 30 samples of brain cortex, liver and spleen. They were divided into 2 parts (15 samples in each), which incubated for 30 min in PS at 20˚C and 7˚C, respectively. In experiments described below the tissue samples were taken after animal decapitation.

For the second series of experiments the data of control group (the tissue samples of which were incubated in PS at 20˚C) were compared with the corresponding data of young as well as of old experimental animal groups being i/p injected with [^{3}H]-ouabain at 10^{-4}M. In these experimental groups 3 young and 3 old rats were taken and the number of samples from each investigated tissue was the same as it is mentioned above.

The third series of experiments were carried out like the second one but the animals of experimental groups were i/p injected with [^{3}H]-ouabain at 10^{-9}M. The obtained data were compared with the same data of control group as in the

second series.

The 4th-6th series of experiments were made in *in vitro* conditions. From 6 animals of each group (young and old) 5 samples of each tissue were taken. So, 30 samples from each tissue were divided into 2 parts (15 samples in each), which were incubated for 30 minutes in the two types of PS (100% Na and 50% Na) in addition to them the radioactive Ca ($^{45}Ca^{2+}$). The 5th and 6th series were performed in the same way as the 4th one and in each corresponding PS (with ^{45}Ca) where incubated their tissue samples were also added the non-radioactive ouabain at 10^{-4}M (5th series) and 10^{-9}M (6th series), respectively.

The 7th-9th series of experiments were carried out on animals drinking (for 10 days) the distilled water (DW) and after being i/p injected by PS. In each series 3 young and 3 old animals were taken. The obtained data from 7th series were compared with that received in the 1st series (data from tissue samples of animals were incubated in PS at 20˚C). After 10 days of drinking DW the animals of 8th and 9th series were being i/p injected by [^{3}H]-ouabain at 10^{-4}M (8th series) and 10^{-9}M (9th series), respectively. The results of these experiments were compared with the corresponding data received in 2nd and 3rd series, respectively.

2.5. Definition of Water Content of Brain Tissues

The water content of brain cortex, liver and spleen tissues was determined by traditional "tissue drying" method [11]. After measuring the wet weight (w.w.) of tissue samples they were dried in oven (Factory of Medical Equipment, Odessa, Ukraine) for 24 h at 105˚C for determination of dry weight (d.w.). The quantity of water in 1 g of d.w. tissue was counted by the following equation: (w.w.–d.w.)/d.w.

2.6. Counting of [^{3}H]-Ouabain Molecules

The tissue samples in *in vivo* experiments, which were subjected to [^{3}H]-ouabain, were homogenized in 50 µl of 68% HNO_3 solution after determination of wet and dry weights. Then 2 ml of Bray's scintillation fluid was added and chemo luminescence of samples was quantified with 1450-Micro Beta liquid scintillation counter (Wallac, Turku, Finland). The number of [^{3}H]-ouabain molecules' binding with cell membranes was defined per mg of dry weight of samples. The same procedure (the definition of number of [^{3}H]-ouabain molecules) was performed on the tissue samples from in *in vitro* experiments after removing them from the oven and determining their water content.

2.7. Measurement of $^{45}Ca^{2+}$ Uptake

PS with the radioactive $^{45}Ca^{2+}$ (PerkinElmer, Massachusetts, USA) was received by substituting 0.0115 mM of $CaCl_2$ from 1.8 mM $CaCl_2$ by radioactive one (with 11.2 mCi/l activity). The measurement of $^{45}Ca^{2+}$ uptake was carried out as in the case of definition of [^{3}H]-ouabain molecules. The quantity of $^{45}Ca^{2+}$ in tissue slices was expressed by cpm/mg d. w.

2.8. Statistical Analysis

Microsoft Excel and Sigma-Plot (Version 8.02A, NY, USA) were used for data analyses. The statistical significance in comparison with the control group was calculated with Student's t-test with the following symbols (*$p < 0.05$; **$p < 0.01$; ***$p < 0.001$).

3. Results

It is known that aging is connected with the dysfunction of metabolic processes in the living objects. In order to find out the difference between the metabolic sensitivity of tissues, the effect of cold (7˚C) PS on ET and NET hydration of young and old animals are studied. As can be seen in **Figure 1**, in the group of young as well as old animals i/p injected by PS, the incubation of brain cortex tissue samples in cold PS lead to significant dehydration (**Figure 1(a)**), while in liver and spleen tissues it brings to pronounced opposite effect, *i.e.* to over-hydration (**Figure 1(b)** and **Figure 1(c)**).

It is worth to note that the temperature-dependent tissue hydration has more pronounced age-dependent increasing character in the brain and liver tissues (**Figure 1(a)** and **Figure 1(b)**), while in the spleen tissues the temperature sensitivity of tissue hydration is higher in young animals than in the old ones (**Figure 1(c)**).

The previous research data have established the key role of Na^+/K^+ pump in the regulation of cell volume [1] [7] [12]. To estimate the age-dependent effect of Na^+/K^+ pump on cell hydration and ouabain binding in the second series of experiments the effect of i/p injected [^{3}H]-ouabain at 10^{-4}M in ET and NET is studied. The received data have been compared with those of animal group i/p injected by PS (data of black bars in **Figure 1**). At first sight, the opposite results of water content can be noted in ET (brain cortex) and NET (liver, spleen) in young as well as in old animals, *i.e.* the increase of water content (**Figure 2(a)**)

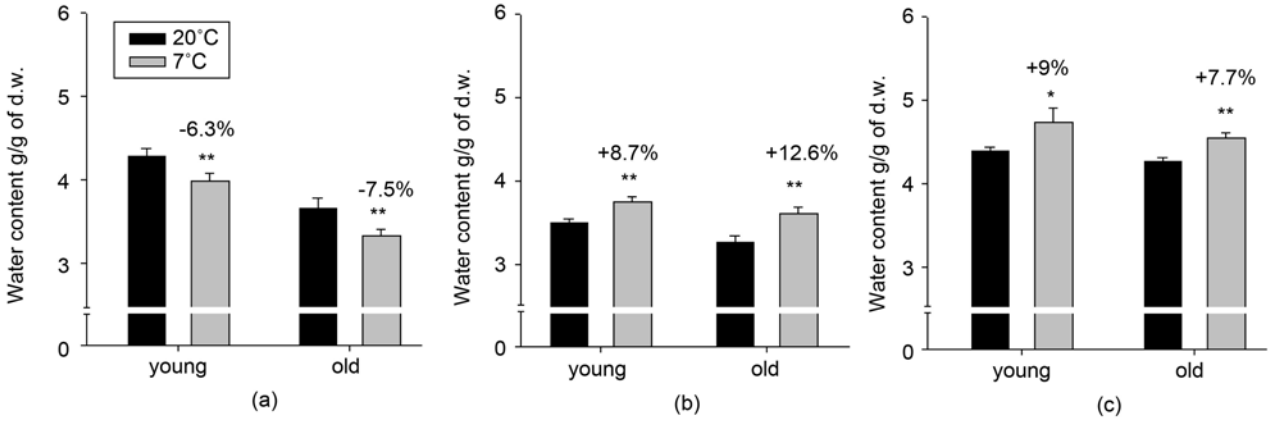

Figure 1. The variation of water content in brain cortex, liver and spleen tissue samples after their incubation in PS at 20˚C (black bars) and 7˚C (gray bars), respectively. Each bar represents the mean ± SEM (n = 45). The symbols (*), (**) indicate $p < 0.05$ and $p < 0.01$, respectively. The numbers in % indicate the difference between levels of hydration in each group. All data were obtained from three independent experiments.

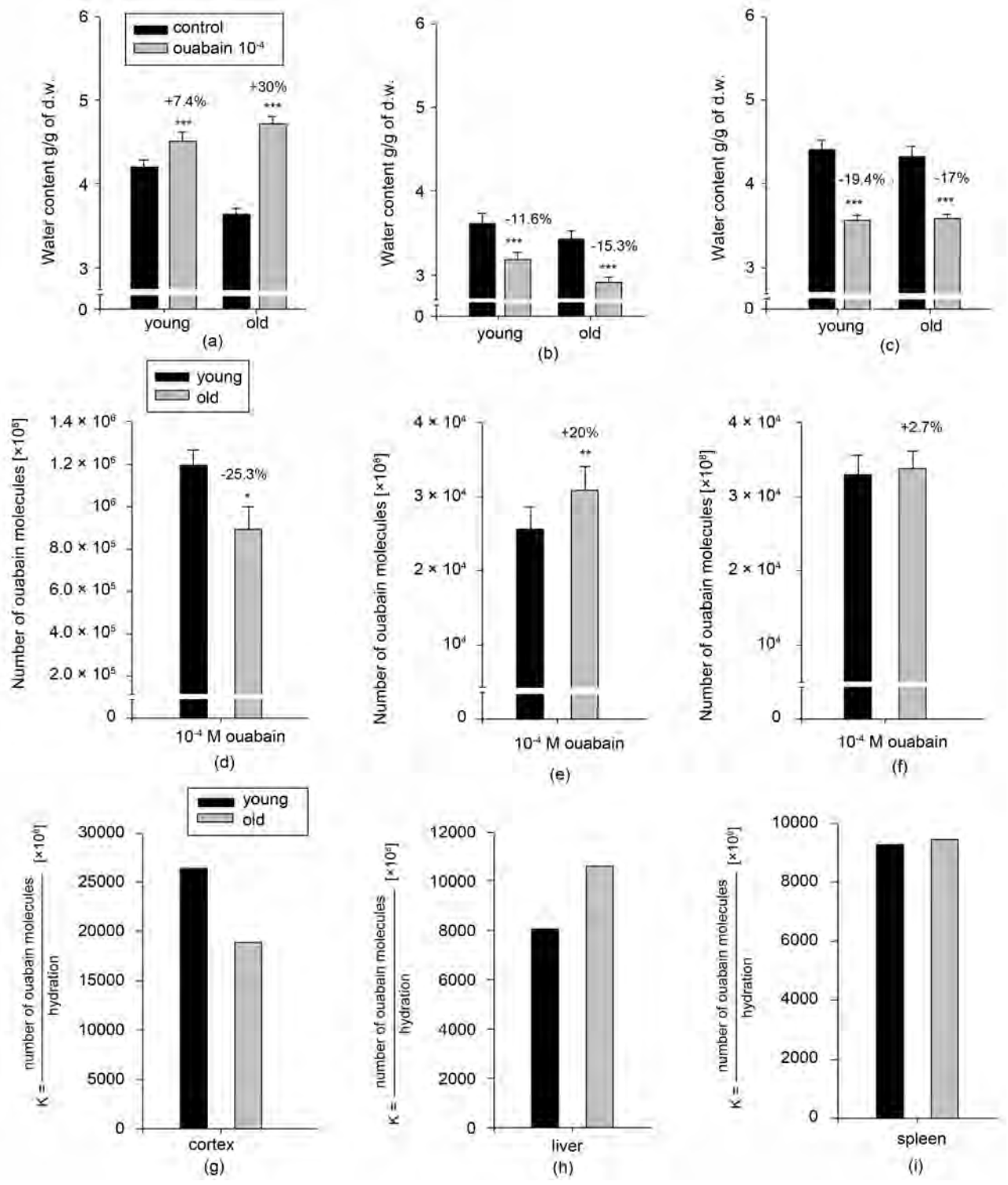

Figure 2. The effect of [^{3}H]-ouabain at 10^{-4}M on water content and number of ouabain molecules in brain cortex, liver and spleen tissues. Black bars on (a)-(c) indicate the mean value of water content in the tissues of control animal group (i/p injected by PS). Gray bars on (a)-(c) indicate the mean value of water content in the tissues of experimental animal group (i/p injected by [^{3}H]-ouabain at 10^{-4}M). Each bar represents the mean ± SEM (n = 45). (d)-(f) demonstrate the number of ouabain molecules in young (black bars) and old (gray bars) animal tissues. The numbers in % indicate the difference between levels of hydration and the number of ouabain molecules. (g)-(i) indicate the ratio between the number of ouabain molecules and the level of water content. The symbol (***) indicates $p < 0.005$. All the data were obtained from three independent experiments.

in ET and its decrease in NET (**Figure 2(b)**, **Figure 2(c)**). As can be seen in **Figure 2(a)**, the over-hydration is more pronounced in the brain cortex tissue of old animals than in young ones. The effect of dehydration in liver tissue of old animals (**Figure 2(b)**) is higher than that in young animals, while in spleen tissue the percent of dehydration is higher in case of young animals in comparison to the old ones (**Figure 2(c)**). From these data it is suggested that on the basis of cell hydration in ET and NET lay different mechanisms.

In spite of the fact that [^{3}H]-ouabain at 10^{-4}M in ET of old animals leads to more expressed over-hydration than that in young ones, the number of ouabain molecules in cortex tissue of old animals is lower than in young ones (**Figure 2(d)**). As for the ouabain binding in NET (**Figure 2(e)**, **Figure 2(f)**), it must be noted that the number of ouabain molecules in old animal tissues is higher than in young ones. The coefficients reflecting the ratio between the number of ouabain molecules and cell hydration (**Figure 2(g)**, **Figure 2(h)**) are similar to those of corresponding ratio between their numbers of ouabain molecules (**Figure 2(d)**, **Figure 2(f)**).

The previous data [13] have observed that nM ouabain stimulates Na^+/Ca^{2+} exchange in the reverse (R) mode and leads to age-dependent weakening of hydration effect in ET. To find out the role of RNa^+/Ca^{2+} exchange in the regulation of NET cell hydration and its age-dependency, in the next (3rd) series of experiments the comparative study of i/p injection of nM[^{3}H]-ouabain is studied. As in case of the abovementioned experiments (**Figure 2**), the injection of nM [^{3}H]-ouabain brings to the same results: the increase of water content in ET (**Figure 3(a)**) and its decrease in NET (**Figure 3(b)**, **Figure 3(c)**). As can be seen in **Figure 3(a)**, the over-hydration in ET of young animals is higher than that in ET of old ones, but the number of ouabain molecules in ET of old animals is higher than that in ET of young ones (**Figure 3(d)**). The ouabain binding in NET (**Figure 3(e)**, **Figure 3(f)**) demonstrates the correlation between the level of hydration and the number of ouabain molecules. Clearer correlation between the number of ouabain molecules binding with membrane and its cell hydration can be detected by means of the coefficients determined their relationship (**Figure 3(g)**, **Figure 3(i)**).

It is known that the decrease of Na gradient on the cell membrane leads to the activation of RNa^+/Ca^{2+} exchange [14]. In order to check the sole role of Na^+/Ca^{2+} exchange in the next (4th) series of experiments, the variation of hydration and $^{45}Ca^{2+}$ uptake in tissues are investigated by incubation of tissue samples in 100% Na and 50% Na PS. As can be seen in **Figure 4**, the incubation of tissue samples in 50% Na PS with $^{45}Ca^{2+}$ leads to the dehydration in ET of young and old animals (**Figure 4(a)**). The same effect is observed in liver tissue of young animals (**Figure 4(b)**) and also in the spleen tissue of young and old ones (**Figure 4(c)**). In liver tissue of old animals there is weak increase of hydration (**Figure 4(b)**). There must be checked the increase of $^{45}Ca^{2+}$ uptake in ET and its high level in ET of old animals than that in ET of young ones (**Figure 4(d)**). The decrease of $^{45}Ca^{2+}$ uptake in 50% Na PS is observed in NET of young rats (**Figure 4(e)**,

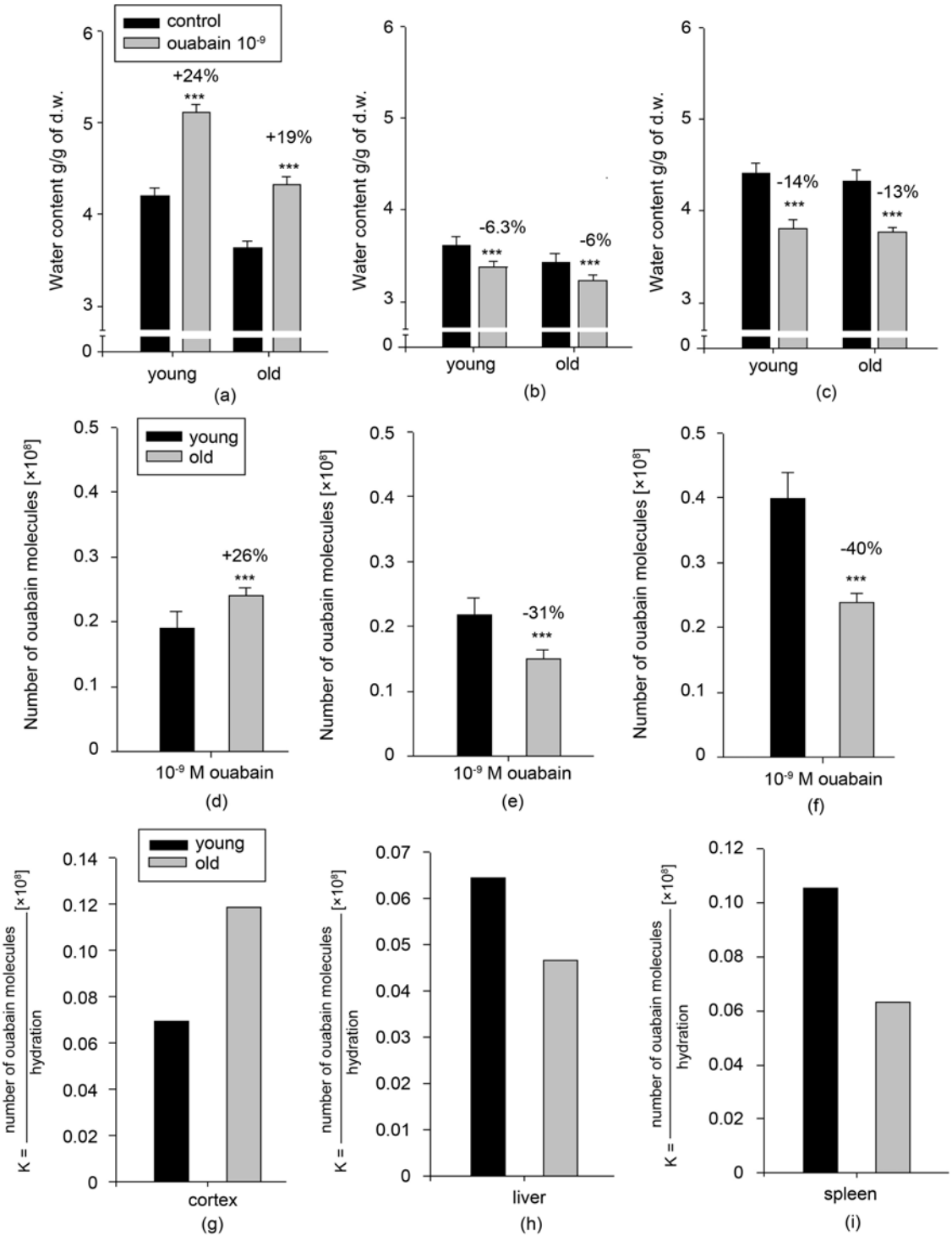

Figure 3. The effect of [^{3}H]-ouabain at 10^{-9}M on water content and number of ouabain molecules in brain cortex, liver and spleen tissues. Black bars on (a)-(c) indicate the mean value of water content in the tissues of control animal group (i/p injected by PS). Gray bars on (a)-(c) indicate the mean value of water content in the tissues of experimental animal group (i/p injected by [^{3}H]-ouabain at 10^{-9} M). Each bar represents the mean ± SEM (n = 45). (d)-(f) demonstrate the number of ouabain molecules in young (black bars) and old (gray bars) animals' tissues. The numbers in % indicate the difference between levels of hydration and the number of ouabain molecules. (g)-(i) indicate the ratio between the number of ouabain molecules and the level of water content. The symbol (***) indicates $p < 0.005$. All data were obtained from three independent experiments.

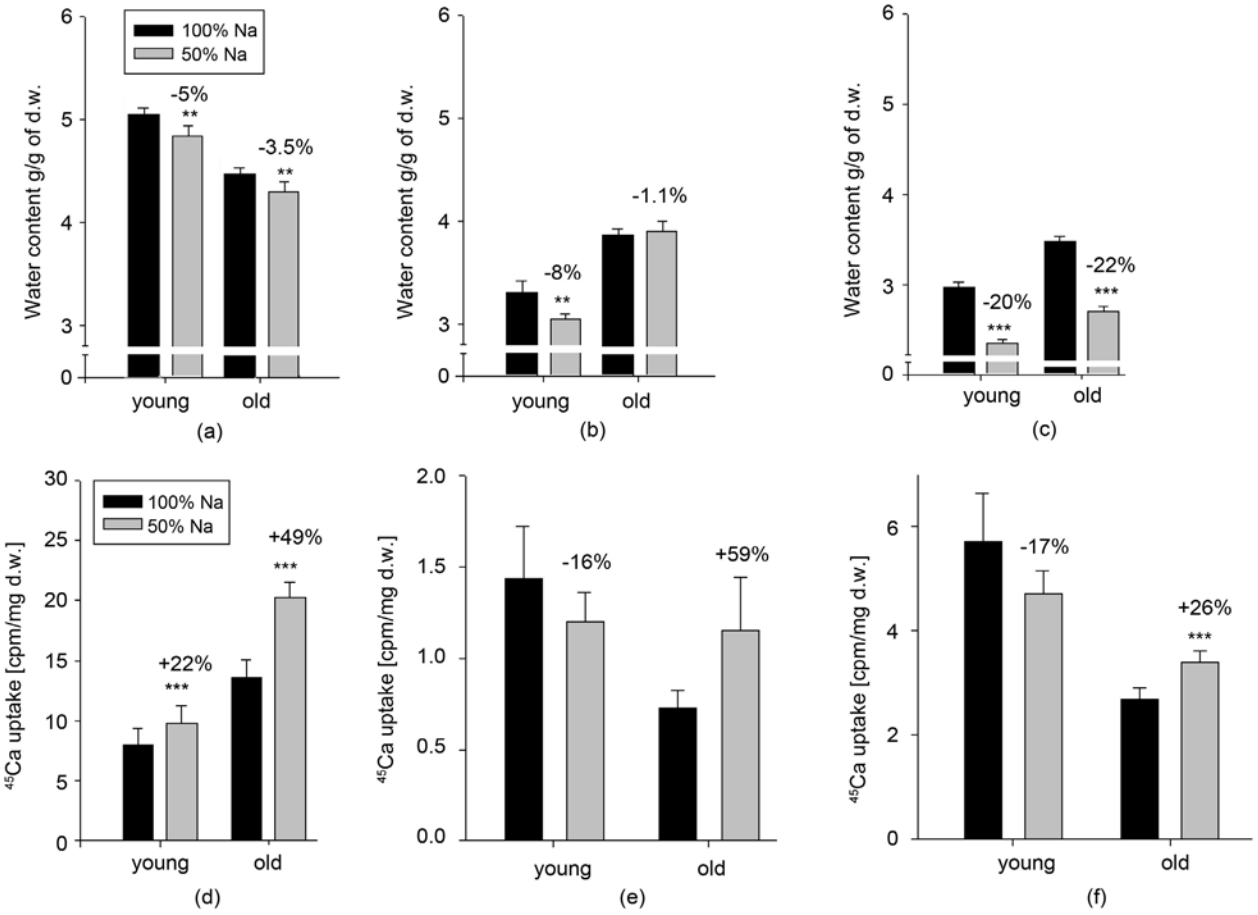

Figure 4. The comparative study of water content (a)-(c) and $^{45}Ca^{2+}$ uptake (d)-(f) in brain cortex, liver and spleen tissues samples incubated in 100% Na PS (black bars) and in 50% Na PS (gray bars). Each bar represents the mean ± SEM (n = 45). The symbols (**) and (***) indicate $p < 0.01$ and $p < 0.005$, respectively. The numbers in % indicate the difference between levels of hydration and $^{45}Ca^{2+}$. All data were obtained from three independent experiments.

Figure 4(f)) and the opposite effect (expressed increase of $^{45}Ca^{2+}$ uptake in 50% Na PS) is received in the same tissues of old animals (Figure 4(e), Figure 4(f)).

To estimate the role of Na^+/K^+ pump in the next (5^{th}) series in incubated solutions, besides $^{45}Ca^{2+}$, there is added non radioactive ouabain at 10^{-4}M. In such case the water content in all investigated tissues (after their incubation in 50% Na PS) is decreased (Figure 5(a), Figure 5(c)). The $^{45}Ca^{2+}$ uptake in ET of young rats is slowly decreased but it is expressively increased in ET of old ones (Figure 5(d)). In liver tissue of young and old rats $^{45}Ca^{2+}$ uptake is decreased (Figure 5(e)), meanwhile in spleen tissue (Figure 5(f)) it has smaller increase in tissues of young animals and expressively higher increase in tissues of old ones.

In the next group of animals (6^{th} series) the effect of nM non-radioactive ouabain is studied. In such conditions the water content in all investigated tissues incubated in 50% Na PS obviously decreases (Figure 6(a), Figure 6(c)) and is very expressive both in young and old rats' spleen tissues (Figure 6(c)). The $^{45}Ca^{2+}$ uptake in brain cortex tissue of young and old rats is expressively increased in 50% Na PS. The identical data have been received in liver tissue of old

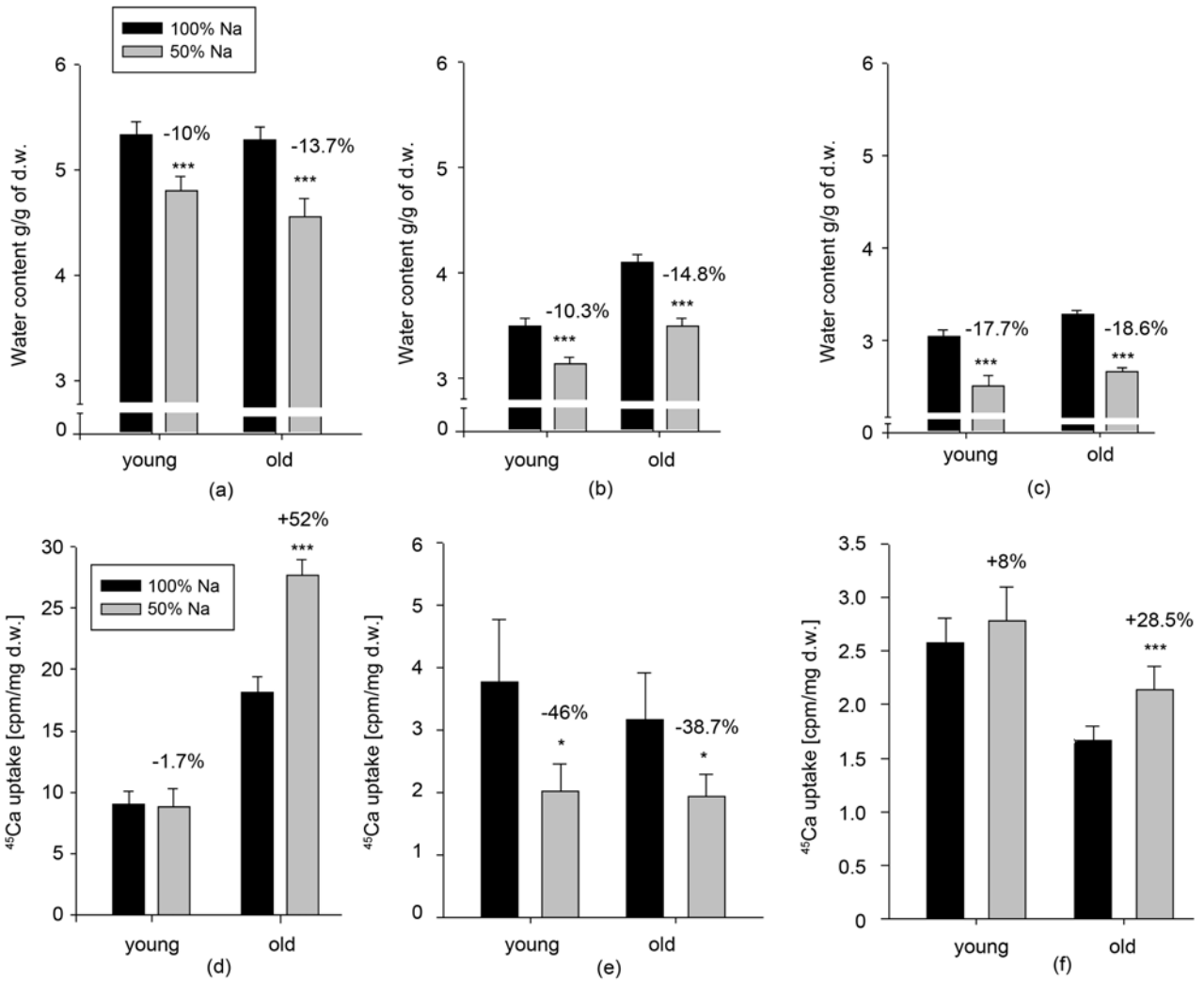

Figure 5. The variation of water content and $^{45}Ca^{2+}$ uptake in tissue samples incubated in 100% Na PS (black bars) and 50% Na PS (gray bars) in addition to non radioactive ouabain at 10^{-4} M ouabain. (a)-(c) the data of water content in brain cortex (a), liver (b) and spleen (c) tissues' samples. (d)-(f) data of $^{45}Ca^{2+}$ uptake in brain cortex (d), liver (e) and spleen (f) tissues. Each bar represents the mean ± SEM (n = 45). The symbols (*) and (***) indicate $p < 0.05$ and $p < 0.005$, respectively. The numbers in % indicate the difference between levels of hydration and $^{45}Ca^{2+}$. All data were obtained from three independent experiments.

animals (Figure 6(e)). The variation of $^{45}Ca^{2+}$ uptake in liver tissue of young animals is not so different in comparison with that in 100% Na PS (Figure 6(e)). The $^{45}Ca^{2+}$ uptake in spleen tissue of young rats in 50% Na PS is higher than that in 100% Na PS (Figure 6(f)). As for the $^{45}Ca^{2+}$ uptake, in spleen tissue of old animals it is lower in 50% Na PS than that in 100% Na PS (Figure 6(f)).

Previously it has been shown that cell swelling leads to the stimulation of cell metabolism by the increase of membrane functionally active protein molecules [12].

To evaluate the metabolic dependency of ET and NET hydration and their age dependency in the next (7^{th}) series of experiments the tissue hydration of animals drinking DW for 10 days is studied. After this the rats are i/p injected by PS and the results of these experiments are compared with that received in control

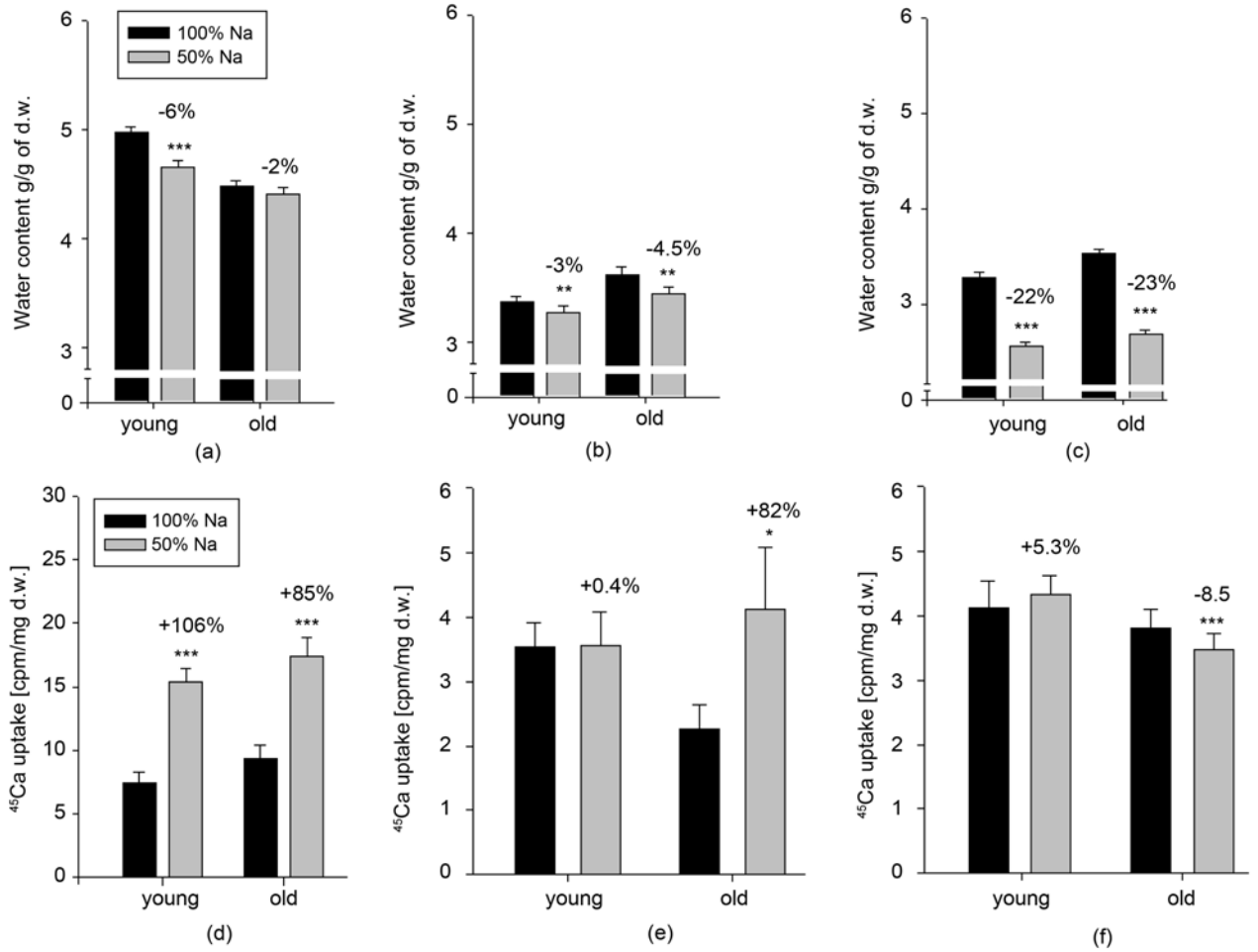

Figure 6. The variation of water content and $^{45}Ca^{2+}$ uptake in tissue samples incubated in 100% Na PS (black bars) and 50% Na PS (gray bars) in addition to non radioactive ouabain at 10^{-9} M ouabain. (a)-(c) the data of water content in brain cortex (a), liver (b) and spleen (c) tissue samples. (d)-(f) data of $^{45}Ca^{2+}$ uptake in brain cortex (d), liver (e) and spleen (f) tissues. Each bar represents the mean ± SEM (n = 45). The symbols (**) and (***) indicate $p < 0.01$ and $p < 0.005$, respectively. The numbers in % indicate the difference between levels of hydration and $^{45}Ca^{2+}$ uptake. All data were obtained from three independent experiments.

groups of animals drinking the tap water and also being injected by PS (**Figure 1**, black bars). In **Figure 7** can be seen that in such experimental conditions the hydration process in ET and NET is also different. In ET the over-hydration is observed both in young as well as in old animals (**Figure 7(a)**), but in NET the opposite effect (dehydration) is demonstrated (**Figure 7(b)**, **Figure 7(c)**).

To evaluate the role of Na^+/K^+ pump on tissue hydration and ouabain binding in the next series the new animal groups are taken. Each (young and old) group of animals drinks DW (as it was shown above) and then is i/p injected by [^{3}H]-ouabain at 10^{-4}M. Data of hydration and ouabain binding are compared with that received in similar experiments where the animals drink tap water and are also i/p injected by [^{3}H]-ouabain at 10^{-4}M (**Figure 2**). The results of this comparative data are different. As can be seen in **Figure 8** in the brain cortex tissue of young animals (drinking DW) over-hydration is observed, while in the similar group of old animals the opposite effect (dehydration) is demonstrated

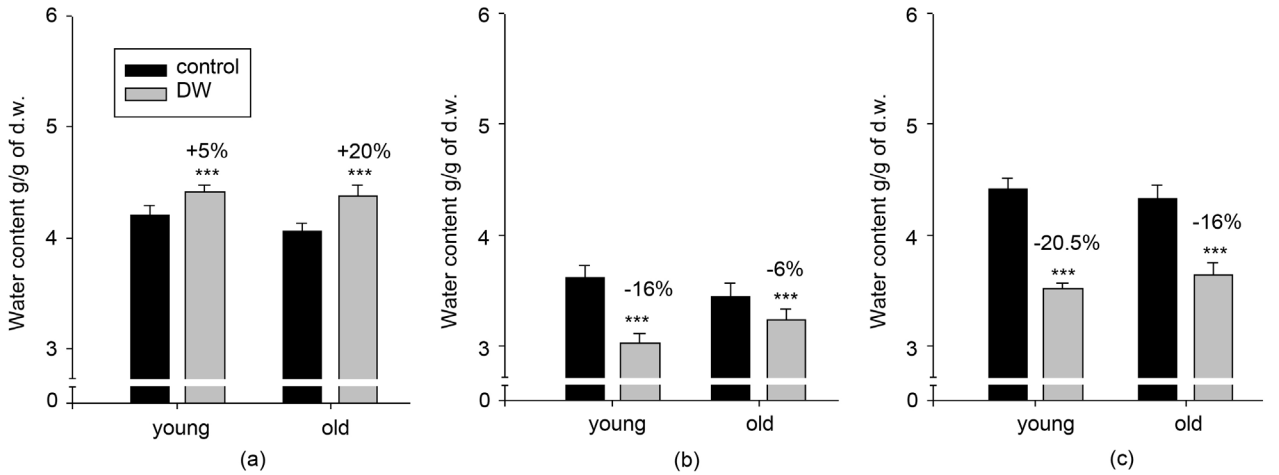

Figure 7. The variation of water content in brain cortex (a), liver (b) and spleen (c) tissues. Black bars indicate the mean value of water content in the tissues of control animal group drinking the tap water and being i/p injected with PS. Gray bars indicate the mean value of water content in the tissues of experimental animal group drinking DW and being i/p injected with PS. Each bar represents the mean ± SEM (n = 45). The symbol (***) indicates $p < 0.005$. The numbers in % indicate the difference between levels of hydration. All data were obtained from three independent experiments.

(Figure 8(a)). In liver tissue of young animals the small dehydration and in old rats an over-hydration are revealed (Figure 8(b)). In spleen tissues of both animal groups weak over-hydration is observed (Figure 8(c)). As for the ouabain binding, it must be noted that in brain cortex and liver tissues of young and old rats (drinking DW) the number of ouabain molecules in cell membrane has significantly been decreased (Figure 8(d), Figure 8(e)) and is expressively low in brain cortex tissue (Figure 8(d)) compared with that of animals drinking tap water. In spleen tissue of young rats the number of ouabain molecules increases but in old ones it decreases (Figure 8(f)). The coefficients of relationship of number of ouabain molecules and the level of hydration in brain cortex of young and old animals are nearly equal to each other (Figure 8(g)). In liver tissue of young rats it is lower compared with that in old ones (Figure 8(h)) and in spleen tissue (Figure 8(i)) this coefficient in young rats is higher than that in old ones. Another data have been received when the identical experiments have been carried out in animals drinking DW but being i/p injected by [^{3}H]-ouabain at 10^{-9}M. The data of these experiments have been compared with similar data where animals drink tap water and are injected by [^{3}H]-ouabain at 10^{-9}M. (Figure 9(a), Figure 9(c)) shows that in ET as well as in NET significant dehydration is observed. Besides, there is a sharp correlation between hydration and binding of ouabain molecules in all investigated tissues (Figure 9(d), Figure 9(f)). It must be noted that the decrease of number of ouabain molecules in young animals' liver and spleen tissues was more pronounced than that in old ones (Figure 9(e), Figure 9(f)). The ratio of the number of ouabain molecules to the level of water content is most pronounced in tissues of brain cortex and liver of old animals (Figure 9(g), Figure 9(h)) and, on the contrary, in the spleen tissue of young rats this ratio is higher (Figure 9(i)) than that in the old ones.

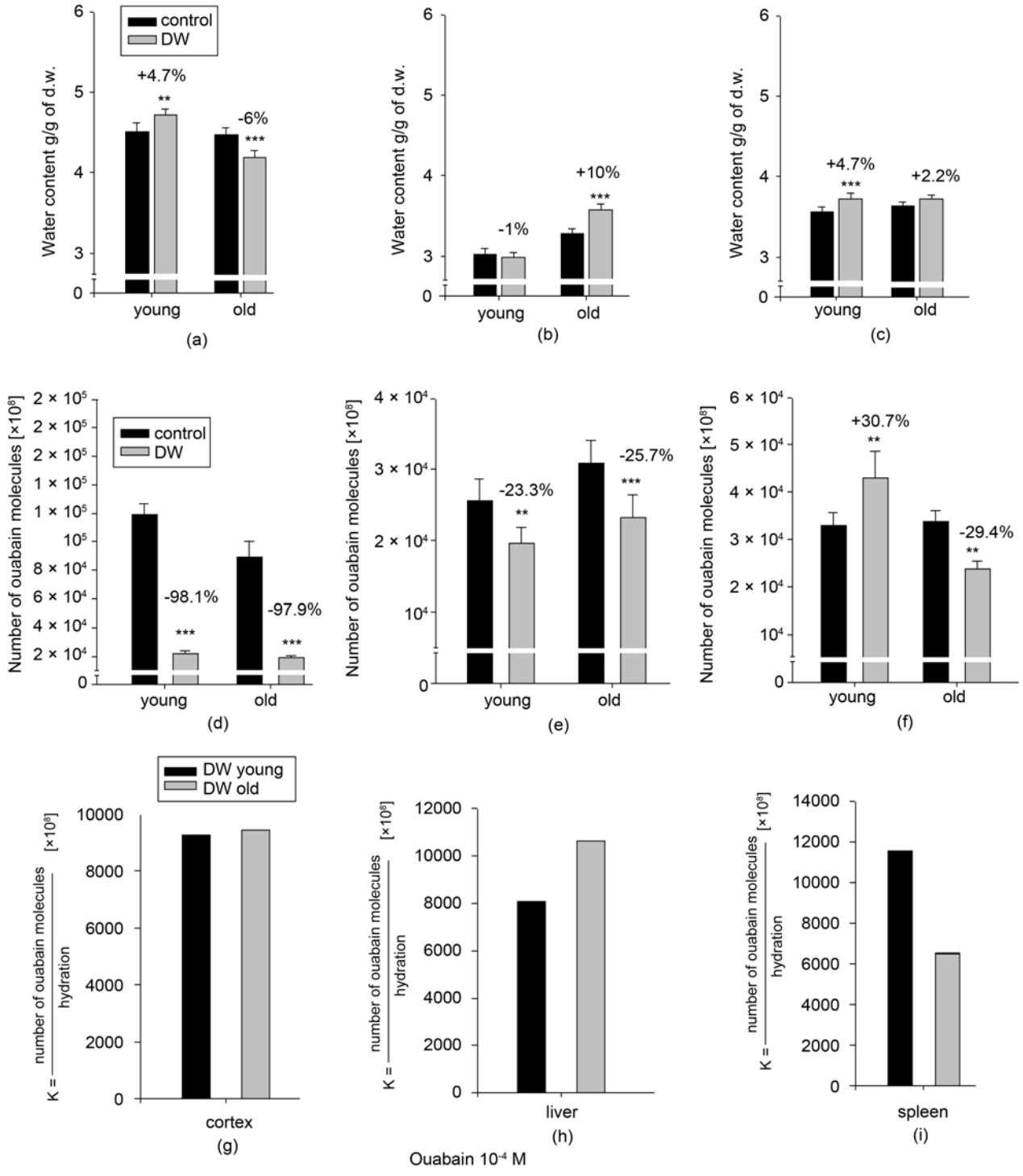

Figure 8. The effect of 10^{-4}M ouabain on hydration and ouabain binding in brain cortex, liver and spleen tissues. Black bars on (a)-(c) indicate the mean value of water content in the tissues of control animal group (i/p injected with [^{3}H]-ouabain at 10^{-4}M). Gray bars on (a)-(c) indicate the mean value of water content in the tissues of experimental animal group drinking DW and after 10 days being i/p injected with [^{3}H]-ouabain at 10^{-4}M. (d)-(f) demonstrate the number of ouabain receptors in tissues of young (black bars) and old (gray bars) animals. Each bar represents the mean ± SEM (n = 45). The symbols (**) and (***) indicate $p < 0.01$ and $p < 0.005$, respectively. The numbers in % indicate the difference between levels of hydration and the number of ouabain molecules. (g)-(i) indicate the ratio between the numbers of ouabain molecules and the level of water content. All data were obtained from three independent experiments.

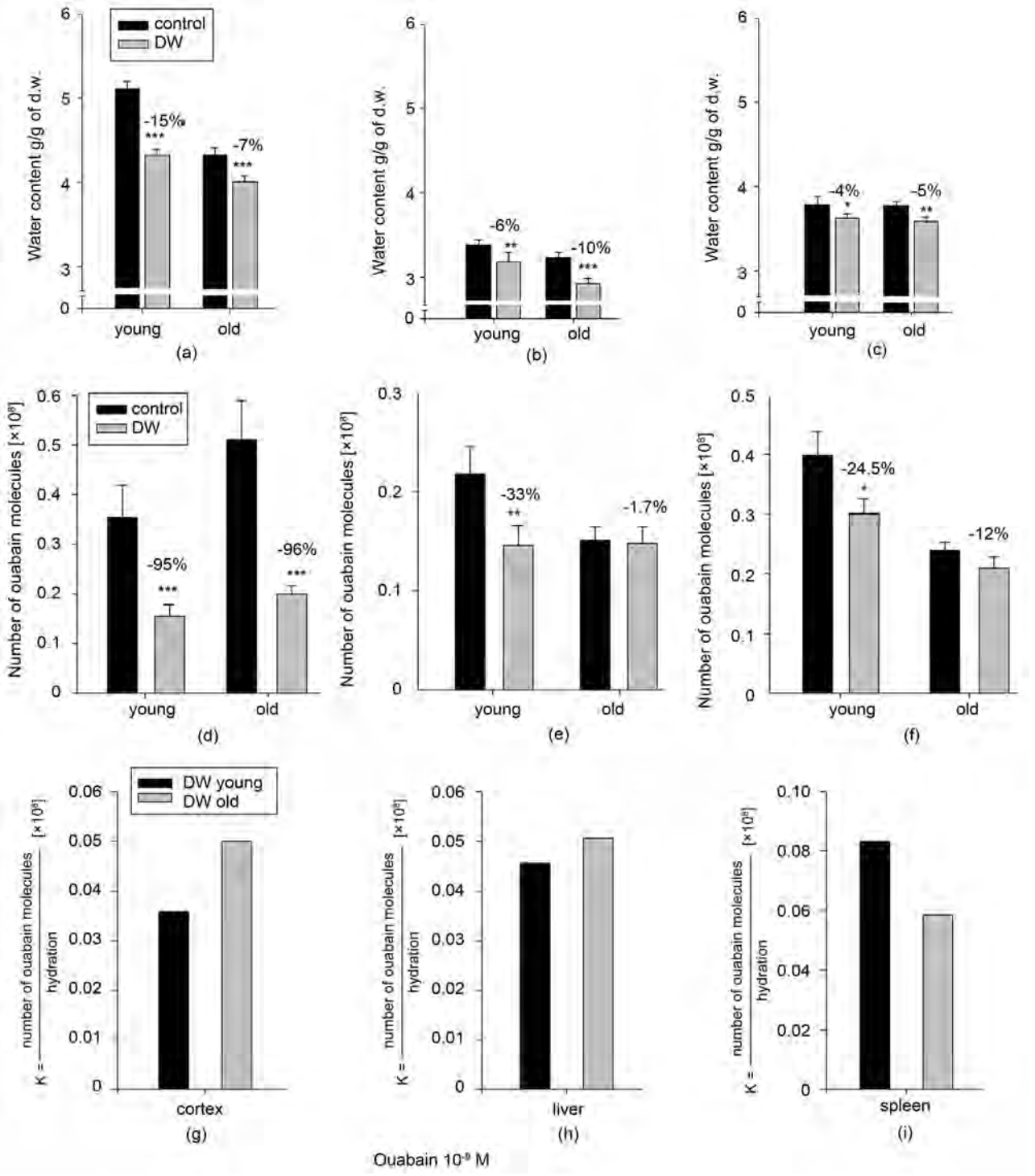

Figure 9. The effect of 10^{-9} M ouabain on hydration and ouabain binding in brain cortex, liver and spleen tissues. Black bars on (a)-(c) indicate the mean value of water content in the tissues of control animal group (i/p injected with [^{3}H]-ouabain at 10^{-9}M). Gray bars on (a)-(c) indicate the mean value of water content in the tissues of experimental animal group drinking DW and after 10 days being i/p injected with [^{3}H]-ouabain at 10^{-9}M. (d)-(f) demonstrate the number of ouabain receptors in tissues of young (black bars) and old (gray bars) animals. Each bar represents the mean ± SEM (n = 45). The symbols (*), (**) and (***) indicate $p < 0.05$, $p < 0.01$ and $p < 0.005$, respectively. The numbers in % indicate the difference between levels of hydration and the number of ouabain molecules. (g)-(i) indicate the ratio between the number of ouabain molecules and the level of water content. All data were obtained from three independent experiments.

4. Discussion

The obtained data that the cooling leads to dehydration in ET and hydration in NET (**Figure 1**) can be explained by low and high permeability of cell membrane for water in ET and NET, respectively. In neuronal tissue (ET) the ionic transporting systems (such as Na^+/K^+ pump and Na^+/Ca^{2+} exchange) are able to generate the osmotic gradients on the cell membrane, while NET cells are unable to generate these gradients on their membranes because of high proton (H^+) permeability [5]. Therefore, the generation of water efflux in ET cells takes place due to the activation of electrogenic ion transporting mechanisms as well as by endogen water formation in process of intracellular oxidation, while in NET cells the water efflux generates only by the formation of the endogen water. From this point of view, it is clear that there are different effects of cooling on ET and NET hydrations. Cooling dehydration effect in ET can be explained by the reciprocal correlation between Na^+/K^+ pump and RNa^+/Ca^{2+} exchange [14]. The cooling induced depression of electrogenic Na^+/K^+ pump activity leads to the activation of RNa^+/Ca^{2+} exchange, which is less sensitive to temperature because of its diffusion nature. Thus, ET dehydration by cooling can be explained by the activation of RNa^+/Ca^{2+} exchange leading to $[Ca]_i$-induced sol-gel transition of cytoplasm by formation of actin networks mediated by actin binding proteins of intracellular filaments and cytoskeleton [15]. The cooling-induced hydration of NET can be a result of depression of intracellular oxidative processes and production of endogen water. The latter has induced the water efflux from the cells, which besides balancing the water uptake has in hibitory effect on diffusion of osmolytes by cells (**Figure 1(b)**, **Figure 1(c)**).

It is well established that Na^+/K^+-ATPase in ET cells has three catalytic isoforms with different affinity to ouabain (inhibitor for Na^+/K^+-ATPase), while in NET cells only the low affinity isoforms (α_1) are expressed [16]. The obtained data indicate that 10^{-4} M ouabain (agonist for α_1 isoform) induces Na^+/K^+ pump inactivation and also leads to the opposite effect on ET and NET hydrations: hydration in the brain cortex and dehydration in the liver and spleen tissues (**Figure 2**). At first sight reverse effects of cooling and [^{3}H]-ouabain at 10^{-4}M on hydration of tissues are controversial to the abovementioned explanation of cooling effect. The Na^+/K^+ pump inhibition on the one side leads to hydration and on the other side to dehydration effect by activation of the RNa^+/Ca^{2+} exchange. In tissues of old animals the initial $[Ca]_i$ level is higher [17] than that in the same tissues of young ones where the rate of RNa^+/Ca^{2+} exchange is low. Therefore, in old animals the brain cortex hydration induced by Na/K pump is more pronounced than that in young animals' brain cortex tissue (**Figure 2(a)**). The dehydration effect in NET induced by Na^+/K^+ pump inhibition can be explained by the decrease of intracellular pH, which brings to the depression of water extrusion from mitochondria [18].

In spite of the fact that [^{3}H]-ouabain at 10^{-4}M in old animals' brain cortex leads to more pronounced hydration effect than that in young ones, the ouabain

binding with cell membrane is decreased in old animals (**Figure 2(d)**). In earlier experiments can be observed that there is a positive correlation between membrane surface and the number of ouabain binding sides in the membrane [12], while the affinity of these receptors to ouabain decreases by the increase of $[Ca]_i$ [19]. Therefore, the decrease of ouabain binding in the brain cortex of old animals compared with that of young ones can be explained by high $[Ca]_i$ in old animals' tissue [17]. It is remarkable that there is an age-dependent increase of ouabain receptors' expression in NET which is more pronounced in liver (**Figure 2(e)**) than in spleen tissue (**Figure 2(f)**).

It is known that the effect of $[^3H]$-ouabain at 10^{-9}M (compared with $[^3H]$-ouabain at 10^{-4}M) has no different effect on Na^+/K^+ pump activity and brings to the activation of RNa^+/Ca^{2+} exchange accompanied by the increase of cAMP in neurons [20]. As the experiments have showed $[^3H]$-ouabain at 10^{-9}M leads to hydration effect on brain cortex and dehydration on liver and spleen cells (**Figure 3(a)**, **Figure 3(c)**). It must be noted that at this ouabain concentration in brain cortex tissue of old animals the age-dependent increase of α_3 isoforms have been observed (**Figure 3(d)**), which is opposite to the effect of $[^3H]$-ouabain at 10^{-4}M (**Figure 2(d)**). In NET there is an age-dependent dehydration effect, which can be explained by cAMP-dependent activation of Ca-pump in the membrane of endoplasmic reticulum (ER), which through ER-mitochondria junction stimulates the generation of water efflux from mitochondria, which leads to transition from sole into gale state [15]. The data of ouabain binding decrease in aging in NET can be explained by accumulation of $[Ca]_i$ because of weakening of cAMP-dependent Ca pump in ER membrane (**Figure 3(e)**, **Figure 3(f)**).

The results in *in vitro* experiments, where the slices of ET and NET have been incubated in 100% and 50% NaCI containing PS with $^{45}Ca^{2+}$, and their metabolic state is depressed, the similar effects have been demonstrated in the brain cortex tissue hydration as in case of cooling (**Figure 1(a)**), the brain cortex tissue is dehydrated (**Figure 4(a)**). In NET, with the exception of liver tissue of old rats, the pronounced dehydration effect has been observed (**Figure 4(b)**, **Figure 4(c)**).

The age-dependent weakening of ET hydration (**Figure 4(a)**) when the concentration of $[Na]_o$ decreased, is accompanied with the activation of the RNa^+/Ca^{2+} exchange. This tissue dehydration brings the $^{45}Ca^{2+}$ uptake to increase in young as well as in old animals (**Figure 4(d)**), but in old animals the level of $^{45}Ca^{2+}$ uptake is higher than that in young ones (because of high content of $[Ca]_i$ in their brain cortex tissue). However, such correlation between the $^{45}Ca^{2+}$ uptake and tissue hydration in liver and spleen tissues are absent (**Figure 4(e)**, **Figure 4(f)**). In NET the decrease of $[Na]_o$ leads to dehydration in young animals, which accompanied by decrease of $^{45}Ca^{2+}$ uptake by cells, while in old animals' liver tissue there is non-significant increase of the $^{45}Ca^{2+}$ uptake (**Figure 4(e)**). Although in the spleen tissue the pronounced dehydration effect has been

observed (**Figure 4(c)**), the results of the $^{45}Ca^{2+}$ uptake are similar to that in liver tissue (**Figure 4(f)**). The data that the initial the $^{45}Ca^{2+}$ uptake by brain cortex tissue is higher than that in NET and the absence of activation effect of decreased $[Na]_o$ on the $^{45}Ca^{2+}$ uptake in young animals allow us to suggest on the non essential direct effect of RNa^+/Ca^{2+} exchange in metabolic regulation of cell hydration in NET. The non significant effect of decreased $[Na]_o$ on NET hydration, which accompanied by the increase of $^{45}Ca^{2+}$ uptake in old animals, probably can by explained by the activation effect of calmodulin on Na^+/Ca^{2+} exchange in the forward mode, which leads to replace the intracellular $^{40}Ca^{2+}$ by $^{45}Ca^{2+}$. This suggestion cannot be final and needs to have a special investigation.

The data of $[^3H]$-ouabain (at $10^{-4}M$) and $^{45}Ca^{2+}$ effects in 50% Na PS, where the role of pump is excluded, demonstrates the dehydration in all tissues (**Figure 5(a)**, **Figure 5(c)**). As it has been predicted, the decrease of $[Na]_o$ when Na^+/K^+ pump is in inactive state, the dehydration and $^{45}Ca^{2+}$ uptake in brain cortex is more pronounced (**Figure 5(a)**, **Figure 5(d)**) than when the pump is active (**Figure 4(a)**, **Figure 4(d)**). In liver tissues the age-dependent weakening dehydration effect is accompanied by depression of $^{45}Ca^{2+}$ uptake (**Figure 5(b)**, **Figure 5(e)**) and in spleen tissue there is an age-dependent strengthening effect (**Figure 5(c)**, **Figure 5(f)**). From these data can be suggested that Na^+/K^+ pump inactivation leads to the activation of Na^+/H^+ exchange in the reverse mode, which brings to inhibition of RNa^+/Ca^{2+} exchange and activation of mitochondrial function leading to tissue dehydration.

The data that 10^{-9} M ouabain in 50% Na PS has effects in ET can be explained by age-dependent weakening RNa^+/Ca^{2+} exchange (**Figure 6(a)**) led to age-dependent decrease of $^{45}Ca^{2+}$ uptake (**Figure 6(d)**). However, in liver tissue the age-dependent weakening dehydration effect leads to the age-dependent increase of $^{45}Ca^{2+}$ uptake (**Figure 6(e)**) but in spleen it is accompanied by age-dependent decreasing effect of Ca^{2+} uptake (**Figure 6(f)**). Since the Na gradient on the membrane serves as the energy source for both, Na^+/H^+ exchange and RNa^+/Ca^{2+} exchange, the effect of $[Na]_o$ on tissue hydration and $^{45}Ca^{2+}$ uptake can be explained by competitive interaction between Na^+/H^+ and RNa^+/Ca^{2+} differences between age-dependent Ca uptake in liver and spleen tissues probably can be explained by different expressions of these exchangers, which could serve as a subject for special investigation. The different age-dependent ion transporting mechanisms between these tissues indicate the age-dependent increase of Na^+/K^+ pump units in liver while it is absent in the spleen (**Figure 2**). The cell hydration leads to the activation of cell metabolism [2] [12]. Therefore, it has been suggested that by supplying animals DW instead of regular tap water, it could stimulate the metabolic activity of tissues. The data obtained on animals drinking during 10 days DW instead of tap water, indicates that in ET there is an age-dependent increase of tissue hydration (**Figure 7(a)**), while in NET an age-dependent dehydration is observed (**Figure 7(b)**, **Figure 7(c)**), *i.e.* there is the opposite picture to that in case of cooling (**Figure 1(a)**, **Figure 1(c)**). From these data can be

concluded that DW-induced activation of mitochondrial activity leads to the water efflux from the cells bringing to dehydration (transition from sole into gel state) in NET. This explanation supports the data that old animals' DW-induced dehydration effect in NET is less than that in young ones (**Figure 7(b)**, **Figure 7(c)**).

The data on Na^+/K^+ pump inactivation by 10^{-4}M ouabain indicate that in ET of young and old animals there are hydration and dehydration effects, respectively (**Figure 8(a)**). It is worth to note that the number of ouabain binding has pronounced decrease in the membrane in case of animals drinking DW compared with those drinking tap water (**Figure 8(d)**). These data indicate on the increase of expression of Na^+/K^+ pump units in ET of old animals (**Figure 7(d)**, **Figure 7(g)**). Probably, the increase of pump units in ET of old animals is the compensated response of brain tissue for weakening pump function because of high $[Ca]_i$. It seems extremely interesting, that Na^+/K^+ pump inactivation leads to non-significant effect on liver dehydration of young animals but has pronounced hydration effect in old ones (**Figure 8(b)**), while in spleen tissue of both age groups the hydration is observed (**Figure 8(c)**), which accompanied by the over-expression of pump units in aging animals, has more pronounced character in liver tissues (**Figure 8(h)**, **Figure 8(i)**). These data clearly indicate that the electrogenic ion transporting mechanisms such as Na^+/K^+ pump and Na^+/Ca^{2+} exchange and endogen water molecules' formation as a result of oxidative processes have the key role in regulation of neuronal hydration. Meanwhile, in NET because of their cell membrane higher permeability to water (H^+), the electrogenic properties of cell membrane are depressed and their hydration controlled by mitochondrial activity in its turn releases the production of water molecules in cytoplasm.

As it has been predicted, 10^{-9} M ouabain has dehydration effect on tissue, which is due to activation of RNa^+/Ca^{2+} exchange in ET (**Figure 9(a)**) and the activation of Na^+/H^+ exchange in NET (**Figure 9(b)**, **Figure 9(c)**). It is interesting that there is an age-dependent increase of α_3 receptors in the membrane (**Figure 9(g)**), which have RNa^+/Ca^{2+} function in neurons [21], while in NET tissues Na^+/H^+ exchange (**Figure 8(g)**). 10^{-9}M ouabain has an age-dependent dehydration effect on liver and spleen tissues, which is accompanied by the age-dependent increase of nM ouabain receptors in liver and its decrease in spleen membranes. Since the Na^+/K^+-ATPase isoforms in NET are absent, nM ouabain induced effect in NET can be explained by the activation of G protein in the membrane leading to the increase of the intracellular cAMP contents, which probably activates Na^+/H^+ exchange [22]. Therefore, it is suggested that in NET the nM ouabain brings to cAMP-dependent dehydration by stimulation of Na^+/H^+ exchange, while the brain tissue dehydration is the result of activation of cAMP-dependent RNa^+/Ca^{2+} exchange. Thus, the summary of the obtained data brings us to the conclusion that the over-expression of Na^+/Ca^{2+} exchanger in the brain cortex and the Na^+/K^+ pump units in the liver could be considered as

markers for aging.

5. Conclusions

1) Metabolic regulation of cell hydration in excitable tissue (brain cortex) is realized by the activation of electrogenic Na^+/K^+ pump and Na^+/Ca^{2+} exchange in the cell membrane and the formation of endogen water by mitochondrial activity.

2) Regulation of cell hydration in non-excitable tissue (liver, spleen) is carried out only by the activity of mitochondrial function.

3) Aging leads to an over-expression of Na^+/K^+ pump units in liver and Na^+/Ca^{2+} exchanger in brain cortex of rats.

Conflicts of Interest

The authors declare no conflicts of interest regarding the publication of this paper.

References

[1] Ayrapetyan, S.N. (1980) On the Physiological Significance of Pump Induced Cell Volume Changes. 28*th International Congress of Physiological Science*, Budapest, Vol. 23, 67-82. (In Russian) https://doi.org/10.1016/B978-0-08-027344-0.50010-7

[2] Parsegian, V.A., Rand, R.P. and Rau, D.C. (2000) Osmotic Stress, Crowding, Preferential Hydration and Binding: A Comparison of Perspectives. *Proceedings of the National Academy of Sciences of the United States of America*, **97**, 3987-3992. https://doi.org/10.1073/pnas.97.8.3987

[3] Lauriola, M., Mangiacotti, A., D'Onofrio, G., Cascavilla, L., Paris, F., *et al.* (2018) Neurocognitive Disorders and Dehydration in Older Patients: Clinical Experience Supports the Hydromolecular Hypothesis of Dementia. *Nutrients*, **10**, 562-576. https://doi.org/10.3390/nu10050562

[4] Damadian, R. (1971) Tumor Detection by Nuclear Magnetic Resonance. *Science*, **171**, 1151-1153. https://doi.org/10.1126/science.171.3976.1151

[5] Hoffman, E.K., Lambert, I.H. and Pedersen, S.F. (2009) Physiology of Cell Volume Regulation in Vertebrates. *Physiological Reviews*, **89**, 193-277. https://doi.org/10.1152/physrev.00037.2007

[6] Ayrapetyan, S.N. and Suleymanyan, M.A. (1979) On the Pump-Induced Cell Volume Changes. *Comparative Biochemistry and Physiology*, **64A**, 571-575. https://doi.org/10.1016/0300-9629(79)90585-1

[7] Ayrapetyan, S.N., Rychkov, G.Y. and Suleymanyan, M.A. (1988) Effects of Water Flow on Transmembrane Ionic Currents in Neurons of Helix Pomatia and in Squid Giant Axons. *Comparative Biochemistry and Physiology*, **89**, 179-186. https://doi.org/10.1016/0300-9629(88)91076-6

[8] Krnjevic, K. (1992) Cellular and Synaptic Actions of General Anaesthetics. *General Pharmacology*, **23**, 965-975. https://doi.org/10.1016/0306-3623(92)90274-N

[9] Heqimyan, A., Deghoyan, A. and Ayrapetyan, S. (2011) Ketamine-Induced Cell Dehydration as a Mechanism of Its Analgesic and Anesthetic Effects. *Journal of International Dental and Medical Research*, **4**, 42-49.

[10] Takahashi, R. and Aprison, M. (1964) Acetylcholine Content of Discrete Areas of

the Brain Obtained by a Near-Freezing Method. *Journal of Neurochemistry*, **11**, 887-892. https://doi.org/10.1111/j.1471-4159.1964.tb06740.x

[11] Adrian, R.H. (1956) The Effect of Internal and External Potassium Concentration on the Membrane Potential of Frog Muscle. *Journal of Physiology*, **133**, 631-658. https://doi.org/10.1113/jphysiol.1956.sp005615

[12] Ayrapetyan, S.N., Suleymanyan, M.A., Saghyan, A.A. and Dadalyan, S.S. (1984) Autoregulation of Electrogenic Sodium Pump. *Cellular and Molecular Neurobiology*, **4**, 367-383. https://doi.org/10.1007/BF00733598

[13] Heqimyan, A., Narinyan, L., Nikoghosyan, A., *et al*. (2012) Age Dependency of High Affinity Ouabain Receptors and Their Magnetosensitivity. *The Environmentalist*, **32**, 228-235. https://doi.org/10.1007/s10669-011-9383-0

[14] Baker, P.F., Blaustein, M.P., Hodgkin, A.L. and Steinhardt, S.A. (1969) The Influence of Calcium on Sodium Efflux in Squid Axons. *The Journal of Physiology*, **200**, 431-458. https://doi.org/10.1113/jphysiol.1969.sp008702

[15] Janmey, P.A. (1991) Gel-Sol Transition of the Cytoplasm and Its Regulation. *AIP Conference Proceedings*, **226**, 304. https://doi.org/10.1063/1.40599

[16] Juhaszova, M. and Blaustein, M. (1997) Na^+ Pump with Low and High Ouabain Affinity Apha Subunit Isoforms Are Differently Distributed in Cells. *Proceedings of the National Academy of Sciences of the United States of America*, **94**, 1800-1805. https://doi.org/10.1063/1.40599

[17] Khachaturian, Z.S. (1989) The Role of Calcium Regulation in Brain Aging: Reexamination of a Hypothesis. *Aging*, **1**, 17-34. https://doi.org/10.1007/BF03323872

[18] Lehninger, A.L. (1970) Mitochondria and Calcium Ion Transport. *Biochemical Journal*, **119**, 129-138. https://doi.org/10.1042/bj1190129

[19] Ayrapetyan, S.N., Heqimyan, A.A. and Nikoghosyan, A.K. (2012) Age-Dependent Brain Tissue Hydration, Ca Exchange and Their Dose-Dependent Ouabain Sensitivity. *Journal of Bioequivalence and Bioavailability*, **4**, 60-68. https://doi.org/10.4172/jbb.10000114

[20] Saghian, A.A., Ayrapetyan, S.N. and Carpenter, D.O. (1996) Low Concentrations of Ouabain Stimulate Na/Ca Exchange in Neurons. *Cellular and Molecular Neurobiology*, **16**, 180-185. https://doi.org/10.1007/BF02150229

[21] Heqimyan, A., Narinyan, L., Nikoghosyan, A. and Ayrapetyan, S. (2015) Age Dependent Magnetic Sensitivity of Brain and Heart Muscles, Electromagnetic Fields in Biology and Medicine. CRC Press, Boca Raton, 217-230. https://doi.org/10.1201/b18148-15

[22] Rosenbaum, D.M., Rasmussen, S.G. and Kobilka, B.K. (2009) The Structure and Function of G-Protein-Coupled Receptors. *Nature*, **459**, 356-363. https://doi.org/10.1038/nature08144

Call for Papers

Open Journal of Biophysics

ISSN Print: 2164-5388 ISSN Online: 2164-5396
http://www.scirp.org/journal/ojbiphy

Open Journal of Biophysics (OJBIPHY) is an international journal dedicated to the latest advancement of biophysics. The goal of this journal is to provide a platform for scientists and academicians all over the world to promote, share, and discuss various new issues and developments in different areas of biophysics.

Subject Coverage

All manuscripts must be prepared in English, and are subject to a rigorous and fair peer-review process. Accepted papers will immediately appear online followed by printed hard copy. The journal publishes original papers including but not limited to the following fields:

- Bioelectromagnetics
- Bioenergetics
- Bioinformatics and Computational Biophysics
- Biological Imaging
- Biomedical Imaging and Bioengineering
- Biophysics of Disease
- Biophysics of Photosynthesis
- Cardiovascular Biophysics
- Cell Biophysics
- Medical Biophysics
- Membrane Biophysics
- Molecular Biophysics and Structural Biology
- Physical Methods
- Physiology and Biophysics of the Inner Ear
- Proteins and Nucleic Acids Biophysics
- Radiobiology
- Receptors and Ionic Channels Biophysics
- Sensory Biophysics and Neurophysiology
- Systems Biophysics
- Theoretical and Mathematical Biophysics

We are also interested in: 1) Short Reports—2-5 page papers where an author can either present an idea with theoretical background but has not yet completed the research needed for a complete paper or preliminary data; 2) Book Reviews—Comments and critiques.

Notes for Intending Authors

Submitted papers should not have been previously published nor be currently under consideration for publication elsewhere. Paper submission will be handled electronically through the website. All papers are refereed through a peer review process. For more details about the submissions, please access the website.

Website and E-Mail

http://www.scirp.org/journal/ojbiphy E-mail: ojbiphy@scirp.org

What is SCIRP?

Scientific Research Publishing (SCIRP) is one of the largest Open Access journal publishers. It is currently publishing more than 200 open access, online, peer-reviewed journals covering a wide range of academic disciplines. SCIRP serves the worldwide academic communities and contributes to the progress and application of science with its publication.

What is Open Access?

All original research papers published by SCIRP are made freely and permanently accessible online immediately upon publication. To be able to provide open access journals, SCIRP defrays operation costs from authors and subscription charges only for its printed version. Open access publishing allows an immediate, worldwide, barrier-free, open access to the full text of research papers, which is in the best interests of the scientific community.

- High visibility for maximum global exposure with open access publishing model
- Rigorous peer review of research papers
- Prompt faster publication with less cost
- Guaranteed targeted, multidisciplinary audience

Scientific Research Publishing

Website: http://www.scirp.org

Subscription: sub@scirp.org

Advertisement: service@scirp.org